AD-A112 725 DAYTON UNIV OH RESEARCH INST F/G 11/4
EXPERIMENTAL AND NUMERICAL ANALYSIS OF AXIALLY COMPRESSED CIRCU--ETC(U)
OCT 81 N R BAULD F33615-79-C-3030
UNCLASSIFIED AFWAL-TR-81-3158 NL

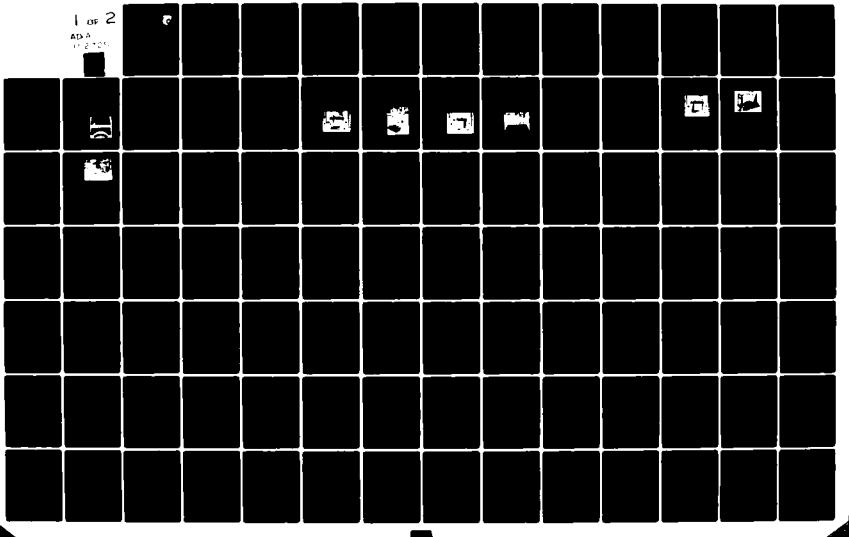

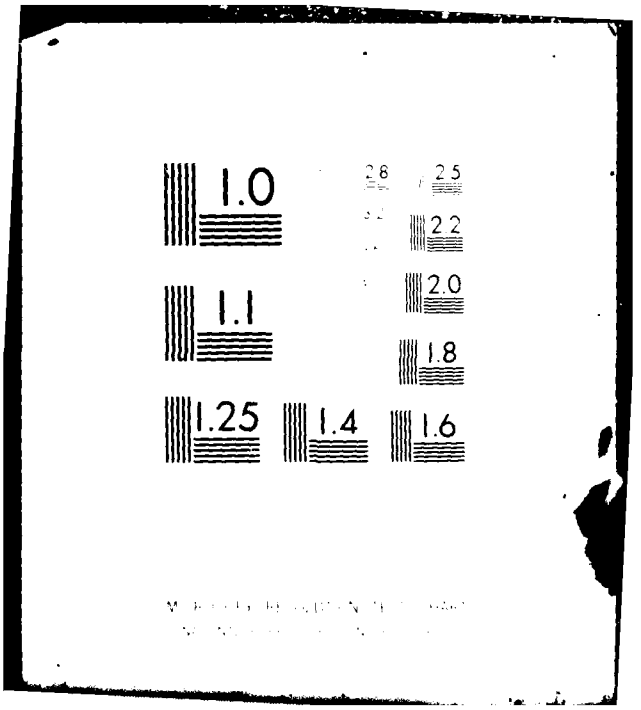
1.0
1.1
1.25
1.4
1.6
2.0
1.8
2.2
2.5

(2)

AFWAL-TR-81-3158

AD A112225

EXPERIMENTAL AND NUMERICAL ANALYSIS OF AXIALLY COMPRESSED CIRCULAR CYLINDRICAL FIBER-REINFORCED PANELS WITH VARIOUS BOUNDARY CONDITIONS

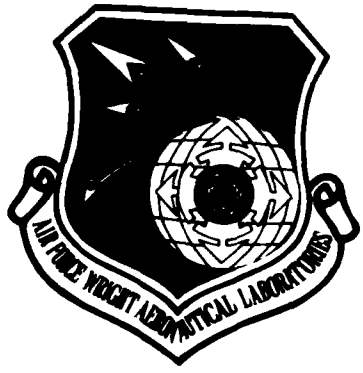

NELSON R. BAULD, JR.

CLEMSON UNIVERSITY
CLEMSON, SC 29631

OCTOBER 1981

TECHNICAL REPORT AFWAL-81-3158
Final Report for Period 1 October 1978 - 30 September 1981

Approved for public release; distribution unlimited.

FLIGHT DYNAMICS LABORATORY
AIR FORCE WRIGHT AERONAUTICAL LABORATORIES
AIR FORCE SYSTEMS COMMAND
WRIGHT-PATTERSON AIR FORCE BASE, OHIO 45433

NOTICE

When Government drawings, specifications, or other data are used for any purpose other than in connection with a definitely related Government procurement operation, the United States Government thereby incurs no responsibility nor any obligation whatsoever; and the fact that the government may have formulated, furnished, or in any way supplied the said drawings, specifications, or other data, is not to be regarded by implication or otherwise as in any manner licensing the holder or any other person or corporation, or conveying any rights or permission to manufacture use, or sell any patented invention that may in any way be related thereto.

This report has been reviewed by the Office of Public Affairs (ASD/PA) and is releasable to the National Technical Information Service (NTIS). At NTIS, it will be available to the general public, including foreign nations.

This technical report has been reviewed and is approved for publication.

Narendra S Khot

NARENDRA S. KHOT
Project Engineer

Fred A. Picchioni

FREDERICK A. PICCHIONI, Lt Col, USAF
Chief, Analysis & Optimization Branch

FOR THE COMMANDER

Ralph L. Kuster Jr.

RALPH L. KUSTER, JR., Col, USAF
Chief, Structures & Dynamics Div.

If your address has changed, if you wish to be removed from our mailing list, or if the addressee is no longer employed by your organization please notify AFWAL/FIBR, W-PAFB, OH 45433 to help us maintain a current mailing list .

Copies of this report should not be returned unless return is required by security considerations, contractual obligations, or notice on a specific document.

AIR FORCE/56780/18 March 1982 — 200

UNCLASSIFIED

SECURITY CLASSIFICATION OF THIS PAGE (When Data Entered)

REPORT DOCUMENTATION PAGE		READ INSTRUCTIONS BEFORE COMPLETING FORM
1. REPORT NUMBER AFWAL-TR-81-3158	2. GOVT ACCESSION NO. AD-A112725	3. RECIPIENT'S CATALOG NUMBER
4. TITLE (and Subtitle) EXPERIMENTAL AND NUMERICAL ANALYSIS OF AXIALLY COMPRESSED CIRCULAR CYLINDRICAL FIBER-REINFORCED PANELS WITH VARIOUS BOUNDARY CONDITIONS		5. TYPE OF REPORT & PERIOD COVERED Final Report for Period 1 October 1978-30 Sept 1981 6. PERFORMING ORG. REPORT NUMBER
7. AUTHOR(s) Nelson R. Bauld, Jr.		8. CONTRACT OR GRANT NUMBER(s) F33615-79-C-3030
9. PERFORMING ORGANIZATION NAME AND ADDRESS Clemson University Clemson, SC 29631		10. PROGRAM ELEMENT, PROJECT, TASK AREA & WORK UNIT NUMBERS Proj 2307, Task 2307N5 Work Unit 2307N501
11. CONTROLLING OFFICE NAME AND ADDRESS University of Dayton Research Institute Dayton, OH 45469		12. REPORT DATE October 1981 13. NUMBER OF PAGES 151
14. MONITORING AGENCY NAME & ADDRESS(if different from Controlling Office) Flight Dynamics Laboratory (AFWAL/FIBRA) Air Force Wright Aeronautical Laboratories (AFSC) Wright-Patterson AFB, Ohio 45433		15. SECURITY CLASS. (of this report) UNCLASSIFIED 15a. DECLASSIFICATION DOWNGRADING SCHEDULE

16. DISTRIBUTION STATEMENT (of this Report)

Approved for public release, distribution unlimited.

17. DISTRIBUTION STATEMENT (of the abstract entered in Block 20, if different from Report)

18. SUPPLEMENTARY NOTES

19. KEY WORDS (Continue on reverse side if necessary and identify by block number)

Buckling Load
Composite Structures
Plates and Shells
Finite Difference Methods
Experiments

20. ABSTRACT (Continue on reverse side if necessary and identify by block number)

This report presents comparisons between the experimental and numerical buckling behaviors of fiber-reinforced, circular cylindrical panels under prescribed uniform end-displacements. Numerical predictions used in the comparisons were obtained from the energy-based, finite-difference computer program CLAPP. Test specimens were clamped along both curved edges and were either simply supported or unsupported along the straight edges.

DD FORM 1 JAN 73 1473 EDITION OF 1 NOV 65 IS OBSOLETE

UNCLASSIFIED

SECURITY CLASSIFICATION OF THIS PAGE (When Data Entered)

FOREWORD

This report was prepared by Dr Nelson R. Bauld, Jr., Professor, Department of Mechanical Engineering, Clemson University, Clemson, South Carolina, in partial fulfillment of the requirements under Contract F33615-79-C-3030. The effort was initiated under Project No. 2307, "Research in Flight Vehicle Structures," Task 2307N501, "Basic Research in Structures and Dynamics." The project monitor for the effort was Dr Narendra S. Khot of the Structures and Dynamics Division (AFWAL/FIBRA).

The technical work was performed during the period October 1978 through September 1981. Review report was submitted in October 1981 and the final report in January 1982.

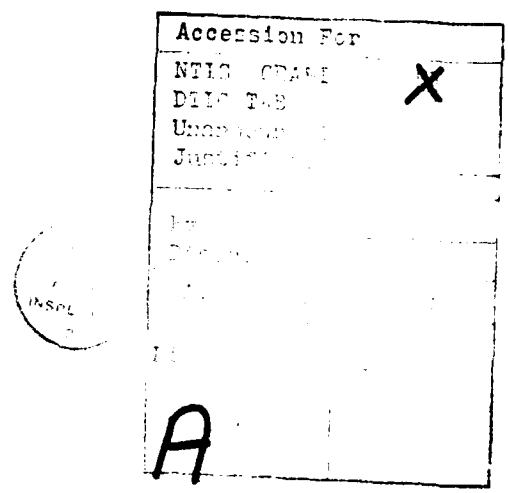

TABLE OF CONTENTS

LIST OF ILLUSTRATIONS

LIST OF TABLES

SECTION I

INTRODUCTION

The principal purpose of this investigation is to provide a basis for assessing the capability of the computer program CLAPP [1] to predict buckling loads for fiber-reinforced, circular cylindrical panels under prescribed uniform axial end-displacements.

Two testing programs were undertaken to accomplish this objective. They are designated as Program A and Program B in this report.

Program A. Experimental buckling loads were determined for 20 specimens having identical fiber patterns of $[0/90]_{2s}$ and 20 specimens having identical fiber patterns of $[0/\pm45/90]_{s}$. The specimens of a particular fiber pattern were characterized geometrically by five different aspect ratios and by two different sets of boundary conditions. The aspect ratios were a/b = 1/2, 3/4, 1, 4/3, and 2, where a and b are the dimensions of the projection of a panel into its base plane as shown in Figure 1. Boundary conditions along the straight edges of a specimen corresponded to either an unsupported edge or a simply-supported edge. For the simply-supported edge a distinction between unconstrained and constrained circumferential displacements is also made. Boundary conditions along the curved edges corresponded to a clamped edge for all specimens.

Program B. Experimental buckling loads were determined for 6 specimens with the same fiber pattern ($[0/90]_{2s}$), the same aspect ratio (a/b = 1.247, a = 16 in. and b = 12.83 in.), and the same boundary conditions (unsupported straight edges and clamped curved edges). Similarly, experimental buckling loads were obtained for 5 specimens with the fiber pattern $[0/\pm45/90]_{s}$,

aspect ratio a/b = 4/3 (a = 16 in. and b = 12 in.), and boundary conditions consisting of simply-supported straight edges and clamped curved edges.

A second purpose of this investigation is to modify the computer program CLAPP so as to minimize the effort required to input necessary data. This phase of this investigation is contained as a USER'S MANUAL in Appendix D.

Finally, a third purpose is to modify CLAPP so that it can be used to predict the buckling behavior of fiber-reinforced, circular cylindrical panels and flat plates that are augmented by longitudinal stiffeners. This is accomplished for isotropic stiffeners with a variety of cross sections and for a quasi-isotropic stiffener with a hat shaped cross section.

SECTION II

TESTING PROCEDURE

(II-1). TEST SPECIMENS. Each of the circular cylindrical specimens of Program A and Program B was laminated from graphite-epoxy, and each specimen was cured in a mold for which the external radius was 12 inches.[1] The external radius of a specimen tended to be slightly less than 12 inches upon removal from the mold. The thickness of a test specimen was taken as an average of the thicknesses at 32 locations along a perimeter located uniformly 1-1/2 inches from the exterior perimeter of the specimen. The average thickness for each specimen of Program A is shown in column 2 of Table 1. The average thickness for each specimen of Program B is shown in column 2 of Table 2. Figure 1 indicates pertinent geometrical parameters of a typical specimen. The radius, R = 12.0 in., is the radius of a perfectly circular panel installed in the testing fixture, and the thickness shown is the average thickness of a typical panel.

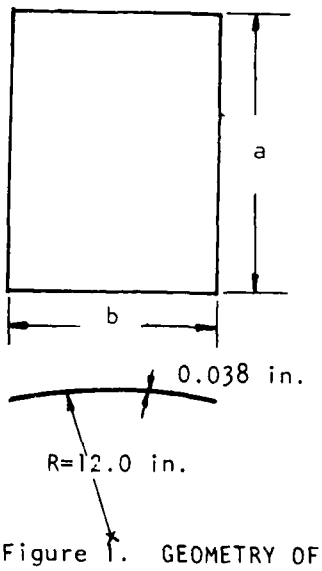

Figure 1. GEOMETRY OF CURVED PANEL SPECIMEN

Laminate stiffness properties were calculated by lamination theory [2] using the following lamina properties:

---

(1) All specimens were fabricated and cut by the Air Force Flight Dynamics Laboratory, Air Force Wright Aeronautical Laboratories, Air Force Systems Command, Wright-Patterson Air Force Base, Ohio.

E_{11} = 20,524 ksi, E_{22} = 1,333 ksi, G_{12} = 752 ksi, ν_{12} = 0.335, and ν_{21} = 0.022. E_{11} and E_{22} are Young's moduli of elasticity parallel and perpendicular to the fiber direction, G_{12} is the shearing modulus associated with these two directions, and ν_{12} and ν_{21} are Poisson ratios.

Program A. The specimens of Program A were distinguished by aspect ratio (a/b), laminate fiber pattern, and boundary conditions.

Specimens having five different aspect ratios (a/b = 1/2, 3/4, 1, 4/3, and 2) were tested. It is convenient to perceive of specimens that are associated with a specific aspect ratio to form a group. Thus, five separate groups of specimens are identifiable.

Each group of specimens consisted of two sub-groups: one sub-group being associated with simply-supported straight edges, and one sub-group being associated with unsupported straight edges. Boundary conditions along the curved edges were clamped for all specimens in each group.

Two laminate fiber-patterns ($[0/90]_{2s}$ and $[0/\pm45/90]_s$) were considered for each sub-group. Moreover, each member of each group was duplicated to provide a means to assess repeatibility of experimental results.

From the foregoing discussion it will be observed that each group contained eight specimens: four with simply-supported straight edges and four with unsupported straight edges. Of the four specimens in a sub-group (either simply-supported or unsupported straight edges) two were characterized by a fiber-pattern of $[0/90]_{2s}$ and two were characterized by a fiber-pattern of $[0/\pm45/90]_s$. The complete experimental effort amounted to forty specimens. Table 1 has been organized to ref'ect the foregoing classification of specimens.

The physical dimensions of the base-planes (projected area of a specimen) of the specimens associated with the five aspect ratios were 8 x 16, 12 x 16, 16 x 16, 16 x 12, and 16 x 8 (all dimensions are in inches). These dimensions correspond to the inside dimensions of the specimens after installation in the testing fixture.

Program B. As was stated in the introduction, the specimens of Program B can be categorized into two groups: one group with fiber pattern $[0/90]_{2s}$, aspect ratio 16/12.83 = 1.247, and unsupported straight edges; and one group with fiber pattern $[0/\pm45/90]_{s}$ aspect ratio 16/12 = 4/3, and simply-suported straight edges. The results of buckling tests on these specimen are tabulated in Table 2.

(II-2). TEST FIXTURE. The testing fixture used in both testing programs was a modification of a test fixture used by Wilkins [3]. Modifications of the Wilkins' testing fixture were necessary to accommodate specimens of different aspect ratios. Figure 2 shows the head-plate and the base-plate (with their auxilliary pressure blocks and clamping plates) through which an axial compressive load was applied to a specimen. All surfaces of the head-plate, and of the base-plate, were carefully machined so that they were within 0.001 in. of being parallel.

FIGURE 2. Head-plate and base-plate with auxiliary pressure blocks and clamping plates.

TABLE 1. EXPERIMENTAL AND NUMERICAL BUCKLING RESULTS FOR CIRCULAR CYLINDRICAL PANELS FOR TESTING PROGRAM A.

DIMENSIONS (in)	AVERAGE THICKNESS (in)	ASPECT RATIO	PANEL LABEL DESIGNATION	BOUNDARY CONDITION	LAMINATE PATTERN	EXPERIMENTAL BUCKLING LOAD (lb)	THEORETICAL BIFURCATION LOAD (lb)	RATIO MODIFIED EXP LOAD TO THEO. LOAD
8 x 16	0.0357	1/2	BCP-9824-A2-1	S.S.*	[0/±45/90]s	5825	12,020	0.458
	0.0389		BCP-9824-A2-2	S.S.	[0/±45/90]s	6710		0.528
	0.0378		BCP-9810-B4-1	S.S.	[0/$\bar{9}$0]2s	5175	9,402	0.521
	0.0362		BCP-9810-B4-2	S.S.	[0/90]2s	5350		0.538
	0.0373		BCP-9824-A2-1	F.E.**	[0/±45/90]s	3900	3,724	1.047
	0.0396		BCP-9824-A2-2	F.E.	[0/±45/90]s	3970		1.066
	0.0384		BCP-9810-B4-1	F.E.	[0/$\bar{9}$0]2s	3850	2,020	1.906
	0.0402		BCP-9810-B4-2	F.E.	[0/90]2s	3300		1.634
12 x 16	0.0397	3/4	BCP-9921-A5-1	S.S.	[0/±45/90]s	5600	9,954	0.532
	0.0378		BCP-9921-A5-2	S.S.	[0/±45/90]s	5910		0.562
	0.0376		BCP-8910-B2-1	S.S.	[0/$\bar{9}$0]2s	4750	8,770	0.516
	0.0380		BCP-8910-B2-2	S.S.	[0/90]2s	4950		0.538
	0.0374		BCP-9921-A6-1	F.E.	[0/±45/90]s	2775	1,557	1.782
	0.0404		BCP-9921-A6-2	F.E.	[0/±45/90]s	3050		1.959
	0.0382		BCP-9817-B5-1	F.E.	[0/$\bar{9}$0]2s	3140	1,456	2.157
	0.0400		BCP-9817-B5-2	F.E.	[0/90]2s	3200		2.198

* The designation S.S. signifies that the straight edges of the panel were simply-supported.

** The designation F.E. signifies that the straight edges of the panel were unsupported.

(CONT) TABLE 1. EXPERIMENTAL AND NUMERICAL BUCKLING RESULTS FOR CIRCULAR CYLINDRICAL PANELS FOR TESTING PROGRAM A.

DIMENSIONS (in)	AVERAGE THICKNESS (in)	ASPECT RATIO	PANEL LABEL DESIGNATION	BOUNDARY CONDITION	LAMINATE PATTERN	EXPERIMENTAL BUCKLING LOAD (lb)	THEORETICAL BIFURCATION LOAD (lb)	RATIO MODIFIED EXP LOAD TO THEO. LOAD
16 x 16	0.0388	1	BCP-9824-A3-1	S.S.	[0/±45/90]s	4750	8,228	0.539
	0.0390		BCP-9824-A3-2	S.S.	[0/±45/90]s	6400		0.727
	0.0386		BCP-9810-B3-1	S.S.	[0/90]2s	5010	8,125	0.583
	0.0393		BCP-9810-B3-2	S.S.	[0/90]2s	5700		0.664
	0.0375		BCP-9824-A4-1	F.E.	[0/±45/90]s	2850	1,861	1.531
	0.0384		BCP-9824-A4-2	F.E.	[0/±45/90]s	2750		1.478
	0.0391		BCP-9817-B8-1	F.E.	[0/90]2s	2740	1,511	1.813
	0.0393		BCP-9817-B8-2	F.E.	[0/90]2s	3100		2.052
16 x 12	0.0385	4/3	BCP-9921-A8-1	S.S.	[0/±45/90]s	3500	5,277	0.667
	0.0391		BCP-9921-A8-2	S.S.	[0/±45/90]s	5575		0.979
	0.0399		BCP-9810-B1-1	S.S.	[0/90]2s	4600	4,893	0.871
	0.0388		BCP-9810-B1-2	S.S.	[0/90]2s	4710		0.892
	0.0387		BCP-9824-A1-1	F.E.	[0/±45/90]s	2300	800	2.875
	0.0389		BCP-9824-A1-2	F.E.	[0/±45/90]s	2090		2.6125
	0.0383		BCP-9817-B6-1	F.E.	[0/90]s	1930	796	2.425
	0.0387		BCP-9817-B6-2	F.E.	[0/90]s	2110		2.651
16 x 8	0.0390	2	BCP-9921-A7-1	S.S.	[0/±45/90]s	3440	3,088	0.992
	0.0396		BCP-9921-A1-2	S.S.	[0/±45/90]s	3320		0.958
	0.0380		BCP-9817-B7-1	S.S.	[0/90]2s	2450	2,693	0.810
	0.0393		BCP-9817-B7-2	S.S.	[0/90]2s	3240		1.072
	0.0356		BCP-9921-A7-1	F.E.	[0/±45/90]s	840	643	1.322
	0.0382		BCP-9921-A7-2	F.E.	[0/±45/90]s	1046		1.627
	0.0387		BCP-9817-B7-1	F.E.	[0/90]2s	1065	476	2.238
	0.0363		BCP-9817-B7-2	F.E.	[0/90]2s	1090		2.290

TABLE 2. EXPERIMENTAL AND NUMERICAL BUCKLING RESULTS FOR CIRCULAR CYLINDRICAL PANELS FOR TESTING PROGRAM B.

PANEL LABEL DESIGNATION	AVERAGE THICKNESS, (in)	LAMINATE PATTERN	BOUNDARY CONDITIONS	EXP. BUCKLING LOAD, (lb)	THEO. BUCKLING LOAD, (lb)
DS-B9-1	0.0357	$[0/90]_{2s}$	F.E.	2165	
DS-B9-2	0.0378	$[0/90]_{2s}$	F.E.	2410	
DS-B10-1	0.0369	$[0/90]_{2s}$	F.E.	2300	* 3320 lb
DS-B10-2	0.0380	$[0/90]_{2s}$	F.E.	2500	
DS-B11-1	0.0374	$[0/90]_{2s}$	F.E.	2460	
DS-B11-2	0.0382	$[0/90]_{2s}$	F.E.	2715	
DS-A9-1	0.0375	$[0/\pm45/90]_{s}$	S.S.	4600	
DS-A9-2	0.0382	$[0/\pm45/90]_{s}$	S.S.	4975	* 6950 lb
DS-A10-1	0.0378	$[0/\pm45/90]_{s}$	S.S.	5775	
DS-A10-2	0.0371	$[0/\pm45/90]_{s}$	S.S.	5510	** 5622 lb
DS-A11-1	0.0383	$[0/\pm45/90]_{s}$	S.S.	5160	

* Theoretical buckling load for perfect panel corresponding to prescribed uniform end displacements and a 20 x 11 finite difference grid.

** Theoretical buckling load for an imperfect panel corresponding to prescribed uniform end displacements and a 20 x 11 finite difference grid.

(11-3). TESTING MACHINE. An axial compressive load was applied to a specimen through a 120,000 lb Tinius-Olsen hydraulic testing machine. Most experimental buckling loads were of such a magnitude that the intermediate range (12,000 lb range) of the testing machine could be used effectively. The finest division for this range is 50 lb. The low range (3000 lb range) was used to test several specimens with unsupported straight edges. The finest division for this range is 5 lb.

The surfaces of the platten and the cross-head of the testing machine were dressed so that they were nearly plane.

The head-plate and the base-plate of the testing fixture are shown installed in the Tinius-Olsen testing machine in Figure 3.

Early in testing Program A it became apparent that the cross-head would tilt as the reactive force of the specimen on the cross-head tended to lift it off the threads of the vertical columns. To eliminate the tilting action two large aluminum nuts were machined and placed on the vertical screws

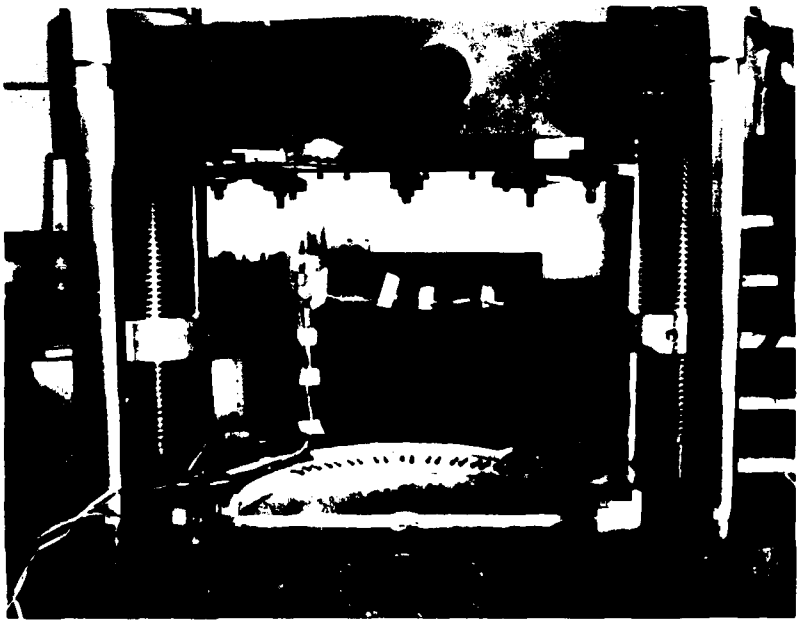

FIGURE 3. Testing fixture installed in the Tinius-Olsen hydraulic testing machine.

beneath the cross-head. At an appropriate point during the installation of a specimen these nuts were tightened against the lower surfaces of the cross-head causing it to lock in place. These aluminum locking nuts are shown in Figure 3.

(11-4). IMPERFECTION DEVICE. Figure 4 shows the mechanical device that was used to measure deviations of a specimen from a perfect cylindrical form; that is, to measure the initial geometric imperfections of a specimen.

Components of this device were constructed so that the vertical sides of the circular groove in the platform of the device were concentric with the vertical sides of the circular groove in the base-plate of the testing fixture. The imperfection device was secured to the base-plate of the testing fixture so that its slotted vertical platform-supports were perpendicular to the base-plate. This ensured concentricity of the platform groove with the groove in the base-plate for any platform level.

To position the imperfection device relative to the base-plate of the testing fixture, the dial indicator mechanism shown in Figure 4

FIGURE 4. Imperfection measuring device attached to the base-plate of the testing fixture.

was designed so that it could be moved smoothly and snugly in the circular groove of the platform of the imperfection measuring device. With the tip of the dial indicator extension resting against the vertical side of the circular groove in the base-plate, the mechanism was moved along the platform groove. By trial the imperfection measuring device was adjusted relative to the base-plate so that the pointer of the dial indicator was undisturbed for a complete cycle along the platform groove. Once the proper position was located the imperfection measuring device was secured to the base-plate of the testing fixture by machine bolts. Positioning pins were installed so that the correct position could be duplicated. This procedure resulted in a variation of less than 0.001 in. for a complete traverse of the platform groove.

Holes for positioning pins were drilled at one-inch intervals along the slotted vertical platform supports. This ensured that the position of the imperfection measuring device relative to the base-plate of the testing fixture could be duplicated at appropriate levels. Once the platform was located at a specified level by the positioning pins, it was locked in that position by cap screws.

Figure 5 shows the imperfection measuring

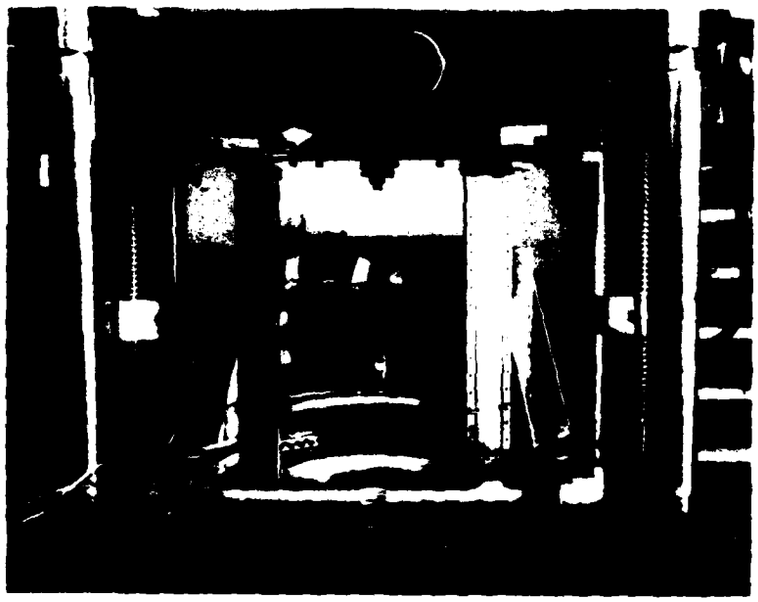

FIGURE 5. Imperfection measuring device in position to measure initial geometric imperfections of a specimen.

device installed on the testing fixture. Deviation of a specimen from perfect circularity were measured by moving the dial indicator mechanism along the platform groove.

(11-5). POSITIONING OF HEAD-PLATE AND BASE-PLATE. Two requirements were essential for proper alignment of the head-plate relative to the base-plate of the testing fixture. First, the circular arc associated with an edge of the circular groove in the head-plate and the corresponding circular arc of the circular groove in the base-plate must lie in parallel planes. This requirement is realized when the head-plate (when attached to the cross-head of the testing machine) and the base-plate (when attached to the platten of the testing machine) are parallel. Secondly, these two arcs must lie in a common circular cylindrical surface that is perpendicular to the base-plate (and, hence, perpendicular to the head-plate).

Parallelism of the head-plate and the base-plate was assessed using the device shown in Figure 6. This device consists of a rigid base that was machined to fit snugly in the circular groove of the base-plate, and that could be moved smoothly along the groove. A dial indicator was attached to a stiff steel rod which was affixed to

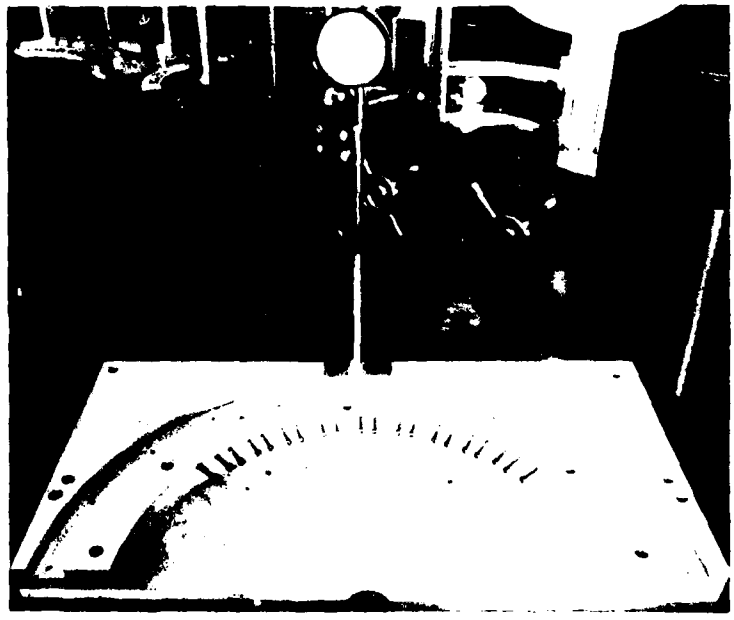

FIGURE 6. Device used to establish the relative parallelism of the head-plate and the base-plate of the testing fixture.

the moveable base. With the plunger of the dial indicator resting against the surface of the circular groove in the head-plate, the device was moved along the circular groove in the base-plate. Using the centerline of the circular groove as a reference, it was observed that the variation in the distance between the surfaces of the grooves in the head-plate and the base-plate did not exceed 0.0035 in. on either side of the centerline for the maximum arc of 18.5 in. (circumferential arc length of the widest specimen). This variation was accordingly smaller for narrower specimens. Once the head-plate and the base-plate had been assessed to be as parallel as reasonable efforts would allow, they were securely clamped to the crosshead and to the platten of the Tinius-Olsen testing machine by specially designed clamps. These clamps can be seen in Figure 5.

The imperfection device was used to bring corresponding circular arcs in the head-plate and in the base-plate into concentricity. To accomplish this alignment the platform of the imperfection measuring device was positioned at an appropriate level and the tip of the dial indicator extension shown in Figure 4 was allowed to rest against the vertical side of the circular groove in the head-plate. Since the groove in the platform of the imperfection measuring device is concentric with the vertical edge of the circular groove in the base-plate, the corresponding edge of the circular groove in the head-plate will be concentric with its counterpart in the base-plate when the pointer of the dial indicator is undisturbed as the indicator mechanism is moved smoothly along the platform groove. Thus, appropriate alignment of the head-plate and the base-plate of the testing fixture was accomplished.

(11-6). SPECIMEN INSTALLATION. The procedure used to install specimens in the testing fixture was similar for specimens with unsupported straight edges and for specimens with simply-supported straight edges. It is convenient to describe the installation procedure for the specimens with unsupported straight edges first, and, subsequently, describe the additional installation features associated with the specimens for which the straight edges were simply-supported. In either case the curved edges of all specimens were clamped.

In preparation for buckling tests of specimens with unsupported straight edges, a specimen was centered in the circular groove of the base-plate of the testing fixture and the pressure blocks were adjusted by finger tightening appropriate screws. The platten of the testing machine was then raised to allow the upper curved edge of the specimen to enter the circular groove of the head-plate to approximately three-quarters of the groove depth. Pressure blocks in the head-plate were then adjusted by finger tightening appropriate screws in the head-plate. Generators at several locations along the circumference of a specimen were aligned vertically with a precision square. The platten of the testing machine was then raised until the specimen experienced a compressive force of 25 lb. Pressure blocks in the base-plate and in the head-plate were adjusted to their final positions by applying a 40 in-lb torque to appropriate screws while the 25 lb pre-load was maintained.

Preparation for buckling tests of specimens with a simply-supported straight edges was similar to that for specimens with unsupported straight edges. A specimen was centered in the circular groove of the base-plate and its straight edges were inserted in the slots of the vertical edge supports (hence forth referred to as book-ends) as shown in Figure 7.

Pressure blocks in the base-plate and at each book-end were adjusted to the finger tight position. The platten of the testing machine was then raised to allow the upper curved edge of the specimen to enter the circular groove of the head-plate to approximately three-quarters of the groove depth. Pressure blocks in the head-plate were then adjusted to the finger tight position. Generators at several locations along the circumference of the specimen were aligned vertically with a precision square. The platten of the testing machine was then raised until the specimen experienced a compressive force of 50 lb. Pressure blocks in the base-plate and in the head-plate were adjusted to the 40 in-lb position, and the vertical pressure blocks in the book-ends (see Figure 8) were adjusted to the finger tight position for specimens of Program A.

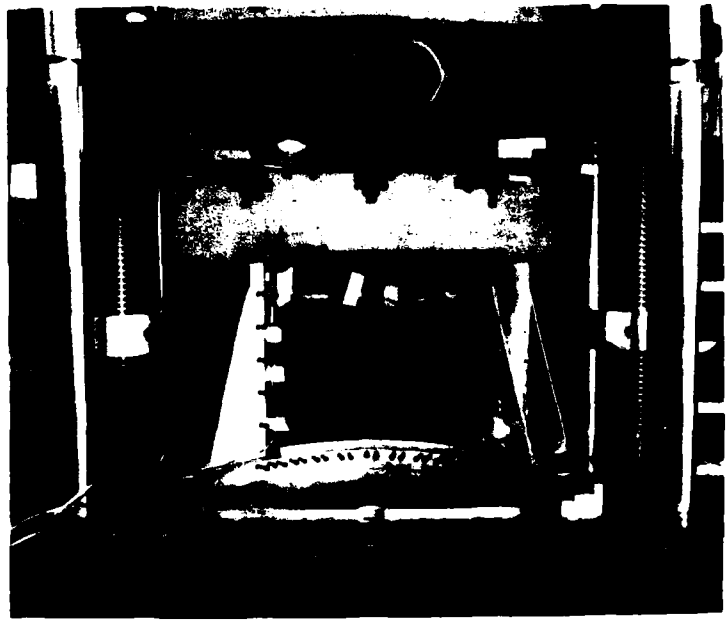

FIGURE 7. Test specimen installed in the base-plate and book-ends that supply simply-supported edge conditions.

For Program B the pressure exerted on the specimen by the vertical pressure blocks was adjusted to different amounts.

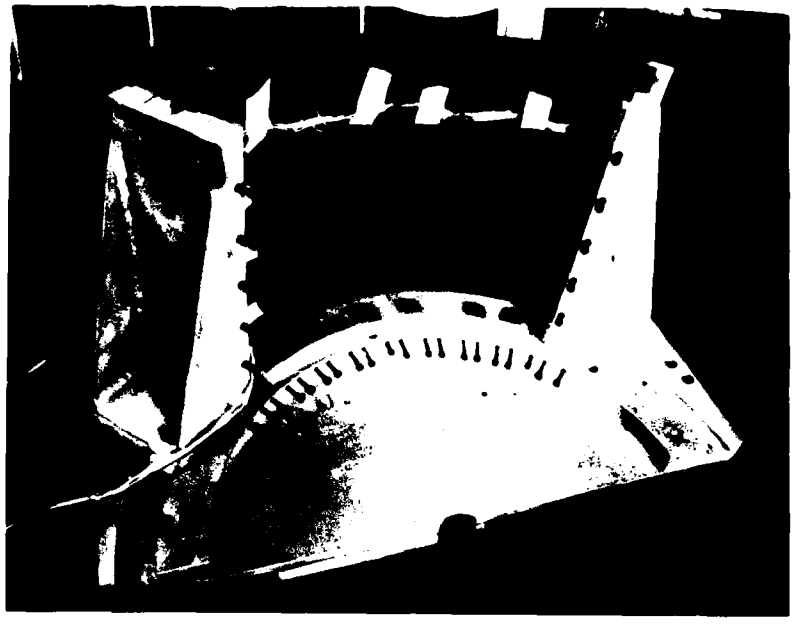

FIGURE 8. Simply-supported edge of a test specimen showing vertical pressure blocks.

SECTION III

EXPERIMENTAL DATA

(III-1). INITIAL GEOMETRICAL IMPERFECTIONS. Initial deviations of a specimen from a perfect cylindrical surface are referred to in this report as initial geometric imperfections. Imperfection measurements were obtained at the nodes of a rectangular grid drawn on the inner surface of a specimen. Details of the imperfection grids for specimens with different aspect ratios are listed in Appendices A and B for specimens with simply-supported straight edges and unsupported straight edges, respectively. This data corresponds to testing Program A. Details of the imperfection grids used in testing Program B are listed in Appendix C.

For testing Program A, the reference point for imperfection measurements lies on the specimen centerline two inches below the upper clamped edge. Measurements were made at equal intervals on either side of the specimen centerline, and at equal intervals along the generators of a specimen. Measurements for specimens with unsupported edges were obtained along these edges, while measurements for specimens with simply-supported edges were obtained as close to the straight edges as the imperfection measuring device would permit. These observations are reflected in the imperfection data contained in Appendices A and B. Actual spacing dimensions for the imperfection grid associated with each panel aspect ratio are shown in these appendices also.

For testing Program B a specially constructed device, with two circular members that were concentric with the groove in base-plate, was used to establish the reference point for imperfection measurements. Measurements for imperfections were made at the locations described for Program A.

Actual spacing dimensions for imperfection grids associated with panels with unsupported straight edges and simply-supported straight edges are indicated in Appendix C. The imperfection measurements for Program B are also presented in Appendix C.

(III-2). STRAIN MEASUREMENTS. It was of interest to determine if the axial compressive end-load was applied uniformly along the curved edges of a specimen.

Program A. For testing Program A, axial strains were measured along an arc lying one inch below the upper clamped edge on the specimen centerline and at two other equally spaced points on both sides of the centerline. Electrical resistance strain gages were bonded at identical locations on both sides of a specimen so that, by means of an appropriate four-arm bridge, only axial strains were sensed. Locations of the strain gages on the surface nearest the center of curvature of a specimen can be observed in Figure 7. Appendices A and B contain details for strain gage locations for Program A.

Program B. For testing Program B, axial strains were measured at the five locations described in Program A for specimens with unsupported edges. Axial strains were measured at only three locations for specimens with simply-supported edges: on the centerline and at two points symmetrically located relative to the centerline. Appendix C contains details for strain gage locations for Program B.

Strain gage readings were obtained using a Vishay/Ellis-20 digital strain indicator and a Vishay-Ellis-21 ten channel switching and balancing unit. This equipment is shown in Figure 9. Strain data associated with

testing Program A are presented in Appendix A for specimens with simply-supported straight edges, and in Appendix B for specimens with unsupported straight edges. Strain data associated with testing Program B are presented in Appendix C.

FIGURE 9. Simply-supported specimen partially installed in the testing fixture and associated strain measuring equipment.

The strain data indicates that the distribution of force on the curved edge of a specimen is essentially uniform in the very early stages of the loading process, but quickly becomes nonuniform. These observations remain valid for all specimens in each testing program.

Consider specimens with unsupported straight edges. As was stated previously, specimens were not perfectly circular cylindrical as they emerged from the mold. Consequently, installation in the testing fixture caused regions near the ends to assume a circular cylindrical shape of radius 12 inches, while cross sections away from the ends assumed noncircular shapes with the unsupported edges "dishing" toward the center of curvature. Generally, the centerline and generators in the regions on either side of the centerline were straighter than generators near the edges. Since the axial stiffness of a small strip of specimen parallel to a generator depends on

its flexural stiffness as well as its in-plane stiffness, the strains associated with strips located at various sites on a specimen should be expected to be different. Indeed, the non-uniformity of the strain distribution should be expected to be intensified as the loading process proceeds. It is noted, from the strain data for specimens with unsupported straight edges in Appendix B, that the strains near the straight edges actually changed from compression to tension during the early stages of loading. This reversal of strain near the straight edges is associated with the bifurcation load for the specimen under an essentially uniform end-load (as opposed to uniform end-displacement). A more detailed discussion of this behavior is presented in a later section.

Now consider specimens with simply-supported straight edges. These specimens experienced the same "dishing" effects as specimens with unsupported straight edges; however, the book-ends forced the edges to become straight with the consequent configuration change on the interior of a specimen. Accordingly, since these initial installed configurations occur in an essentially random manner, nonuniform strain distributions should be expected during the loading process.

Another possible reason for the nonuniform strain distributions exhibited by specimens with simply-supported edges is the asymmetry in the axial displacements that can be introduced at the book-ends. The strain distribution on the interior of a specimen will deviate from uniformity if the axial displacement distributions along the two simply-supported edges differ.

The further observation should be made that not only do the initial imperfections influence the buckling resistance of a specimen, but a certain unknown initial stress distribution is associated with the installed initial configuration that also influences the buckling resistance. The influence of the

initial stress distribution on the buckling resistance is rather capricious. The initial geometric imperfections that are incorporated in CLAPP assume that the imperfect configuration is stress free.

(III-3). END-SHORTENING. The end-shortening of each specimen in testing Programs A and B was measured with a dial indicator that was positioned so as to determine the relative displacement between the platten and the cross-head of the Tinius-Olsen testing machine. The axial compressive load applied to the specimen was read directly from the testing machine. Load and corresponding end-shortening data are listed in Appendices A and B for specimens of testing Program A and in Appendix C for specimens of testing Program B.

(III-4). BUCKLING BEHAVIORS. Experimental buckling loads for the 40 specimens associated with testing Program A are listed in column 7 of Table 1 and those associated with the 10 specimens of testing Program B are listed in column 5 of Table 2. The recorded experimental buckling load for each specimen of either testing program was characterized by a distinct loss in load carrying capacity. Loss of load carrying capacity was detected readily from the load-dial of the Tinius-Olsen hydraulic testing machine, and was always accompanied by a sudden shift in the equilibrium configuration of the specimen that was clearly audible and visible.

SECTION IV

EXPERIMENTAL AND NUMERICAL RESULTS

(IV-1). ANALYSIS OF RESULTS OF TESTING PROGRAM A. The theoretical buckling loads shown in column 8 of Table 1 were calculated assuming that each panel was subjected to a force that was uniformly applied along its curved edge. The bifurcation branch of CLAPP was used to calculate these buckling loads. Consequently, the theoretical buckling loads listed in Table 1 correspond to bifurcation under a uniformly applied axial compression using both a 12 x 12 and a 20 x 12 finite difference grid. For this bifurcation analysis the 20 x 12 grid yielded a bifurcation load less than three percent smaller than the 12 x 12 grid. Nevertheless, numerical calculations for the bifurcation load for each of the remaining specimens were obtained using either a 20 x 12 or a 16 x 12 finite difference grid. The clamped boundary condition along a curved edge of a specimen requires the transverse displacements be zero along a line of nodal points coincident with the curved boundary and along a parallel line of nodal points just inside the boundary. The larger number of grid points was always taken along the generators of a specimen to minimize this internal constraint.

SPECIMENS WITH SIMPLY-SUPPORTED STRAIGHT EDGES. Table 1 shows that the bifurcation load predicted by CLAPP was greater than its corresponding set of experimental buckling loads except for one specimen. The ratio of the modified experimental load to the numerical bifurcation load is shown in the last column of Table 1 for each specimen. The modified experimental buckling load was obtained by assuming that the observed experimental buckling load was uniformly distributed along the curved edge of a specimen and only the portion

of the curved edge between the book-ends contributed to the buckling of a specimen.

The ratio of the modified experimental buckling load to the theoretical bifurcation load fell in the range $0.5 < \rho < 1.0$ for eighteen of the twenty specimens with simply-supported straight edges. The ratio was 0.458 for one specimen and 1.072 for another. We remark that theoretical bifurcation loads predicted by the energy method represent upper bounds to the classical bifurcation loads associated with the test specimens. Moreover, in the presence of initial geometric imperfections the experimental buckling loads can be expected to be less than the classical bifurcation load if the specimen is imperfection sensitive. If a specimen is not sensitive to initial imperfections its experimental buckling load can be expected to compare favorably with the theoretical bifurcation load.

Another complicating factor is the nature of the simply-supported boundary condition. Actually two different types of the simply-supported boundary conditions must be recognized. Normally, a simply-supported boundary condition implies the bending moment and transverse displacement are zero. In addition to these conditions, in-plane displacements or membrane forces must be specified. Consequently, with reference to the simply-supported test specimens, circumferential displacement can be prevented, can be allowed to occur freely, or, there can be some intermediate partial restriction of circumferential displacements. The theoretical bifurcation loads listed in Table I correspond to freely occurring circumferential displacements along the straight edges.

The foregoing observations are offered in explanation of the rather large difference between the experimental buckling load and the theoretical bifurcation load for some test specimens and the much better agreement

between the two loads for other specimens. The ratio 1.072 for one test specimen is believed to be a quirk arising out of the way the modified experimental buckling load is defined.

Figure 10 shows the experimental and numerical load versus end-shortening curves for a 16 in. x 16 in. panel with simply-supported straight edges. The numerical load vs end-shortening curve was obtained using measured initial imperfections. A plot of the normalized buckling determinant is also shown in the figure. We note that the numerical curve is essentially linear even though initial imperfections are present. Furthermore, the panel buckled apparently by bifurcation as indicated by the system buckling determinant becoming negative.

CLAPP was modified to provide the capability of prescribing uniform end displacements as opposed to prescribing uniform end load.

Figure 11 shows the experimental and theoretical load versus end-shortening curves for the 16 in. x 8 in. specimen with the $[0/90]_{2s}$ fiber pattern. The theoretical bifurcation loads for conceptual models with simply-supported edges are 2522 lb when circumferential displacements occur freely, and 4311 lb when circumferential displacements are prevented at the straight edges. The experimental buckling loads for the two test specimens are 2500 lb and 3240 lb.

There is, perhaps, better agreement between the theoretical bifurcation loads and the experimental buckling loads than is immediately obvious. Consider the experimental curve labeled 1 in Figure 11. The unusual shape of this load versus end-shortening curve appears to be the result of the panel slipping circumferentially in the book-ends at a load near 300 lb. In this test it becomes clear that the friction forces exerted by the vertical

pressure blocks on the specimen was not sufficient to prevent circumferential displacements. Consequently, at approximately 300 lb the book-ends allowed circumferential displacements to commence. However, the specimen edges apparently made contact with back surfaces of the book-ends and circumferential displacements were prevented from approximately 1500 lb onward. One expects the experimental buckling load for this specimen to fall between the two theoretical bifurcation loads.

The behavior exhibited by the experimental curve labeled 2 in Figure 11 can be explained in a similar manner. Initially the friction forces exerted by the vertical pressure blocks on the specimen is sufficient to prevent circumferential displacements. At a load of approximately 800 lb a gradual slippage occurs and, finally at a load of approximately 2250 lb the friction forces were not sufficient to prevent or restrict these displacements any longer. A sudden slippage occurred that resulted in the buckling of the specimen before its straight edges made contact with the back surfaces of the book-ends. Accordingly, one expects the experimental buckling load for this specimen to agree closely with the theoretical bifurcation load corresponding to the simple-support condition when circumferential displacements occur freely.

The experimental strain distribution shown in Figure 12 shows an encouraging resemblance to the calculated nodal load distribution shown in Figure 13.

SPECIMENS WITH UNSUPPORTED STRAIGHT EDGES. Table 1 shows that the bifurcation load predicted by CLAPP was less than its corresponding set of experimental loads for every specimen. This unexpected behavior can be explained as follows. Because the radius of a specimen was less than 12.0 in,

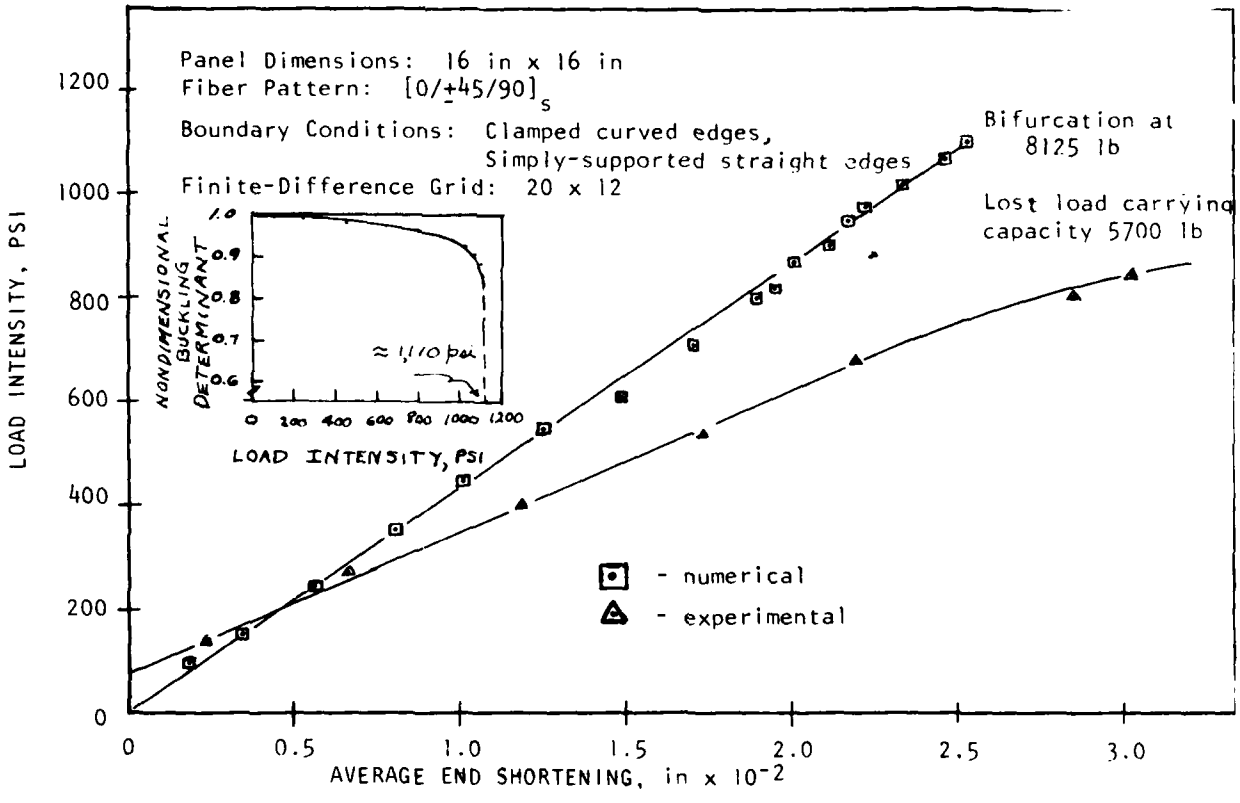

FIGURE 10. Numerical and experimental load versus end-shortening curves for a 16 in x 16 in panel with simply-supported straight edges.

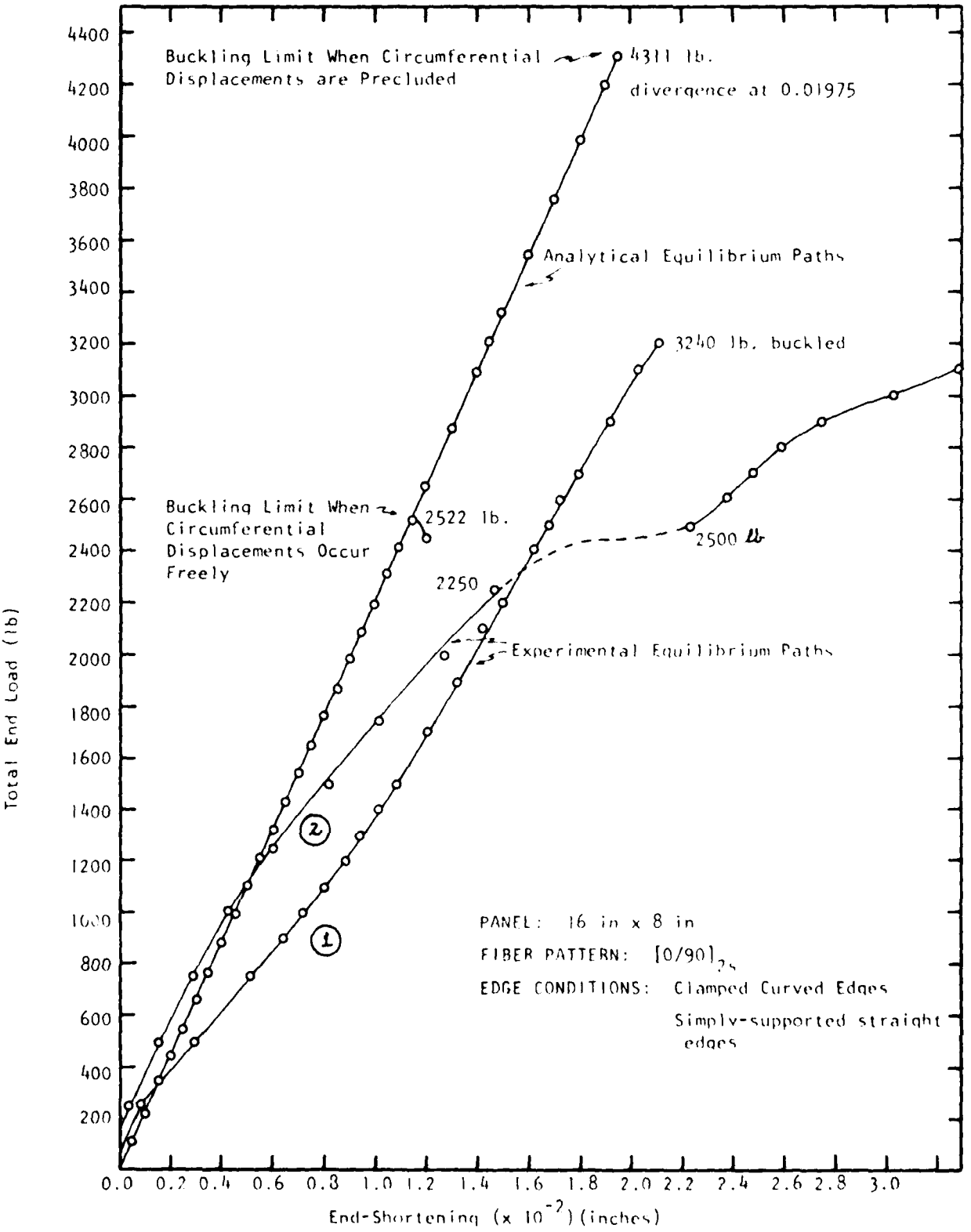

FIGURE 11. Analytical and experimental load vs. end-shortening curves for panels with simply-supported straight edges.

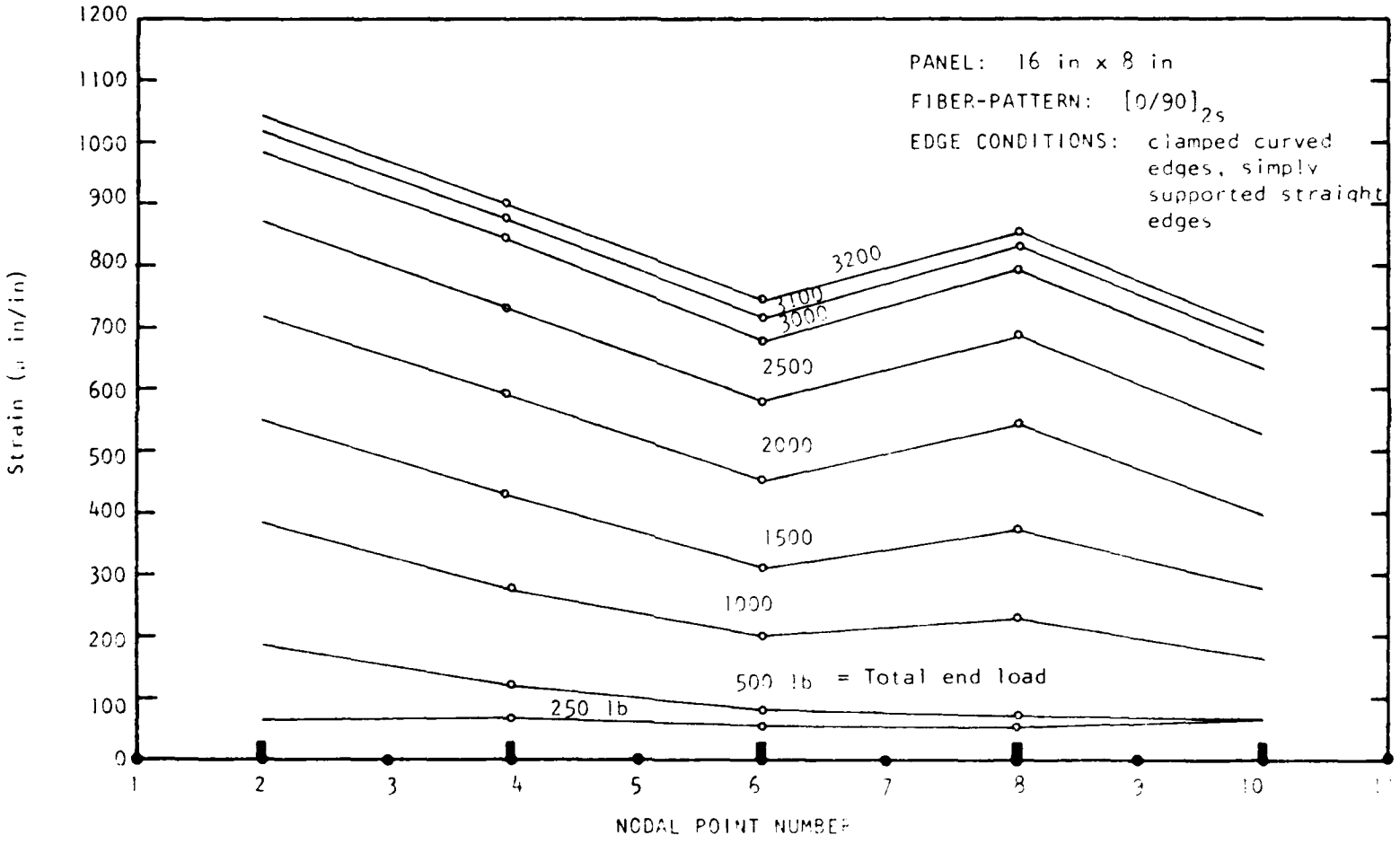

FIGURE 12. Experimental strains corresponding to prescribed values of end-displacement [illegible] with simply supported straight edges and constrained circumferential [illegible]

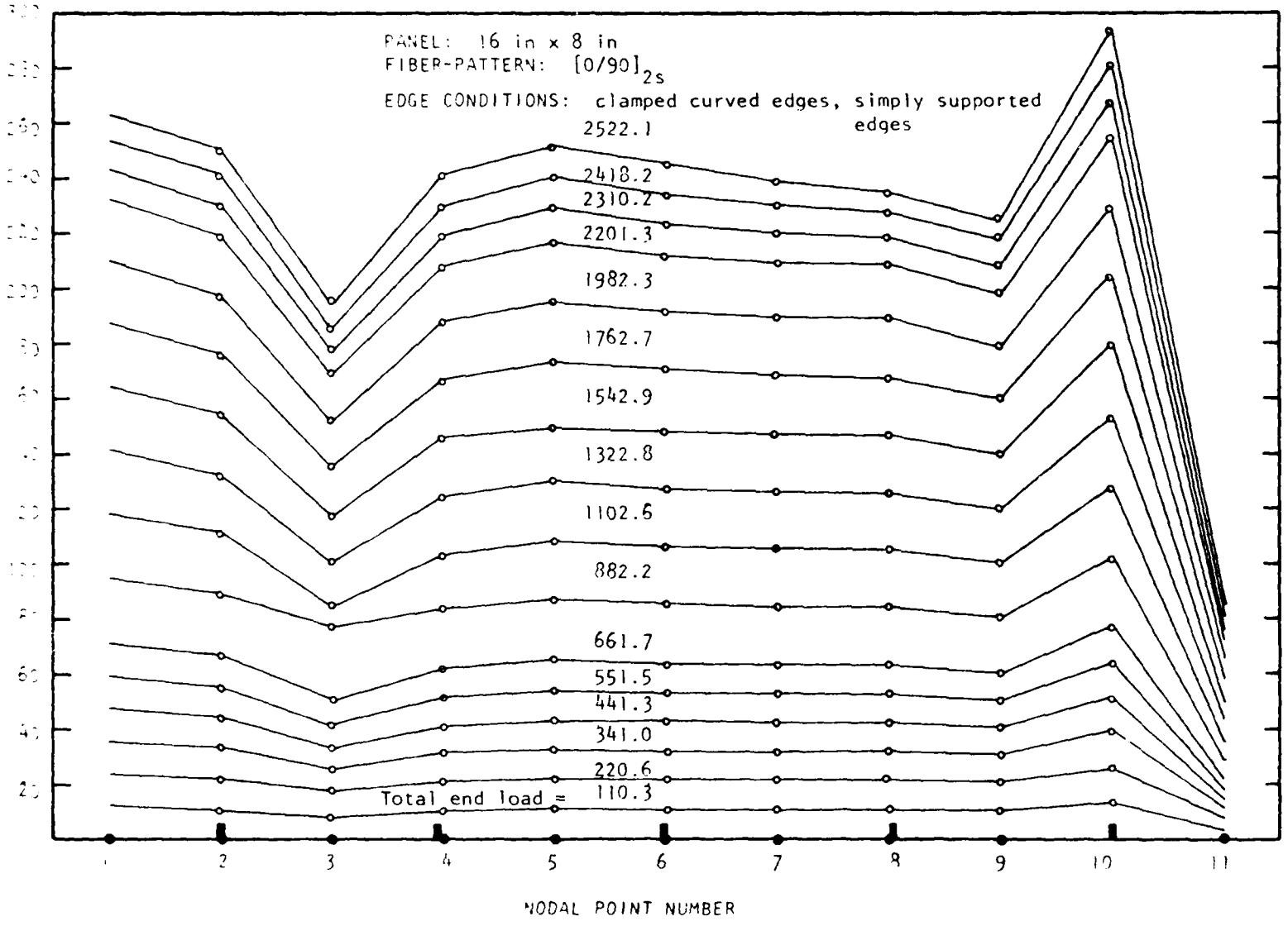

FIGURE 13 Analytical nodal loads corresponding to prescribed values of end-shortening for a specimen with simply supported straight edges with constrained circumferential displacements.

distortions of the straight edges of a specimen occurred upon clamping its curved edges in the testing fixture. The experiment buckling load is believed to correspond to a limit point load that is greater than the bifurcation load for a perfectly cylindrical geometry. In other words, the initial distortion of the straight edges of a specimen prevents an experimental detection of a bifurcation load corresponding to a wrinkling of these edges for a perfect cylindrical geometry under a uniformly distributed edge compression.

We remark that the bifurcation loads predicted by CLAPP correspond to cylindrical specimens without initial imperfections under forces that are uniformly distributed along the curved edges. It is important to note that axial and circumferential displacements along the curved edges are not specified. Consequently, theory predicts a specimen will collapse at the bifurcation load.

The experimental model is clamped tightly in the head-plate and in the base-plate so that circumferential displacements along the curved edges are prevented. More importantly, axial deformations are restricted by the relative movement of the cross-head and the platten of the testing machine. Consequently, when the straight edges buckle the testing fixture prevents the collapse that theory predicts for the specimen under uniform load. As a result of the clamp conditions the specimen retains significant load carrying capacity. In fact, the experimental buckling loads correspond to limit points in the post buckled region.

A close inspection of the strain data indicates the strain at the straight edges changed sign at loads that are in the appropriate neighborhoods of the theoretical bifurcation loads. The sign change on the edge

strains corresponds to the observed severe distortion of the straight edges of a specimen. The load levels at which the sign change occurred depended on the initial imperfection in the specimen.

CLAPP was modified so that the buckling behavior of specimens under prescribed uniform end-displacements could be studied.

Figure 14 shows the experimental equilibrium paths for the 16 in. x 8 in. specimens with the $[0/90]_{2s}$ fiber pattern. It also shows equilibrium paths predicted by CLAPP for initial imperfections of the form $W_o(x,y) = WI(1+\cos\pi x/2a)$ for amplitudes WI = 0.0, +0.005, and -0.010. The limit point buckling loads discussed previously are clearly evident. The ratios of the experimental buckling loads to the theoretical limit load for a perfectly cylindrical specimen are 0.85 and 0.83. The ratios of the experimental buckling loads to the theoretical limit load for an initial imperfection of amplitude 0.005 are 0.93 and 0.91. Even better agreement is expected for the exact imperfection distributions.

Figure 15 shows the strain distribution at various load levels for the specimen discussed in the previous paragraph. Evidently, the force applied to the curved edges of the specimen was uniform during the early stages of the loading process; that is, during the initial increments of prescribed end-displacements. Accordingly, the bifurcation load predicted by CLAPP for a uniformly applied end-load should agree qualitatively with the load at which the sign change occurred for the edge strains. The theoretical bifurcation load from Table 1 is 476 lb and the load at which the axial edge strain ceased to increase was near 600 lb.

Figure 16 shows the nodal forces predicted by CLAPP for the same specimen distribution. During the initial increments of prescribed end-

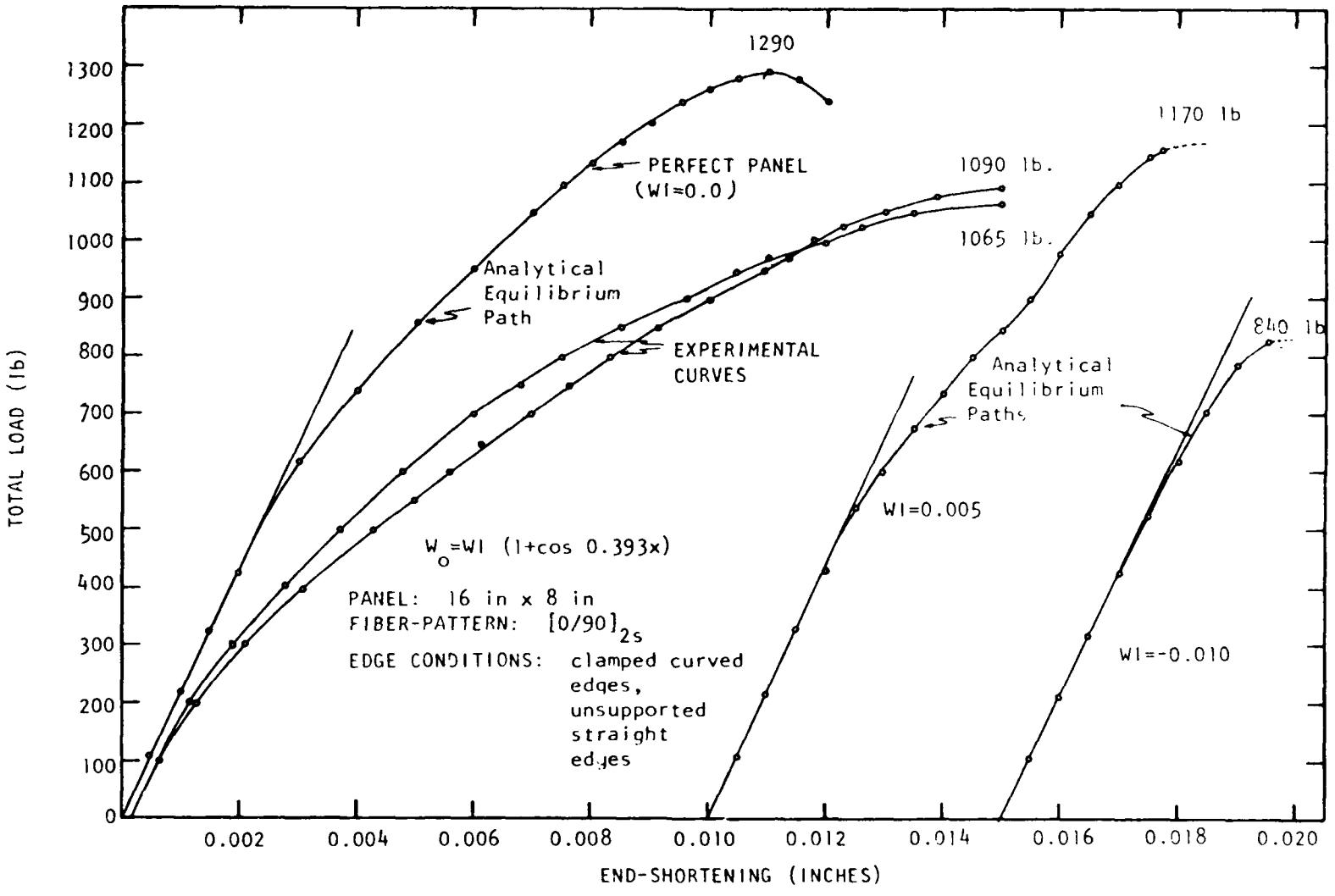

FIGURE 14. Analytical and experimental load vs end-shortening curves for the perfect and the imperfect panel with unsupported straight edges.

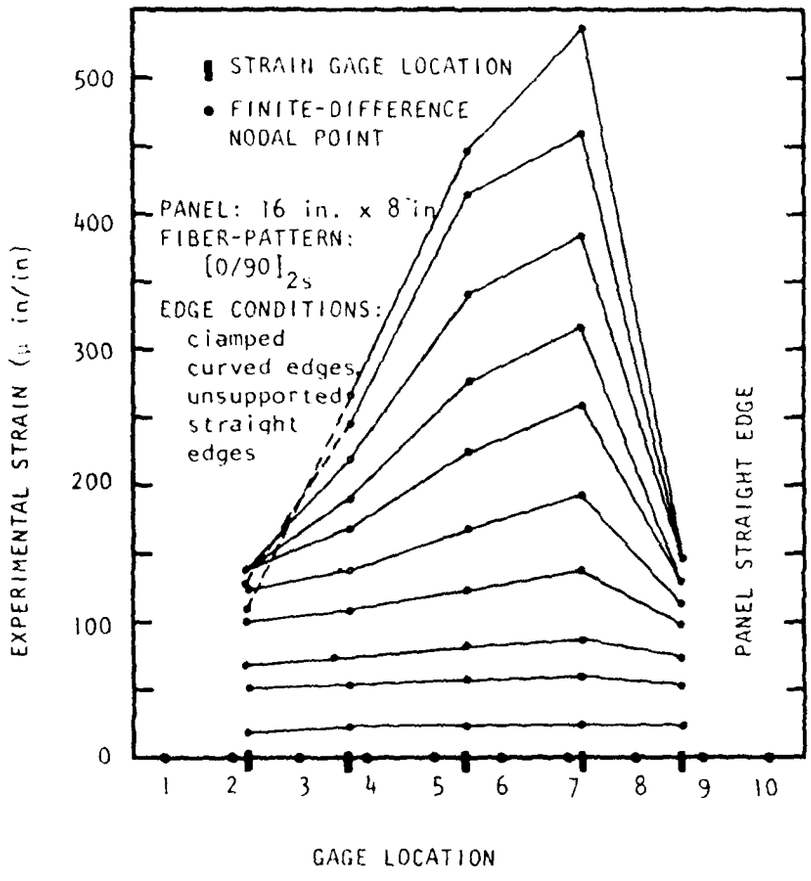

FIGURE 15. Experimental strains corresponding to prescribed values of end-shortening for test specimens with unsupported straight edges.

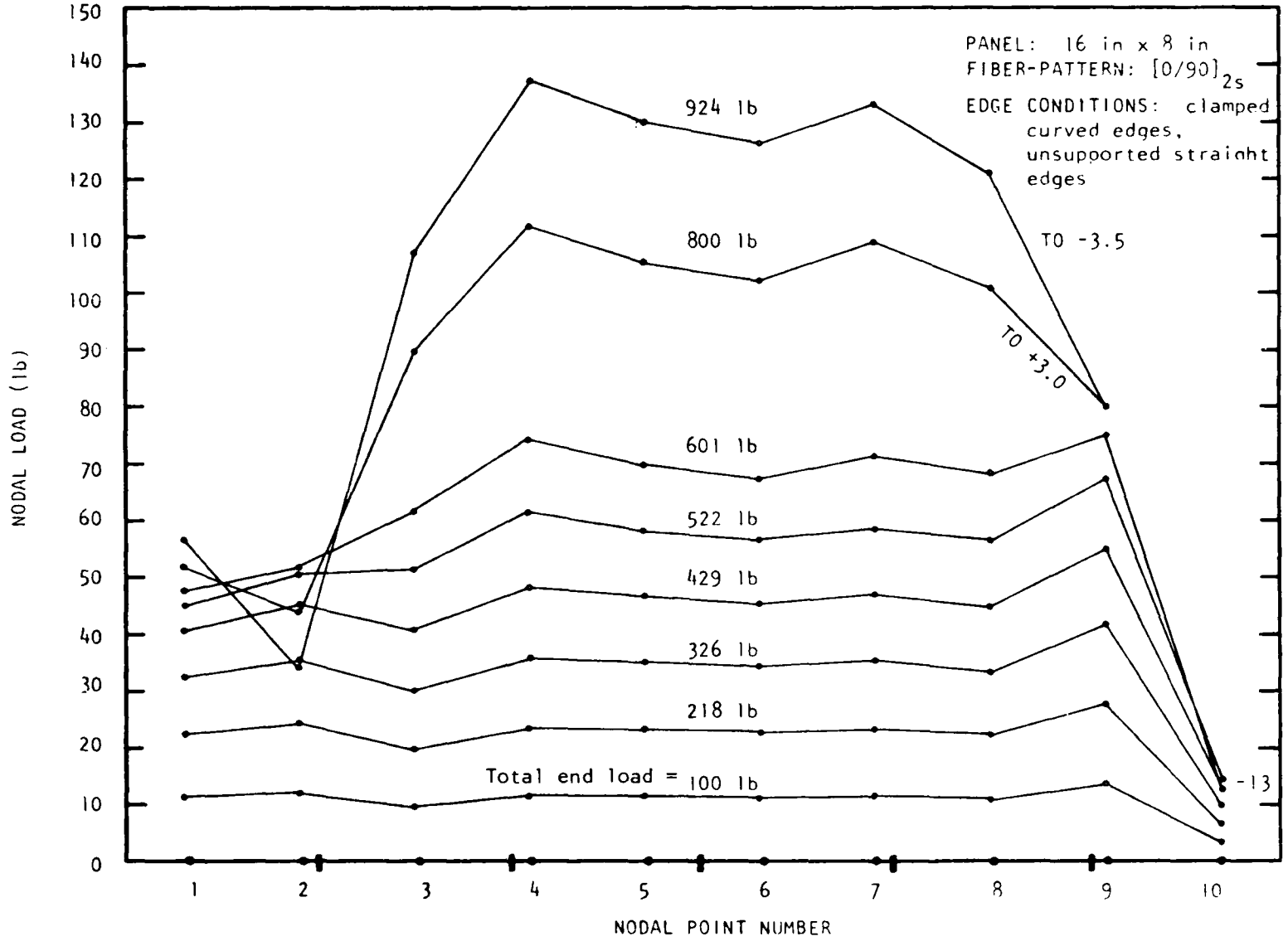

FIGURE 16. Analytical nodal loads corresponding to prescribed values of end-shortening for an initial imperfection of the form $W_o = 0.005 (1 + \cos \pi\xi/a)$ for specimens with unsupported straight edges.

displacements the strain distributions and the nodal force distributions are nearly uniform. These distributions become nonuniform as the loading process continues; however, there is a visible agreement between the experimental strain distribution and the calculated nodal load distribution for all levels of prescribed end-displacements.

(IV-2). ANALYSIS OF RESULTS OF TESTING PROGRAM B. The theoretical buckling loads shown in column 6 of Table 2 were calculated assuming that each panel was subjected to prescribed end-displacements that were uniform along the curved edges. Calculations were made for 16 x 11 and 20 x 11 finite-difference grids to check the convergence of the numerical process.

SPECIMENS WITH SIMPLY-SUPPORTED EDGES. The experimental equilibrium paths for five 16 in. x 12.83 in. specimens with the $[0/\pm45/90]_s$ fiber pattern and simply-supported straight edges are shown in Figure 17. The load at which each specimen buckled is marked on the graph beside the corresponding equilibrium path. The theoretical equilibrium path is also shown in the same figure for the perfect panel and for an initial imperfection amplitude of -0.010 in. The two paths essentially coincide except that their termination points (buckling loads) are different (8064 and 6608 lb. for the perfect and imperfect panels, respectively). These buckling loads correspond to a 16 x 11 finite-difference grid. A 20 x 11 finite-difference grid was also used to calculate the buckling loads for the same perfect and imperfect panels. The equilibrium paths in this case were indistinguishable from those obtained using the 16 x 11 finite-difference grid except that their termination points (buckling loads) are somewhat less (6950 and 5622 lb. for the perfect and imperfect panels, respectively) than those associated with the 16 x 11 finite-difference grid.

Figure 18 shows theoretical equilibrium paths for the perfect panel and the imperfect panel (WI = -0.010 in.) where, instead of using end-displacement as a measure of the system displacement, the norm of the transverse displacements is used. These curves exhibit more clearly the nonlinear character of the equilibrium path. These curves correspond to the 20 x 11 finite-difference grid. Also note the mathematical form of the geometric initial imperfection shown on the same figure.

The theoretical buckling load was detected numerically as a change in the system buckling determinant from positive to negative. This indicates that the simply-supported panel experienced bifurcation buckling. A plot of the normalized buckling determinant versus total end load for an initial imperfection amplitude of -0.010 in. is shown in the upper left hand corner of Figure 18.

The initial imperfection amplitude corresponds to a radial deviation from a perfect cylinder of 0.020 inches at the geometric center of the panel, which is approximately equal to one half the panel thickness. This is a rather large initial imperfection. The magnitudes of the measured initial imperfections were frequently larger than 0.020; however, the distribution of the imperfections were different. Generally, the largest imperfections occurred near the edges of a specimen with somewhat smaller ones occurring near the centerline.

The 16 x 11 and 20 x 11 finite-difference grids gave 8064 lb and 6950 lb as the bifurcation loads for the perfect panel. That is, the 20 x 11 grid predicted a bifurcation load 13.8% lower than the 16 x 11 grid. Further improvement in the theoretical buckling load is expected with a further refinement in the finite-difference grid. CLAPP is presently dimensioned to

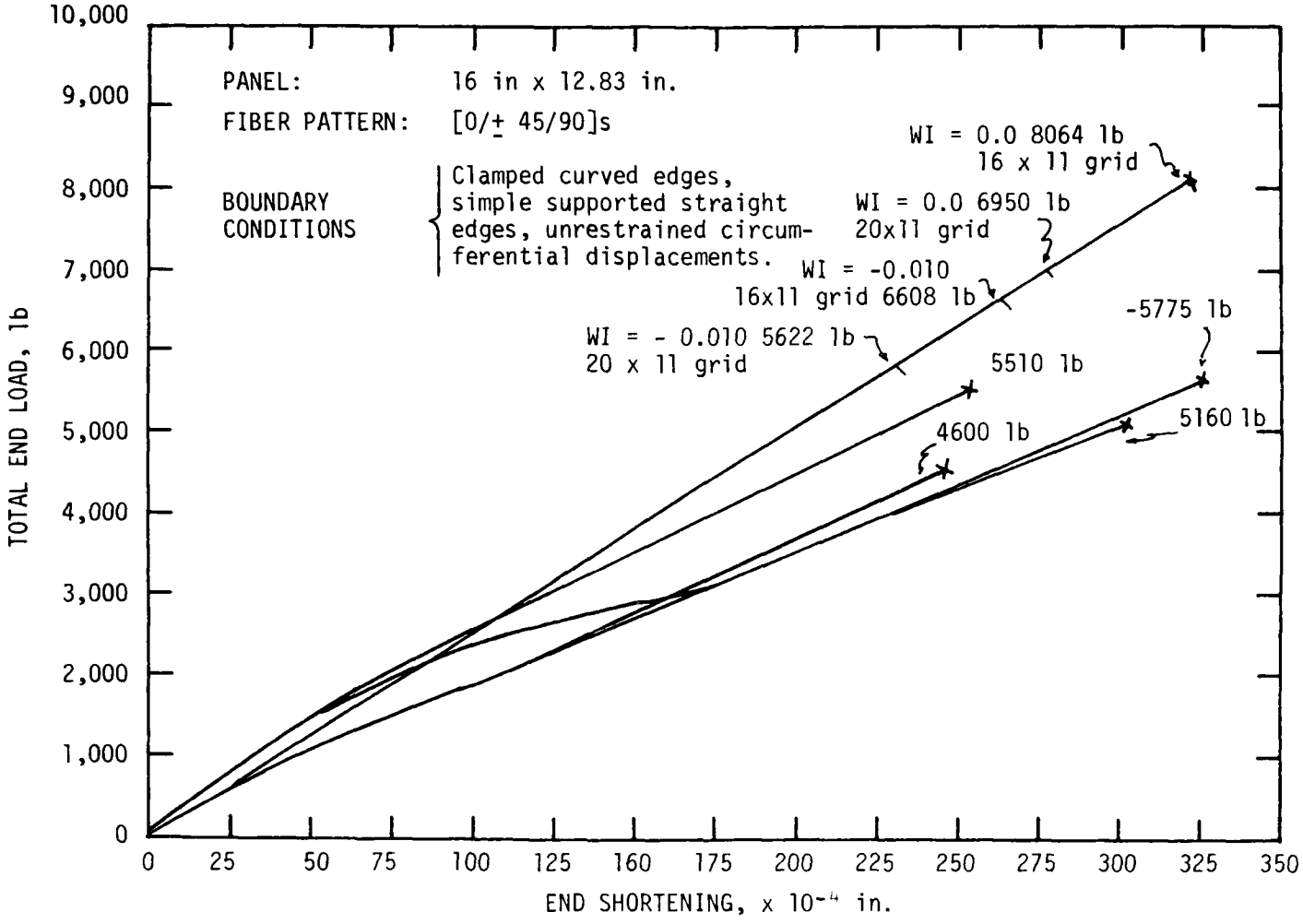

Figure 17. Theoretical and experimental equilibrium paths for simply-supported test specimens for testing Program B.

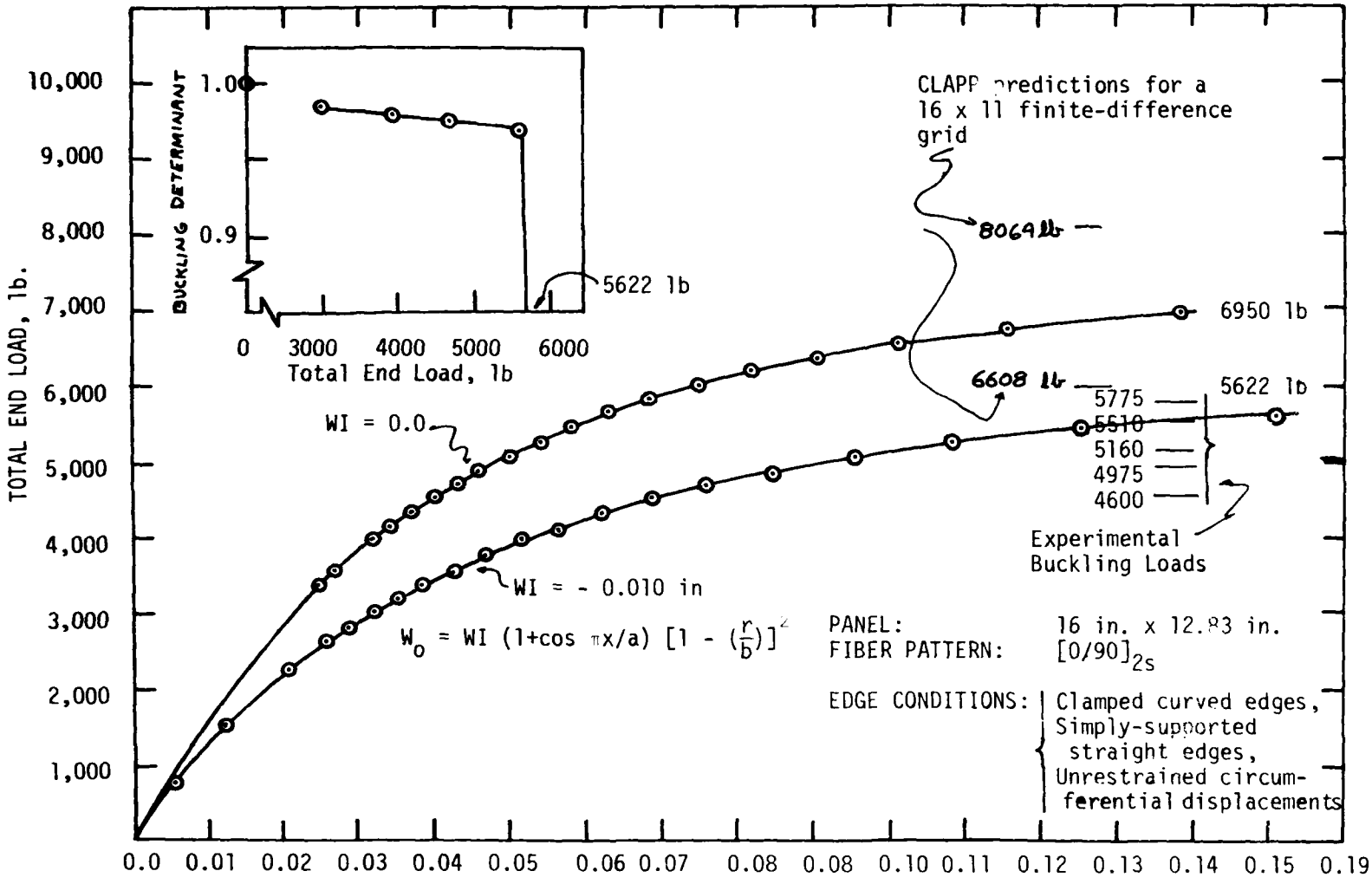

Figure 18. Analytical load versus deflection curves for the perfect and imperfect panel with simply supported straight edges and unconstrained circumferential displacements.

handle a maximum 20 x 12 finite-difference grid, so that further refinements were not undertaken in this investigation.

The 16 x 11 and 20 x 11 finite-difference grids predicted bifurcation loads of 6608 and 5622 lb for the imperfect panel (WI - -0.010 in.). Thus, the 20 x 11 grid predicted a bifurcation load 14.9% lower than the 16 x 11 grid for the imperfect panel. Again, improvement in the theoretical buckling load for the imperfect panel can be expected for a more refined finite-difference grid.

Figure 18 shows that the experimental buckling loads are not grossly misrepresented by the buckling load predicted by the 20 x 11 grid for the imperfect panel. Based on the buckling load predicted by the 20 x 11 grid for the perfect panel (6950 lb) the ratios of the experimental to the theoretical buckling load for the five specimens are 0.831, 0.793, 0.741, 0.716, and 0.668. The last ratio really should not be counted because this specimen had been tested previously with very loose straight edges. Based on the buckling load predicted by 20 x 11 grid for imperfect panel (5622 lb) these ratios become 1.03, 0.980, 0.918, 0.885, and 0.818.

The theoretical curves, and thus the theoretical buckling loads, upon which the foregoing ratios are based correspond to simply-supported straight edges for which circumferential displacements are unrestrained. It is impossible to be certain of the nature of the boundary condition along the straight edges of the test specimens. As an example of the uncertainty of the type of boundary condition that existed along the straight edges of a test specimen consider the test specimen for which the experimental buckling load was found to be 5775 lb, the largest of the buckling loads of the five specimens. For this test the shoulders of the vertical pressure blocks

were filed to a rounded configuration so that the blocks contacted the specimen along a straight line. In the other tests these contacting surfaces were flat and tended to bend the panel when the pressure was applied. The former, it is expected, allowed a more freely occurring rotation at the edge for which the corresponding buckling load should be expected to be less than that for the latter case. As can be seen this was not the case. All this suggests that the edge conditions at the straight edges of the test panel are uncertain.

It is felt that the conditions along the straight edges of the test specimens is the principal source of the difference exhibited between the experimental and theoretical buckling loads. It is also felt the CLAPP is much less at fault for the difference referred to.

It should also be noted that any pressure exerted by the vertical pressure blocks on the panel tends to retard the free occurrence of axial displacements along the straight edges. This could give rise to shearing stresses in the panel which would lead to lower axial buckling loads. Finally, the clamping mechanism prevents circumferential displacements from occurring freely along the curved edges. This could cause local distortions near the curved edges that could lead to lower buckling loads. The model for which the theoretical buckling loads were computed assumed that axial displacements along the straight edges and circumferential displacements along the curved edges are unimpeded.

SPECIMENS WITH UNSUPPORTED STRAIGHT EDGES. The experimental equilibrium paths for six 16 in. x 12.83 in. specimen with the $[0/90]_{2s}$ fiber pattern and unsupported straight edges are shown in Figure 19. The load at which each specimen buckled is marked on the graph beside the corresponding

equilibrium path. The theoretical equilibrium path is also shown in the same figure for initial imperfection amplitudes of -0.0025 and -0.005. As was the case for specimens with simply-supported straight edges, the theoretical equilibrium paths for the 16 x 11 finite-difference grid essentially coincide for initial imperfection amplitudes of -0.0025, -0.0050, and -0.010 in. Moreover, the buckling loads corresponding to these initial imperfection amplitudes differed only slightly, as can be seen from Figure 20. The equilibrium path corresponding to a 20 x 11 finite-difference grid differs only slightly from that corresponding to a 16 x 11 grid. The buckling loads for the 16 x 11 and 20 x 11 grids for an initial imperfection amplitude of -0.01 in. are 3416 and 3320 lb, respectively. In this case the refined finite-difference grid did not influence the buckling load nearly as much as it influenced the buckling loads for the simply-supported panel.

The experimental equilibrium paths depicted in Figure 19 indicate that the stiffness of each test specimen changes noticeably in the load range 400-1000 lb. This change in stiffness coincides also with the observed reversal of the axial strains at the straight edges of the test specimens. Consequently, it is believed that this change in stiffness signifies the load-level at which the straight edges of a specimen lost their capability to resist greater axial loads.

The theoretical equilibrium paths shown in Figure 20 for various initial imperfection amplitudes reveal that a bifurcation occurs at approximately 1134 lb for a perfect panel This agrees well with the experimental loads corresponding to the changes in stiffness of the test specimens as shown in Figure 19.

Using the limit load (3320 lb) corresponding to an initial imperfection amplitude of -0.010 and the 20 x 11 finite-difference grid, the ratios of the experimental limit load to the theoretical limit load are 0.818, 0.753, 0.741, 0.693, and 0.652. The theoretical limit load used to calculate these ratios are based on an axially symmetric distribution of initial imperfections (W_o = WI (1+cos$\pi\xi$/a)). The actual distributions of initial imperfections indicated a pronounced distortion of the straight edges of the general shape represented by the mathematical equation expressed above, that dimenished as the specimen centerline was approached. Actually the center region of the test specimens were relatively straight in comparison to the straight edges. This observation is revealed by the imperfection data listed in Appendix C.

The equilibrium path for an initial imperfection distribution given by W_o = WI (1+cos$\pi\xi$/a) $(\eta/b)^2$ is shown in Figure 20. This distribution more closely represents the actual imperfection distributions. This equilibrium path coincided with the other paths shown in Figure 20. The limit point load for this imperfection was 3460 lb. which is essentially the same as the limit point loads for the other initial imperfections.

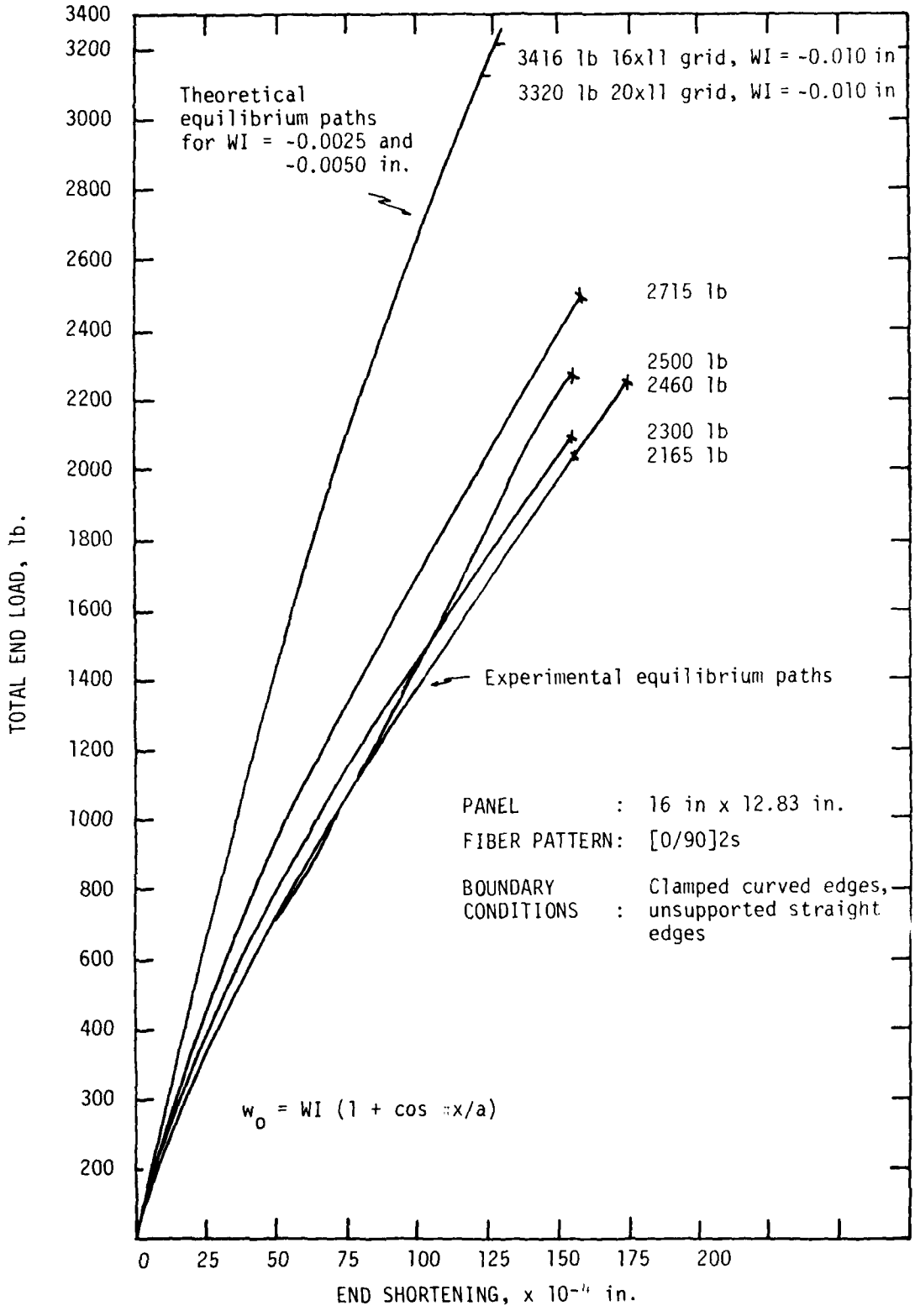

Figure 19. Theoretical and experimental equilibrium paths for specimens of Program B with unsupported straight edges.

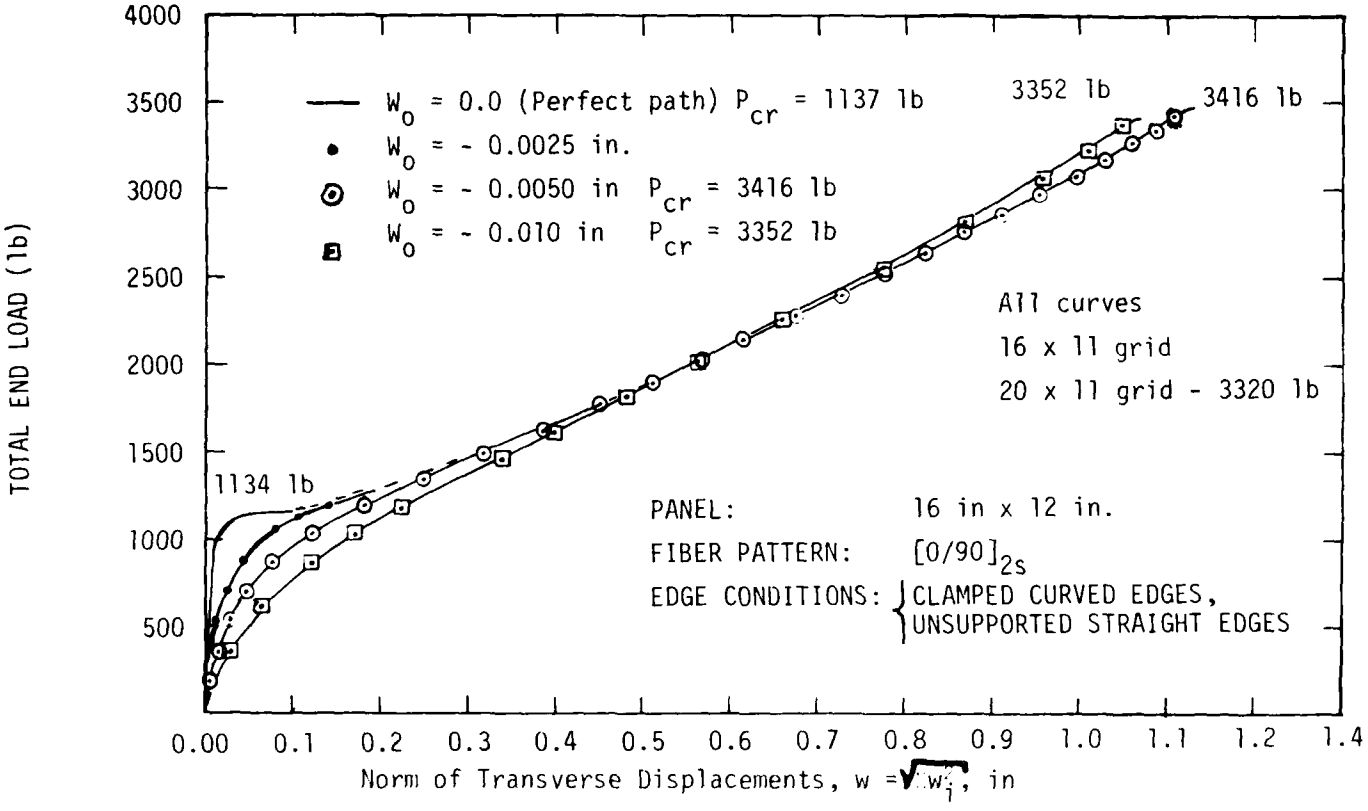

Figure 20. Equilibrium paths for axially compressed panel with unsupported straight edges.

SECTION V

LONGITUDINAL STIFFENERS

(V-1). INTRODUCTION. The computer program CLAPP was modified to include the effect of longitudinal stiffeners on the buckling behavior of fiber-reinforced panels by adding the total potential energy of the stiffeners to the total potential energy of the panel. Accordingly, the total potential energy of a stiffener element is developed in this section.

The stiffeners considered in this section have thin-wall open cross sections and are assumed to coincide with the finite difference grid lines that are parallel to the generators of the panel. It is not necessary that a stiffener be associated with every finite difference grid line.

A stiffener is assumed to be made from an homogeneous isotropic material; however, the developments remain valid for quasi-isotropic, fiber-reinforced stiffeners. The special properties of quasi-isotropic, fiber-reinforced stiffeners are described later. It is further assumed that the cross section of a stiffener does not vary along its length, and that each stiffener is free of externally applied forces.

Each stiffener is assumed to be rigidly attached to the panel along a finite-difference grid line. A point of attachment is defined as the point on the reference surface of the panel that lies on the normal through the centroid of the stiffener cross section. Mathematically, the displacement components associated with the panel and the displacement components associated with the stiffener are required to be continuous along this contact line.

(V-2). STIFFENER STRAIN ENERGY. An expression for the strain energy associated with small displacements of straight beams with thin-wall, open cross sections is given by Bleich and Bleich [4]

$$U = \frac{1}{2}\int_0^{\ell} \left\{ EI_{\eta\eta}(U_s'')^2 + EI_{\xi\xi}(V_s'')^2 + JG(\beta')^2 + EA(w_c')^2 + \Gamma(\beta'')^2 \right\} dz \qquad (V\text{-}1)$$

The quantities appearing in Eq. (V-1) are defined as follows. The rectangular coordinates ξ and η coincide with the principal centroidal axes of inertia, and z signifies a coordinate measured along the centroidal axis of the beam. Thus, $I_{\xi\xi}$ and $I_{\eta\eta}$ are principal centroidal moments of inertia, A denotes the cross sectional area, J is the torsional constant, and Γ is the warping coefficient for the cross section. Young's modulus and the shearing modulus are denoted by E and G, respectively. Finally, U_s and V_s are components of displacement of the shear center parallel to the ξ and η axes, respectively, W_c is the axial displacement of the centroid of the cross section, and β is the unit angle of twist that the section experiences.

The first two terms in Eq. (V-1) represent strain energy due to bending about the principal axes of inertia, while the next two terms represent strain energy caused by twisting and axial deformation, respectively. The last term represents strain energy associated with warping of the cross section. The strain energy associated with warping is usually discarded in stiffener analyses; it is also discarded in the present analysis.

Since it is assumed that every stiffener is free of externally applied forces, Eq. (V-1) also represents the total potential energy of a stiffener.

Energy methods have been employed by several investigators to examine the effect of stiffeners on the buckling behavior of plates and panels.

These investigators do not agree universally on the terms that need to be retained in the stiffener energy expression. Donnell [5] discards the strain energies associated with axial deformations and bending about an axis perpendicular to the reference surface of the panel. Thus Donnell assumes that the dominant actions of a stiffener are bending about an axis parallel to a circumferential tangent, and twisting. Szilard [6] adopts the same reasoning, but argues that strain energy due to twisting can be discarded for closely spaced stiffeners. Palamarchuk and Polyakov [7] retain the same bending and twisting energies, but include terms that represent the effects of externally applied forces and initial geometric imperfections.

The investigations cited consider only stiffeners with symmetrical cross sections. Stiffeners with unsymmetrical cross sections are treated in the present developments.

(V-3). STIFFENER ENERGY IN MATRIX FORM. The total potential energy for a stiffener can be expressed in matrix form as

$$V = \tfrac{1}{2} \int_0^{\ell} \begin{bmatrix} U_s'', & V_s'', & \beta', & w_c \end{bmatrix} \begin{bmatrix} EI_{\eta\eta} & 0 & 0 & 0 \\ 0 & EI_{\xi\xi} & 0 & 0 \\ 0 & 0 & JG & 0 \\ 0 & 0 & o & EA \end{bmatrix} \begin{bmatrix} U_s'' \\ V_s'' \\ \beta' \\ w_c' \end{bmatrix} dz \qquad (V\text{-}2)$$

As was stated previously, U_s and V_s are components of displacement of the shear center along the ξ and η axes, w_c is the axial displacement of the centroid, and β is the rotation of the cross section per unit length.

Connectivity of a stiffener to the panel is accomplished by expressing these displacement variables in terms of the displacements (U_D, V_D) of the

point of contact of a stiffener with the panel. The situation is depicted in Figure 21.

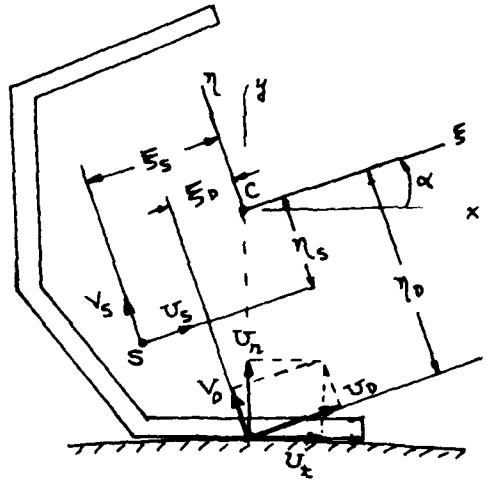

FIGURE 21. General thin-wall open cross section.

It is shown in Ref. [4] that, for small displacements, the displacement components for a generic point in the rigid cross section of a stiffener are

$$\left.\begin{aligned} U &= U_s + (\eta_s - \eta)\beta \\ V &= V_s - (\xi_s - \xi)\beta \end{aligned}\right\} \tag{V-3}$$

At the contact point D, $\xi = \xi_D$ and $\eta = \eta_D$, so that, with the aid of Eqs. (V-3),

$$\begin{bmatrix} U_s \\ V_s \\ \beta \end{bmatrix} = \begin{bmatrix} 1 & 0 & -(\eta_s - \eta_D) \\ 0 & 1 & (\xi_s - \xi_D) \\ 0 & 0 & 1 \end{bmatrix} \begin{bmatrix} U_D \\ V_D \\ \beta \end{bmatrix} \tag{V-4}$$

Because plane sections remain plane ($\Gamma = 0$) the axial displacement of the contact point, w_D, is

$$w_D = w_c - \xi_D U_c' - \eta_D V_c' \tag{V-5}$$

where u_c and v_c are centroidal displacements along the ξ and η axes as shown in Figure (21), and $(\ )'$ indicates differentiation with respect to z. From Eq. (V-3),

$$\left.\begin{aligned} U_c &= U_s + \eta_s \beta \ , \\ V_c &= V_s - \eta_s \beta \ , \end{aligned}\right\} \tag{V-6}$$

so that Eq. (V-5) becomes

$$w_D = w_c - \xi_D U_D' - \eta_D V_D' . \tag{V-7}$$

Eqs. (V-4) and (V-5) lead to the following transformation

$$\begin{bmatrix} U_s'' \\ V_s'' \\ \beta'' \\ \beta' \\ w_c' \end{bmatrix} = \begin{bmatrix} 1 & 0 & -(\eta_s - \eta_D) & 0 & 0 \\ 0 & 1 & (\xi_s - \xi_D) & 0 & 0 \\ 0 & 0 & 1 & 0 & 0 \\ 0 & 0 & 0 & 1 & 0 \\ \xi_D & \eta_D & 0 & 0 & 1 \end{bmatrix} \begin{bmatrix} U_D'' \\ V_D'' \\ \beta'' \\ \beta' \\ w_D' \end{bmatrix} \tag{V-8}$$

Eq. (V-8) permits the strain energy of a stiffener to be expressed in terms of the displacements experienced by the point of contact of a stiffener with the panel.

(V-4). DISPLACEMENT CONTINUITY. To enforce the required displacement continuity along the line of contact of a stiffener with the panel, it is necessary to project the displacement vector of the contact point along the circumferential tangent and along a normal to the panel. According to Figure 21,

$$\begin{bmatrix} U_D \\ V_D \end{bmatrix} = \begin{bmatrix} \cos\alpha & \sin\alpha \\ -\sin\alpha & \cos\alpha \end{bmatrix} \begin{bmatrix} U_t \\ U_n \end{bmatrix} , \tag{V-9}$$

where U_t and V_n are the circumferential and normal components of displacement of the contact point D.

Accordingly, the contact point displacement vector appearing on the right-hand side of Eq. (V-8) is expressed as

$$\begin{bmatrix} U''_D \\ V''_D \\ \beta'' \\ \beta' \\ w'_D \end{bmatrix} = \begin{bmatrix} \cos\alpha & \sin\alpha & 0 & 0 & 0 \\ -\sin\alpha & \cos\alpha & 0 & 0 & 0 \\ 0 & 0 & 1 & 0 & 0 \\ 0 & 0 & 0 & 1 & 0 \\ 0 & 0 & 0 & 0 & 1 \end{bmatrix} \begin{bmatrix} U''_t \\ U''_n \\ \beta'' \\ \beta' \\ w'_D \end{bmatrix} \qquad \text{(V-10)}$$

The assumption is made that the panel thickness is small compared to the dimensions of a stiffener normal to the panel. This permits the contact point D to lie in the reference surface of the panel.

Continuity of the displacements associated with the contact point on the stiffener and the displacements associated with the contact point on the panel requires that

$$\left.\begin{aligned} U_t &= V, & \beta &= W_{,y}, \\ U_n &= W, & \beta' &= W_{,yx}, \\ w_D &= U, & \beta'' &= W_{,yxx}, \end{aligned}\right\} \qquad \text{(V-11)}$$

Here U, V, W are the displacement components of a point on the reference surface of the panel.

Eqs. (V-2), (V-8), (V-10), and (V-11) yield the following matrix formulation for the strain energy of a stiffener:

$$V = \tfrac{1}{2} \int_0^{\ell} [d]^T[A]^T[B]^T[S][B][A][d]\, dz, \qquad \text{(V-12)}$$

where

$$[A] = \begin{bmatrix} \cos\alpha & \sin\alpha & 0 & 0 & 0 \\ -\sin\alpha & \cos\alpha & 0 & 0 & 0 \\ 0 & 0 & 1 & 0 & 0 \\ 0 & 0 & 0 & 1 & 0 \\ 0 & 0 & 0 & 0 & 1 \end{bmatrix} \tag{V-13}$$

$$[B] = \begin{bmatrix} 1 & 0 & -(\eta_s - \eta_D) & 0 & 0 \\ 0 & 1 & (\xi_s - \xi_D) & 0 & 0 \\ 0 & 0 & 0 & 1 & 0 \\ \xi_D & \eta_D & 0 & 0 & 1 \end{bmatrix} \tag{V-14}$$

$$[S] = \begin{bmatrix} EI_{\eta\eta} & 0 & 0 & 0 \\ 0 & EI_{\xi\xi} & 0 & 0 \\ 0 & 0 & JG & 0 \\ 0 & 0 & 0 & EA \end{bmatrix} \tag{V-15}$$

and

$$[d]^T = [V_{,xx}, W_{,xx}, W_{,xxy}, W_{,xy}, U_{,x}] \tag{V-16a}$$

To interface with the computer program CLAPP, the elements of the stiffener displacement vector [d] are rearranged so that

$$[d]^T = [U_{,x}, V_{,xx}, W_{,xx}, W_{,xxy}, W_{,xy}] \tag{V-16b}$$

The total potential energy of a stiffener becomes

$$V = \tfrac{1}{2} \int_0^{\ell} [d]^T [PAS2] [d] \, dz \tag{V-17}$$

The matrix [PAS2) results from carrying out the operations indicated in Eq. (V-12) taking into account the alterations of the matrices [A], [B], and [S] because of the rearrangement of the elements in the [d] matrix. The elements of [PAS2] are given in Figure 22.

A final transformation is required to express the total potential energy in terms of the finite-difference grid point displacements.

(V-5). FINITE-DIFFERENCE CONSIDERATIONS. The strain energy density of a stiffener element is assumed to be constant over the length of the element. Moreover, the strain energy density is assumed to be equal to its values at the midpoint of the element length. Consequently, the total potential energy for a stiffener-element is taken as the product of the strain energy density at the midlength of the element and the length of the element. Symbolically,

$$V_e = \tfrac{1}{2} [d]^T [PAS2][d] \times \ell \qquad (V\text{-}18)$$

where [d] is the displacement vector associated with the midpoint of the stiffener-element.

Nine different stiffener-elements are required. These stiffener-elements correspond to the nine types of area-elements used in CLAPP; one interior stiffener-element, four boundary stiffener-elements, and four corner stiffener-elements. The nine stiffener-elements are shown in Figure 23, which also shows the stiffener-element orientation and midpoint along with the local numbering system for the surrounding finite-difference grid points.

For each stiffener-element the midpoint displacement vector (Eq. (V-16b)) is transformed to the local grid point displacement vector

EA	$EA\ (\xi_D \cos\alpha - \eta_D \sin\alpha)$	$EA\ (\xi_D \sin\alpha + \eta_D \cos\alpha)$	0	0
	$EI_\eta \cos^2\alpha + EI_\xi \sin^2\alpha$ $+ EA\ (\xi_D^2 \cos^2\alpha$ $- \xi_D\eta_D \sin\alpha \cos\alpha)$ $- EA\ (\xi_D\eta_D \sin\alpha\cos\alpha$ $- \eta_D^2 \sin^2\alpha$	$(I_\eta - I_\xi)E \sin\alpha \cos\alpha$ $+ EA(\xi_D^2 \cos\alpha \sin\alpha$ $- \xi_D\eta_D \sin^2\alpha)$ $+ EA(\xi_D\eta_D \cos^2\alpha$ $- \eta_D^2 \sin\alpha \cos\alpha)$	$- (\eta_s - \eta_D)EI_\eta \cos\alpha$ $- (\xi_s - \xi_D)EI_\xi \sin\alpha$	0
		$EI_\eta \sin^2\alpha + EI_\xi \cos^2\alpha$ $+ EA(\xi_D^2 \sin^2\alpha$ $- \xi_D\eta_D \sin\alpha \cos\alpha)$ $+ EA(\xi_D\eta_D \sin\alpha \cos\alpha$ $+ \eta_D^2 \cos^2\alpha)$	$- (\eta_s - \eta_D)EI_\eta \sin\alpha$ $+ (\xi_s - \xi_D)EI_\xi \cos\alpha$	0
S Y M			$(\eta_s - \eta_D)^2 EI_\eta$ $+ (\xi_s - \xi_D)^2 EI_\xi$	0
				JG

Figure 22. Detail of the Coefficient Matrix [PAS2].

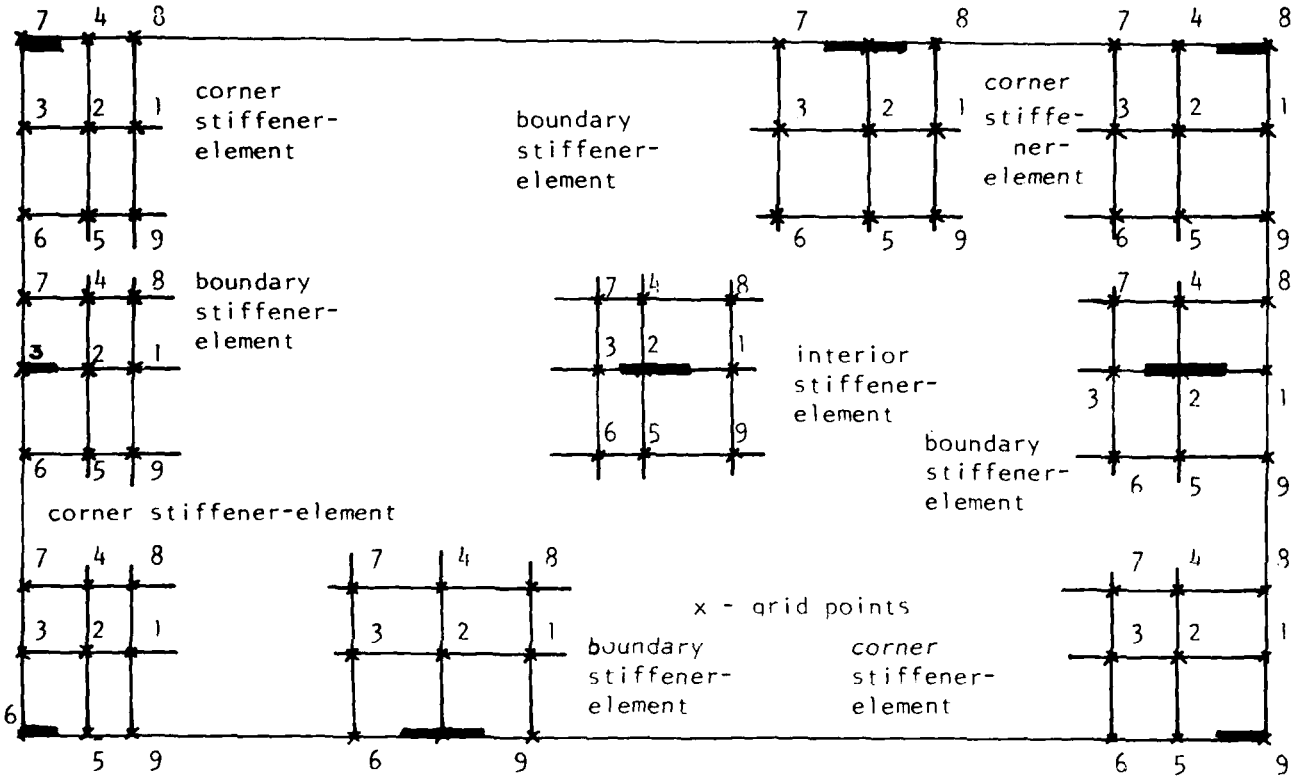

FIGURE 23. Typical stiffener-elements and the local numbering system for the surrounding grid points.

$$[q]^T = [W_1, U_1, V_1, W_2, U_2, V_2, \ldots, W_9, U_9, V_9] \qquad (V\text{-}19)$$

through the relations

$$d_i = c_{ij}\, q_j \qquad (V\text{-}20)$$

where the matrix [C] is composed of coefficients that depend on the variable spacing of the finite-difference grid. Accordingly, the total potential energy for a stiffener-element is

$$V_e = \tfrac{1}{2}\,[q]^T\,[C]^T\,[PAS2][C][q] * \ell \qquad (V\text{-}21)$$

The transformation matrix [C] depends on the location of the stiffener-element in the global system. To illustrate the procedure used to establish these matrices, the transformation matrix for the interior stiffener-element shown in Figure 24 is derived.

In the longitudinal direction, the midpoint (subsequently referred to as the stiffener-element centroid) of the stiffener-element contains the centroid of the corresponding area-element. This follows from the definitions of an area-element and of a stiffener-element. The corners of an area-element are the centroids of the areas contained between adjacent grid lines. The length of the corresponding stiffener-element is equal to the dimension of the area-element parallel to the generator of the panel.

A derivative of a centroidal displacement with respect to the longitudinal direction x, denoted by ( )', can be expressed as a linear combination of displacements at the three finite-difference grid points (i-1, i, i+1) lying on the longitudinal grid line.

A general one-dimensional centroidal function, f, and its derivatives are expressed as linear combinations of the function values at the three

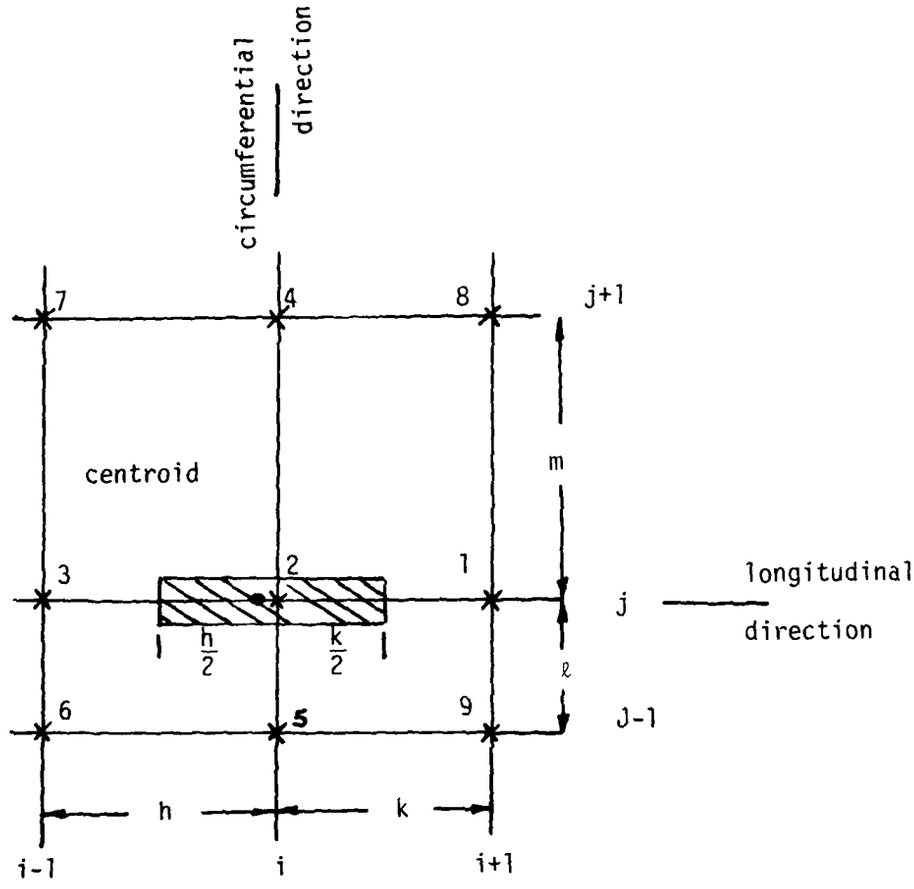

FIGURE 24. Interior stiffener-element with grid spacing and grid line notations.

node points on the jth grid line as

$$\tilde{f}_i = \frac{(k-h)(3h+k)}{16k(h+k)} f_{i+1} + \frac{(h+3k)(3h+k)}{16hk} f_i - \frac{(k-h)(3k+h)}{16h(h+k)} f_{i-1}, \qquad (V\text{-}22)$$

$$\tilde{f}'_i = \frac{1}{2k} f_{i+1} + \left(\frac{1}{2h} - \frac{1}{2k}\right) f_i + \frac{1}{2h} f_{i-1}, \qquad (V\text{-}23)$$

and

$$\tilde{f}''_i = \frac{2}{k(h+k)} f_{i+1} - \frac{2}{hk} f_i + \frac{2}{h(h+k)} f_{i-1}, \qquad (V\text{-}24)$$

where h and k are longitudinal spacings between the grid lines i-1 and i, and i and i+1, respectively.

A derivative of a centroidal displacement with respect to the circumferential coordinate y, denoted by $\dot{(\ )}$, can also be expressed as a linear combination of displacements at suitable finite-difference grid points by means of a Taylor series. Accordingly, a Taylor series expansion about the point (i, j) yields the two linear equations

$$f_{j+1} = f_j + m \dot{f}_j + \tfrac{1}{2} m^2 \ddot{f}_j \qquad (V\text{-}25)$$

and

$$f_{j-1} = f_j - \ell \dot{f}_j + \tfrac{1}{2} \ell^2 \ddot{f}_j, \qquad (V\text{-}26)$$

where ℓ and m are spacings between the j-1 and j, and j and j+1 circumferential grid lines. Eqs. (V-25) and (V-26) lead to the first-order central difference formulas

$$\dot{f}_j = \frac{\ell}{m(\ell+m)} f_{j+1} - \frac{(\ell-m)}{\ell m} f_j - \frac{m}{\ell(\ell+m)} f_{j-1} \qquad (V\text{-}27$$

and

$$\ddot{f}_j = \frac{2}{m(\ell+m)} f_{j+1} - \frac{2}{\ell m} f_j + \frac{2}{\ell(m+\ell)} f_{j-1} \tag{V-28}$$

The centroidal displacement vector [d] includes mixed derivatives also. The coefficients in the transformation matrix [C] that correspond to derivatives with respect to x are obtained from Eqs. (V-23) and (V-24) for an interior stiffener-element. The coefficients in the transformation matrix [C] corresponding to the mixed derivatives are determined by appropriate combinations of Eqs. (V-23), (V-24), and (V-26).

A general two-dimensional centroidal function, $\tilde{g}$, has the mixed derivative

$$\dot{\tilde{g}}' = \frac{1}{2k} \dot{g}_{i+1} + \left(\frac{1}{2h} - \frac{1}{2k}\right) \dot{g}_i + \frac{1}{2h} \dot{g}_{i-1}. \tag{V-29}$$

Using Eq. (V-26) yields

$$\dot{\tilde{g}}' = \frac{1}{2k} \frac{\ell}{m(\ell+m)} g_{i+1,\, j+1} - \frac{(\ell-m)}{\ell m} g_{i+1,\, j} - \frac{m}{\ell(\ell+m)} g_{i+1,\, j+1} \tag{V-30}$$

$$+ \left(\frac{1}{2h} - \frac{1}{2k}\right) \frac{\ell}{m(\ell+m)} g_{i,\, j+1} - \frac{(\ell-m)}{\ell m} g_{i,\, j} - \frac{m}{\ell(\ell+m)} g_{i,\, j-1} \tag{V-31}$$

$$+ \frac{1}{2h} \frac{\ell}{m(\ell+m)} g_{i-1,\, j+1} - \frac{(\ell-m)}{\ell m} g_{i-1,\, j} - \frac{m}{\ell(\ell+m)} g_{i-1,\, j-1} \tag{V-32}$$

Identification of the nine surrounding grid points with the local number system determines the coefficients in the transformation

$$\dot{\tilde{g}}' = c_i\, g_i \qquad i = 1, 2, \ldots, 9. \tag{V-33}$$

The coefficients for the mixed derivative g'' are obtained in a similar manner.

The total potential energy for any stiffener-element is expressed as

$$V_e = \tfrac{1}{2} [q]^T [CAS2][q] \times \ell \qquad (V-34)$$

where

$$[CAS2] = [C]^T [PAS2] [C] \qquad (V-35)$$

Eq. (V-34) is the formulation of the total potential energy for any stiffener-element that interfaces consistently with the area-elements used in CLAPP.

(V-6). INCORPORATION INTO CLAPP. The incorporation of longitudinal stiffeners in the computer program CLAPP is accomplished with three subroutines.

The first of these three stiffener subroutines is named SCOEF. SCOEF calculates the elements of the matrix [PAS2]. Since [PAS2] depends only on the material and geometric properties of the stiffener cross section it is calculated once for each element and stored.

SCOEF permits the user to select any of seven stiffener cross sections. It also provides for any other cross section through a user's choice option. For the various stiffener cross sections included in SCOEF see the user's manual in APPENDIX D.

The second stiffener subroutine is named STFDIF. It calculates the elements of the transformation matrix [C] of Eq (V-20). The subroutine FDIFF of CLAPP performs similar calculations for each area-element. Consequently, when FDIFF is called to calculate [C] for an area-element STFDIF is subsequently called from FDIFF to calculate [C] for the corres-

ponding stiffener element.

The third stiffener subroutine is named ATBAS. It performs the matrix multiplications indicated in Eq (V-35). This subroutine is called from the subroutine STFDIF. ATBAS has been constructed to take advantage of the numerous zeros that occur in the matrix [C].

The main program and the subroutine FDIFF of CLAPP are modified so that longitudinal stiffeners can be included when appropriate. Additions to the main program read in stiffener indices indicating (a) that stiffeners are to be included, (b) the choice stiffener cross section, (c) whether stiffeners are located on the inside or outside of the panel, and (d) if stiffeners occur on every finite-difference grid line. The main program calls SCOEFF to construct the matrix [PAS2]. The additions to the subroutine FDIFF determine when the stiffener energy is required in an analysis that does not include stiffeners at every grid line. When it is appropriate, STFDIF is called to calculate the stiffener-element energy which is immediately added to the correspoinding area-element energy. The procedure used by CLAPP to assemble the system stiffness matrix for area-elements proceeds in precisely the same manner when stiffeners are present.

(V-7). QUASI-ISOTROPIC FIBER-REINFORCED STIFFENERS. A strain energy expression for a quasi-isotropic, fiber-reinforced stiffener that is analogus to the strain energy expression for an isotropic stiffener is established in this section. For the purpose of the present development a quasi-isotropic material is defined as one possessing midplane symmetry and alternate zero and 90 degree fiber directions. Thus, for a stiffener, the zero fiber direction is assumed to coincide with the longitudinal axis of the stiffener, and the 90 degree fiber direction is perpendicular to

this axis.

The stress-strain relations [2] for a general fiber-reinforced laminate are

$$\begin{bmatrix} N_x \\ N_y \\ N_{xy} \end{bmatrix} = \begin{bmatrix} A_{11} & A_{12} & A_{16} \\ A_{12} & A_{22} & A_{26} \\ A_{16} & A_{26} & A_{66} \end{bmatrix} \begin{bmatrix} e_x \\ e_y \\ 2e_{xy} \end{bmatrix} + \begin{bmatrix} B_{11} & B_{12} & B_{16} \\ B_{12} & B_{22} & B_{26} \\ B_{16} & B_{26} & B_{66} \end{bmatrix} \begin{bmatrix} K_x \\ K_y \\ 2K_{xy} \end{bmatrix} \quad \text{(V-36)}$$

$$\begin{bmatrix} M_x \\ M_y \\ M_{xy} \end{bmatrix} = \begin{bmatrix} B_{11} & B_{12} & B_{16} \\ B_{12} & B_{22} & B_{26} \\ B_{16} & B_{26} & B_{66} \end{bmatrix} \begin{bmatrix} e_x \\ e_y \\ 2e_{xy} \end{bmatrix} + \begin{bmatrix} D_{11} & D_{12} & D_{16} \\ D_{12} & D_{22} & D_{26} \\ D_{16} & D_{26} & D_{66} \end{bmatrix} \begin{bmatrix} K_x \\ K_y \\ 2K_{xy} \end{bmatrix} \quad \text{(V-37)}$$

Formulas connecting the elements of the laminate stiffness matrices [A], [B], and [D] with the material properties and the geometric locations of the individual layers are

$$A_{ij} = \sum_{k=1}^{N} \overline{Q}_{ij}{}^{k} (h_k - h_{k-1}), \quad \text{(V-38)}$$

$$B_{ij} = \frac{1}{2} \sum_{k=1}^{N} \overline{Q}_{ij}{}^{k} (h_k^2 - h_{k-1}^2), \quad \text{(V-39)}$$

$$D_{ij} = \sum_{k=1}^{N} \overline{Q}_{ij}{}^{k} (h_k^3 - h_{k-1}^3), \ (i,j = 1, 2, 6). \quad \text{(V-40)}$$

Pertinent geometric quantities appearing in these relations are defined in Figure 25.

The laminate is assumed to possess midplane symmetry so that the B_{ij} are identically zero in Eqs. (V-36) and (V-37). It is also assumed that

the stiffener experiences a membrane state of stress like the one shown in Figure 26. Consequently, the dominant bending action results from the moment caused by the membrane force N_x.

If the cross section of a stiffener is assumed to be rigid, then $e_y = 0$ so that

$$N_x = A_{11}\, e_x + A_{16}\, (2e_{xy}) \tag{V-41}$$

and

$$N_{xy} = A_{16}\, e_x + A_{66}\, (2e_{xy}) \tag{V-42}$$

Now $A_{16} \doteq 0$ because of the laminate fiber directions are either parallel or perpendicular to the longitudinal axis of the stiffener. Consequently, the stress-strain relations appropriate to an analysis of fiber-reinforced stiffeners under the foregoing restrictions are

$$N_x = A_{11}\, e_x \tag{V-43}$$

and

$$N_{xy} = A_{66}\, (2e_{xy}). \tag{V-44}$$

These relations are analogous to the isotropic stress-strain relations used by Bleich and Bleich [4] to arrive at their expression for the strain energy of stiffeners made from isotropic materials. All that is required to make the isotropic strain energy expression valid for quasi-isotropic stiffeners is to appropriately identify E and G of the isotropic case with A_{11} and A_{66} for the quasi-isotropic case.

To do this, consider that

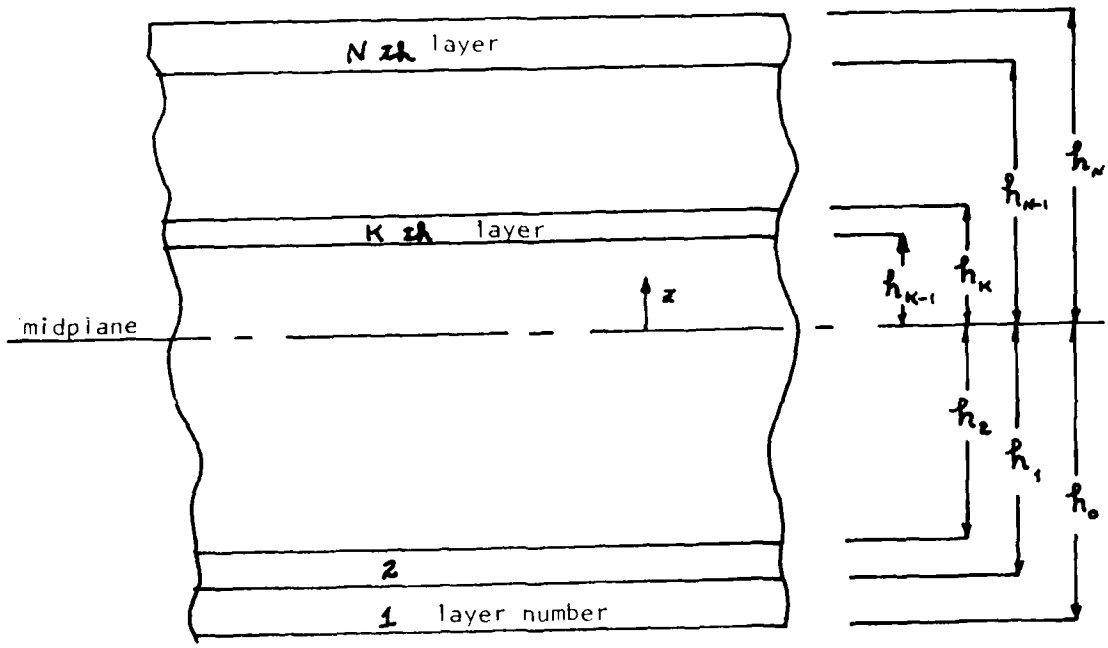

FIGURE 25. Cross section of laminate

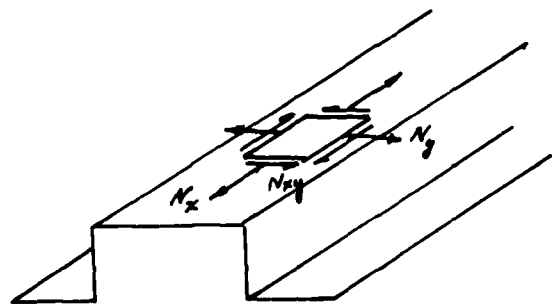

FIGURE 26. Membrane state of stress for a stiffener.

$$A_{11} = \sum_{k=1}^{N} \bar{Q}_{11}{}^{k} (h_k - h_{k-1}) = t \sum_{k=1}^{N} \bar{Q}_{11}{}^{k} \qquad \text{(V-45)}$$

and

$$A_{66} = \sum_{k=1}^{N} \bar{Q}_{66}{}^{k} (h_k - h_{k-1}) = t \sum_{k=1}^{N} \bar{Q}_{66}{}^{k} \qquad \text{(V-46)}$$

if the thickness of each layer is the same.

The subscript k signifies that the k-th layer is under consideration. The $\bar{Q}_{ij}$ are symmetrical and are the material coefficients referred to a generic set of axis. They are expressed in terms of the material coefficients, Q_{ij}, associated with the material axes of a layer through the transformation:

$$\bar{Q}_{11} = Q_{11}\cos^4\theta + 2\,(Q_{12} + 2\,Q_{66})\,\sin^2\theta\,\cos^2\theta + Q_{22}\,\sin^4\theta,$$

$$\bar{Q}_{12} = (Q_{11} + Q_{22} - 4\,Q_{66})\,\sin^2\theta\,\cos^2\theta + Q_{12}\,(\sin^4\theta + \cos^4\theta),$$

$$\bar{Q}_{22} = Q_{11}\,\sin^4\theta + 2(Q_{12} + 2\,Q_{66})\,\sin^2\theta\,\cos^2\theta + Q_{22}\,\cos^4\theta, \qquad \text{(V-47)}$$

$$\bar{Q}_{16} = (Q_{11} - Q_{12} - 2\,Q_{66})\,\sin\theta\,\cos^3\theta + (Q_{12} - Q_{22} + 2\,Q_{66})\,\sin^3\theta\,\cos\theta,$$

$$\bar{Q}_{26} = (Q_{11} - Q_{12} - 2\,Q_{66})\,\sin^3\theta\,\cos\theta + (Q_{12} - Q_{22} + 2\,Q_{66})\,\sin\theta\,\cos^3,$$

$$\bar{Q}_{66} = (Q_{11} + Q_{22} - 2\,Q_{12} - 2\,Q_{66})\,\sin^2\theta\,\cos^2\theta + Q_{66}(\sin^4\theta + \cos^4\theta).$$

The quantities Q_{ij} are related to the engineering material constants through the relations:

$$\left.\begin{aligned} Q_{11} &= \frac{E_{11}}{1-\nu_{12}\nu_{21}}, \\ Q_{12} = Q_{21} &= \frac{\nu_{12}\, E_{11}}{1-\nu_{12}\nu_{21}} = \frac{\nu_{21}E_{22}}{1-\nu_{12}\nu_{21}}, \\ Q_{22} &= \frac{E_{22}}{1-\nu_{12}\nu_{21}}, \\ Q_{66} &= G_{12}. \end{aligned}\right\} \qquad \text{(V-48)}$$

E_{11}, E_{22} are Young's modulii of elasticity parallel and perpendicular to the fiber direction, respectively; G_{12} is the shearing modulus of elasticity associated with the directions parallel and perpendicular to the fiber direction; and ν_{12}, ν_{21} are Poisson ratios. ν_{12} is associated with a strain in the 1-direction due to a stress in the 2-direction and ν_{21} is associated with a strain in the 2-direction due to a stress in the 1-direction. It is convenient to let the 1-direction coincide with the fiber direction.

From Eqs. (V-47) and (V-48)

$$\bar{Q}_{11}{}^{k} = \begin{cases} Q_{11}{}^{k} = \dfrac{E_{11}}{1-\nu_{12}\nu_{21}} & \text{for fibers parallel to the stiffener axis} \\ Q_{22}{}^{k} = \dfrac{E_{22}}{1-\nu_{12}\nu_{21}} & \text{for fibers perpendicular to the stiffener axis} \end{cases} \qquad \text{(V-49)}$$

and

$$\bar{Q}_{66}{}^{k} = Q_{66} = G_{12}, \qquad \text{(V-50)}$$

for either fiber direction.

If N is the number of layers in the laminate, then from Eqs. (V-44) and (V-49)

$$A_{11} = \frac{Nt}{1-\nu_{12}\nu_{21}} \left[\frac{E_{11} + E_{22}}{2} + \lambda \frac{E_{11} - E_{22}}{2N} \right] \tag{V-51}$$

where

$$\lambda = \begin{cases} 0 \text{ if } N \text{ is even} \\ 1 \text{ if } N \text{ is odd.} \end{cases} \tag{V-52}$$

Note that when N is odd, the middle or odd layer is assumed to be parallel to the stiffener axis. If the middle or odd layer is perpendicular to the stiffener axis E_{11} and E_{22} interchange positions in Eq (V-51).

Finally,

$$A_{66} = Nt\, G_{12} \tag{V-53}$$

for N even or odd. Notice that Nt is the total thickness of the laminate from which the stiffener is constructed.

Now if E and G in the isotropic strain energy expression for thin-wall open sections is replaced with

$$E \Rightarrow \frac{A_{11}}{Nt} = \frac{E_{11} + E_{22}}{2} + \lambda \left(\frac{E_{11} - E_{22}}{2N} \right) \tag{V-54}$$

and

$$G \Rightarrow \frac{A_{66}}{Nt} = G_{12}, \tag{V-55}$$

one arrives at a strain energy expression for the quasi-isotropic material considered in this section.

REFERENCES

1. Bauld, Nelson R., and Satymurthy, Kailassam, Collapse Load Analysis for Plates and Panels, AFFDL-TR-79-3038, Air Force Flight Dynamics Laboratory, Air Force Wright Aeronautical Laboratories, Air Force Systems Command, Wright-Patterson Air Force Base, Ohio, May, 1979.

2. Jones, Robert M., Mechanics of Composite Materials, McGraw-Hill, 1975.

3. Wilkins, D. J., "Compression Buckling Tests of Laminated Graphite-Epoxy Curved Panels," AIAA Journal, Vol. 13, No. 4, April, 1975.

4. Bleich, F., Buckling Strength of Metal Structures, H. H. Bleich, Ed., New York: McGraw-Hill, 107-116, 1952.

5. Donnell, L. H., Beams, Plates, and Shells, McGraw-Hill, 204-209, 216-218, 1976.

6. Szilard, R., Theory and Analysis of Plates: Classical and Numerical Methods, Prentice-Hall, Inc., 540-547, 1974.

7. Palamarchuk, V. G., and Polyakov, P. S., "Rational Stringer Reinforcement of a Shell with Initial Deflections," Soviet Applied Mechanics, Vol. 12, No. 3, 229-234, 1976.

APPENDIX A

STRAIN, END-SHORTENING, AND IMPERFECTION MEASUREMENTS FOR TEST PANELS WITH SIMPLY-SUPPORTED STRAIGHT EDGES CLAMPED CURVED EDGES

TESTING PROGRAM A

A-1 EXPERIMENTAL DATA FOR 8 x 16 PANELS WITH SIMPLY-SUPPORTED STRAIGHT EDGES*

BCP 9824-A-2-1 CS**

Axial Load(lb)	End Shortening x 10^{-4}	Axial Strain at Gage Number				
		1	2	3	4	5
50	0	0	-	0	0	0
500	5.0	89	-	60	88	109
1000	24.0	215	-	128	156	257
1500	46.0	339	-	200	228	423
1750	52.0	388	-	226	251	487
2000	57.0	451	-	262	285	589
2250	65.0	531	-	309	329	689
2500	74.5	616	-	353	373	729
2750	86.0	693	-	382	401	743
3000	96.0	775	-	423	448	784
3250	105.0	852	-	446	475	800
3500	114.0	919	-	480	511	845
3750	122.0	972	-	502	534	873
4000	136.0	1035	-	543	572	914
4250	145.5	1102	-	605	619	977
4500	154.0	1176	-	667	662	998
4750	162.0	1243	-	710	684	1016
5000	169.0	1316	-	768	723	1046
5100	174.0	1337	-	784	736	1050
5200	176.5	1356	-	797	745	1056

BCP 9824-A-2-1 CS**

	End Shortening x 10^{-4}	Axial Strain at Gage Number				
		1	2	3	4	5
50	0	0	0	0	0	-
500	3.0	77	64	66	71	-
750	8.0	152	140	134	125	-
1000	20.0	156	156	152	179	-
1250	32.0	177	178	173	218	-
1500	47.0	203	210	201	254	-
1725	60.0	233	253	233	289	-
2000	73.0	281	279	258	348	-
2250	86.0	335	308	284	402	-
2500	101.0	383	335	315	473	-
2750	115.0	417	355	359	541	-
3000	126.0	453	386	411	602	-
3250	136.0	479	400	470	666	-
3500	144.0	504	420	531	737	-
3750	154.0	530	449	599	799	-
4000	168.0	557	473	636	895	-
4250	178.0	586	500	762	990	-
4500	190.0	605	530	855	1072	-
4600	197.0	660	607	891	1091	-
4700	201.0	675	633	919	1114	-

*The last letter in a specimen designator (BCP-9810-B-3-1) indicates the fiber pattern. Thus the letter A denotes the pattern [0/±45/90]s and the letter B denotes the pattern [0/90]2s.

**THESE TWO PANELS HAD THE SAME DESIGNATION LABEL.

BCP 9824-A-2-1 CS (cont'd)

Axial Load(lb)	End Shorten-ing x 10^{-4}	Axial Strain at Gage Number				
		1	2	3	4	5
5300	178.5	1381	-	816	760	1069
5400	184.0	1410	-	839	784	1093
5500	186.0	1428	-	842	798	1093
5600	188.5	1452	-	860	830	1105
5700	194.0	1481	-	905	891	1142
5800	195.0	1508	-	905	903	1136
5900	197.0	1533	-	929	934	1160
6000	200.00	1552	-	936	960	1165
6100	203.5	1571	-	947	985	1175
6200	205.0	1592	-	965	1019	1196
6300	207.0	1609	-	976	1045	1205
6400	209.5	1632	-	991	1084	1220
6500	214.5	1644	-	1000	1115	1223
6600	216.5	1656	-	1020	1146	1235
6700	219.0	1688	-	1043	1186	1254
6710	Buckled					

BCP 9824-A-2-1 CS (cont'd)

	End Shorten-ing x 10^{-4}	Axial Strain at Gage Number				
		1	2	3	4	5
4800	207.0	648	622	903	1108	-
4900	212.0	662	636	937	1140	-
5000	218.5	681	666	1001	1186	-
5100	227.0	718	705	1036	1200	-
5200	236.0	720	711	1071	1212	-
5300	239.0	720	730	1099	1239	-
5400	247.0	738	743	1134	1255	-
5500	270.0	760	780	1205	1276	-
5600	280.0	758	790	1285	1309	-
5700	286.0	772	829	1320	1332	-
5800	294.0	772	852	1353	1346	-
5825	Buckled					

BCP 9810-B-4-1 CS

Axial Load(lb)	End Shortening x 10^{-4}	Axial Strain at Gage Number				
		1	2	3	4	5
50	0	0	0	0	0	0
500	1.0	62	80	52	64	64
1000	10.0	138	160	98	107	140
1500	22.0	205	246	164	161	217
2000	34.0	263	337	249	228	303
2250	38.5	283	371	276	249	334
2500	44.0	310	416	313	281	376
2750	50.0	339	463	352	328	424
3000	53.0	360	500	378	373	460
3250	60.5	389	550	416	434	508
3500	64.0	414	592	446	487	546
3750	72.0	437	633	472	538	582
4000	80.5	468	696	509	611	636
4250	86.5	499	751	522	676	669
4500	93.5	532	797	540	730	700
4750	119.0	608	826	552	749	728
4900	123.5	625	845	569	772	752
5000	124.5	635	866	581	790	772
5100	128.0	645	894	597	810	796
5175	Buckled					

BCP 9810-B-4-2 CS

	End Shortening x 10^{-4}	Axial Strain at Gage Number				
		1	2	3	4	5
50	0	-	0	0	0	0
250	1.0	-	17	30	25	26
500	2.2	-	43	67	60	59
750	4.8	-	72	115	101	110
1000	5.0	-	100	153	123	153
1250	13.5	-	140	214	150	207
1500	15.0	-	178	266	169	256
1750	22.2	-	215	310	193	300
2000	25.0	-	249	346	209	341
2250	33.0	-	284	380	227	379
2500	34.0	-	327	425	260	428
2750	35.0	-	372	467	295	477
3000	43.0	-	411	498	334	503
3250	44.0	-	453	542	393	533
3500	53.0	-	494	573	445	539
3750	55.0	-	534	605	499	552
4000	58.0	-	578	639	559	576
4250	65.0	-	615	655	610	580
4500	67.0	-	657	688	657	603
4750	75.0	-	693	731	679	616
5000	75.0	-	727	780	710	645
5250	84.0	-	755	840	720	663
5350	Buckled	-				

IMPERFECTION MEASUREMENTS

($\times 10^{-3}$ in)

BCP 9824-A-2-1 CS

	-6	-6	-5	0	-6	-2	-6	-4
	-6	-5	-3	2	-5	2	-5	-2
	-6	-6	-5	1	-8	0	-6	-3
	-7	-6	-5	1	-9	-1	-7	-5
	-5	-5	-6	0	-7	-2	-7	-5

BCP 9824-A-2-2 CS

	-7	-4	-4	0	-3	-3	-13	-14
	-7	-6	-3	0	-5	-1	-15	-15
	-7	-9	-4	-2	-6	-2	-17	-13
	-8	-9	-5	-4	-8	-6	-18	-15
	-11	-9	-7	-5	-8	-8	-16	-15

BCP 9810-B-4-1 CS

	-5	-3	-2	0	-1	1	-3	0
	-4	-4	-3	1	-3	-1	-1	-1
	-4	-4	-3	1	-2	1	2	2
	-5	-5	-6	0	-4	-1	1	0
	-8	-6	-5	-1	-5	-2	-2	0

BCP 9810-B-4-2 CS

-12	-15	-7	0	-2	0	-2	2	
-13	-15	-7	-1	-2	-2	-5	0	
-15	-14	-8	-2	-3	-3	-7	-1	
-12	-13	-9	-7	-8	-5	-12	-5	
-11	-11	-11	-8	-11	-9	-13	-9	

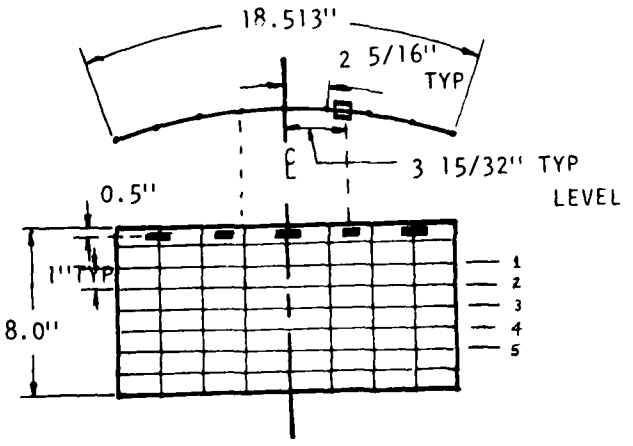

A-2 EXPERIMENTAL DATA FOR 12 x 16 PANELS WITH SIMPLY-SUPPORTED STRAIGHT EDGES

BCP 9121-A-5-1 ES

Axial Load (lb)	End Shortening x 10^{-4}	Axial Strain at Gage Number				
		1	2	3	4	5
50	0	-	0	0	0	0
250	4.0	-	35	34	34	55
500	10.0	-	75	77	68	114
750	17.0	-	121	122	96	184
1000	26.0	-	175	182	124	272
1250	33.5	-	239	256	171	362
1500	42.5	-	290	314	201	435
1750	51.5	-	336	363	219	492
2000	61.5	-	390	425	246	571
2250	70.0	-	433	473	263	630
2500	79.5	-	476	523	273	694
2750	87.5	-	525	580	298	754
3000	97.0	-	588	651	332	822
3250	106.5	-	644	713	357	873
3500	115.5	-	705	783	391	914
3750	123.5	-	756	842	412	926
4000	132.5	-	831	922	457	967
4250	143.0	-	937	1010	549	1013
4500	152.5	-	1010	1046	623	1037
4750	161.0	-	1072	1084	681	1070

BCP 9921-A-5-2 ES

Axial Load (lb)	End Shortening x 10^{-4}	Axial Strain at Gage Number				
		1	2	3	4	5
50	0	0	0	0	0	0
250	4.0	41	24	26	26	41
500	9.5	140	96	91	93	151
750	17.0	202	134	122	122	250
1000	24.5	277	175	161	159	335
1250	33.0	331	201	183	176	400
1500	41.0	400	253	237	217	480
1750	50.0	457	296	288	248	542
2000	59.0	498	289	293	231	532
2250	67.0	522	287	307	223	536
2500	76.5	603	335	383	264	582
2750	87.0	686	379	450	299	606
3000	95.0	854	533	618	446	740
3250	104.0	926	588	677	509	758
3500	113.0	1002	643	728	590	788
3600	117.0	1029	652	725	632	777
3700	120.0	1051	674	745	666	796
3800	124.0	1091	686	752	688	801
3900	128.0	1123	710	767	719	813
4000	132.0	1074	649	692	652	742

BCP 9121-A-5-1 ES (cont'd)

Axial Load(lb)	End Shortening x 10^{-4}	Axial Strain at Gage Number				
		1	2	3	4	5
5000	170.5	-	1148	1116	737	1092
5100	177.0	-	1193	1122	744	1093
5200	181.0	-	1221	1120	732	1083
5350	187.0	-	1241	1129	735	1095
5500	192.0	-	1306	1180	776	1135
5600	Buckled					

BCP 9921-A-5-2 ES (cont'd)

	End Shortening x 10^{-4}	Axial Strain at Gage Number				
		1	2	3	4	5
4100	136.5	1197	769	789	766	828
4200	140.5	1228	795	795	783	832
4300	146.0	1264	827	807	808	840
4400	149.5	1287	849	804	822	831
4500	153.5	1319	876	806	846	823
4600	157.0	1361	920	830	900	866
4700	161.0	1392	951	839	925	875
4800	166.0	1432	997	843	943	883
4900	170.0	1456	1029	829	926	856
5000	176.0	1509	1091	847	950	884
5100	181.5	1540	1115	750	858	790
5200	187.0	1594	1195	855	967	894
5300	192.0	1632	1235	867	981	912
5400	197.0	1654	1268	862	967	886
5500	203.0	1670	1275	837	940	860
5600	208.0	1718	1354	896	985	903
5700	212.0	1769	1375	907	984	900
5800	216.0	1811	1410	938	1001	915
5900	220.0	1839	1429	961	1011	942
5910	Buckled					

BCP 8910-B-21- ES

Axial Load(lb)	End Shortening x 10-4	Axial Strain at Gage Number				
		1	2	3	4	5
50	0	0	0	0	0	0
250	3.5	40	27	30	2	28
500	9.5	100	57	59	18	52
750	16.0	156	91	85	38	76
1000	25.0	240	128	117	65	107
1250	34.0	306	232	215	160	204
1500	44.0	416	286	238	181	231
1750	52.0	406	286	204	141	216
2000	59.0	460	345	238	168	276
2250	67.0	530	442	271	197	348
2500	73.5	582	488	313	235	403
2750	81.0	624	534	338	251	411
3000	88.5	652	576	356	263	409
3250	96.0	686	6k4	379	274	406
3500	101.5	735	669	436	316	442
3750	109.0	777	718	493	336	443
4000	116.0	815	764	552	358	451
4100	119.0	820	820	614	408	490
4200	121.5	853	809	608	395	475
4300	124.0	869	826	629	403	485

BCP 8910-B-2-2 ES

	End Shortening x 10-4	Axial Strain at Gage Number				
		1	2	3	4	5
50	0	0	0	0	0	0
250	3.0	34	34	34	26	36
500	8.0	75	72	76	49	72
750	15.5	123	119	98	61	111
1000	22.0	165	159	127	81	162
1250	29.0	210	206	152	94	222
1500	35.5	250	246	178	115	286
1750	43.0	296	286	204	133	361
2000	49.5	339	333	235	156	430
2250	58.0	379	371	259	169	503
2500	65.0	420	414	291	185	573
2750	73.5	448	447	316	190	624
3000	82.5	489	492	357	203	633
3250	91.5	530	540	405	225	650
3500	98.0	571	582	450	236	648
3600	101.0	586	601	470	246	668
3700	103.5	599	613	484	249	664
3800	106.0	615	638	508	265	681
3900	108.5	628	660	528	275	687
4000	112.0	648	670	543	286	692

BCP 8910-B-2-1 ES (cont'd)

Axial Load(lb)	End Shortening x 10^{-4}	Axial Strain at Gage Number				
		1	2	3	4	5
4400	126.5	885	843	654	411	488
4500	130.0	903	863	679	422	491
4600	132.5	918	380	701	429	490
4700	135.0	927	890	722	433	486
4750	Buckled					

BCP 8910-B-2-2 ES (cont'd)

Axial Load(lb)	End Shortening x 10^{-4}	Axial Strain at Gage Number				
		1	2	3	4	5
4100	115.0	670	692	566	302	701
4200	118.0	686	711	586	318	703
4300	121.5	697	719	595	326	697
4400	124.0	720	746	621	344	713
4500	127.0	724	751	625	349	708
4600	130.0	740	771	646	366	712
4700	133.0	757	783	660	378	715
4800	136.0	780	806	683	395	725
4900	139.0	805	330	710	413	734
4950	Buckled					

IMPERFECTION MEASUREMENTS

($\times 10^{-3}$ in)

BCP 9121-A-5-1 ES

	-10	-1	2	0	5	3	-2	-2
	-13	5	6	2	8	6	-8	0
	-18	3	10	1	8	7	-13	-2
	-16	0	8	2	5	8	-11	0
	-10	3	7	2	5	6	-6	3

BCP 9921-A-5-2 ES

	-9	0	0	0	4	-4	-9	-8
	-12	3	2	2	6	-2	-14	-9
	-16	2	2	0	4	-1	-17	-9
	-20	1	1	-1	2	-5	-18	-7
	-15	-3	-3	-4	-4	-6	-15	-7

BCP 8910-B-2-1 ES

	-16	-7	-2	0	-2	1	-3	-6
	-21	-6	1	1	-3	0	-5	-5
	-22	-9	2	0	-3	-1	-4	3
	-22	-8	2	-2	-4	-3	-4	3
	-17	-8	-3	-5	-8	-6	-8	-1

BCP 8910-B-2-2 ES

	-6	1	0	0	-1	-3	-8	-12
	5	5	2	1	0	-6	-13	-10
	-5	5	2	2	0	-7	-12	-7
	-8	-1	-2	-3	-2	-9	-11	-4
	-8	-3	-5	-5	-5	-7	-8	-1

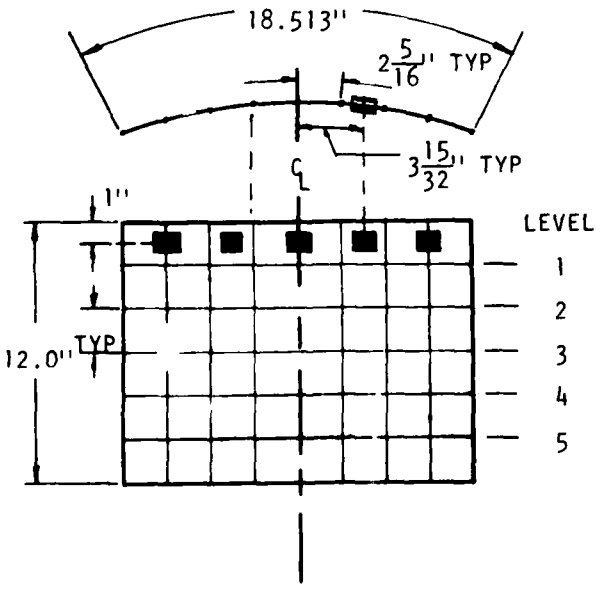

A-3 EXPERIMENTAL DATA FOR 16 x 16 PANELS WITH SIMPLY-SUPPORTED STRAIGHT EDGES

BCP 9810-B-3-1

	End Shortening x 10^{-4}	Axial Strain at Gage Number				
		1	2	3	4	5
50	0.0	0	0	0	0	0
250	2.2	26	16	13	13	23
500	9.0	63	45	57	43	58
750	14.5	115	83	96	70	89
1000	23.0	183	108	-	95	120
1250	32.0	234	136	-	119	162
1500	42.0	283	161	-	138	213
1750	52.0	330	188	-	161	279
2000	61.2	377	244	-	189	342
2250	72.0	417	252	-	206	396
2500	81.0	450	282	-	223	435
2750	92.2	492	321	-	238	496
3000	102.0	527	361	-	258	542
3250	111.2	556	403	-	266	576
3500	120.0	592	455	-	299	629
3750	131.0	643	519	-	318	673
4000	143.0	689	590	-	340	693
4250	152.0	723	636	-	358	747
4500	161.5	760	680	-	373	788
4750	170.5	802	731	-	401	839

BCP 9810-B-3-2

Axial Load(lb)	End Shortening x 10^{-4}	Axial Strain at Gage Number				
		1	2	3	4	5
50	0.0	0	0	0	0	0
250	1.0	22	17	13	12	22
500	5.5	62	43	36	36	55
750	11.0	117	80	57	50	105
1000	17.0	174	124	73	66	159
1250	24.5	237	171	94	85	218
1500	30.0	290	196	114	106	265
1750	37.0	337	214	127	120	298
2000	46.5	388	237	144	140	337
2250	55.5	436	268	163	162	368
2500	65.0	479	300	184	185	400
2600	68.0	494	312	193	195	411
2700	71.0	509	324	200	204	425
2800	76.0	527	343	213	217	444
2900	79.0	541	459	223	229	459
3000	84.0	551	372	230	236	472
3100	87.5	557	387	237	245	485
3200	91.0	567	401	246	254	497
3300	96.0	590	427	265	275	525
3400	100.0	593	440	268	279	535

BCP 9810-B-3-1 (cont'd)

	End Shortening x 10^{-4}	Axial Strain at Gage Number				
		1	2	3	4	5
5000	181.0	782	329	-	437	915
5010	Buckled					

BCP 9810-B-3-2 (cont'd)

Axial Load (lb)	End Shortening x 10^{-4}	Axial Strain at Gage Number				
		1	2	3	4	5
3500	105.0	603	461	281	295	556
3600	108.0	608	472	286	298	564
3700	112.5	615	488	293	306	580
3800	117.0	620	509	300	314	595
3900	123.0	623	536	309	324	618
4000	129.0	619	578	321	338	641
4100	135.0	628	611	333	349	657
4200	138.5	637	635	341	359	674
4300	144.0	650	662	351	370	701
4400	148.5	650	691	358	378	729
4500	154.0	660	719	364	383	749
4600	159.0	662	757	369	390	785
4700	165.0	654	788	369	389	804
4800	170.0	662	820	382	404	838
4900	176.0	672	850	390	412	-
5000	181.0	686	881	403	427	-
5100	185.0	694	897	408	535	-
5200	193.0	699	932	416	513	-
5300	196.5	705	953	424	516	-
5400	203.0	712	977	431	516	-
5500	208.0	712	1006	436	519	-
5600	214.0	709	1033	439	523	-
5700	Buckled just as this load was reached					

BCP 9824-A-3-1 AS

Axial Load(lb)	End Shortening x 10^{-4}	Axial Strain at Gage Number				
		1	2	3	4	5
50	0.0	0	0	-	0	0
250	4.5	42	24	-	19	49
500	8.2	112	67	-	47	113
750	18.0	179	139	-	66	179
1000	28.0	230	195	-	79	198
1250	41.0	299	255	-	103	252
1500	54.0	366	303	-	131	305
1750	68.0	435	345	-	173	353
2000	81.0	503	399	-	224	406
2250	93.0	558	453	-	263	460
2500	105.0	616	507	-	299	519
2750	120.0	681	577	-	331	601
3000	131.0	726	623	-	358	663
3250	142.0	774	681	-	380	737
3500	152.0	826	742	-	409	816
3750	166.0	880	805	-	428	907
4000	177.0	933	884	-	480	1008
4100	181.0	972	904	-	485	1037
4200	186.0	984	918	-	485	1063
4300	191.5	1003	937	-	485	1100

BCP 9824-A-3-2 AS

	End Shortening x 10^{-4}	Axial Strain at Gage Number				
		1	2	3	4	5
50	0.0	0	0	0	0	0
250	3.0	51	34	27	30	46
500	9.0	79	93	76	78	116
750	16.0	145	146	104	98	182
1000	24.0	183	184	134	119	253
1250	35.0	226	225	166	150	335
1500	46.0	260	254	184	162	390
1750	57.0	300	290	211	184	452
2000	67.0	355	339	251	216	528
2250	79.0	416	398	296	253	613
2500	90.0	466	456	332	282	689
2750	106.0	511	527	370	312	746
3000	118.0	552	596	404	341	798
3250	131.0	590	669	453	387	834
3500	145.0	622	746	500	444	862
3750	159.0	643	847	572	537	945
4000	170.0	691	905	605	584	1008
4100	176.0	673	910	594	583	1017
4200	180.0	683	940	612	610	1042
4300	184.0	707	975	638	642	1087

BCP 9824-A-3-1 AS (cont'd)

Axial Load(lb)	End Shortening x 10^{-4}	Axial Strain at Gage Number				
		1	2	3	4	5
4400	196.0	1016	955	-	489	1122
4500	199.0	1030	968	-	489	1147
4600	205.0	1052	990	-	500	1173
4700	210.0	1068	1002	-	493	1193
4750	Buckled					

BCP 9824-A-3-2 AS (cont'd)

	End Shortening x 10^{-4}	Axial Strain at Gage Number				
		1	2	3	4	5
4400	188.0	719	999	648	663	1112
4500	192.0	726	1027	660	688	1142
4600	200.0	733	1053	673	713	1166
4700	206.0	750	1076	689	741	1201
4800	209.0	767	1104	706	769	1229
4900	214.0	782	1130	720	796	1259
5000	220.0	793	1158	732	828	1295
5100	226.0	808	1179	747	861	1334
5200	231.0	815	1187	751	878	1356
5300	237.0	832	1202	766	902	1387
5400	241.0	852	1219	785	929	1430
5500	247.0	871	1236	800	941	1454
5600	252.0	886	1246	825	952	1480
5700	259.0	922	1270	866	980	1510
5800	265.0	943	1275	896	998	1520
5900	271.0	965	1282	922	1020	1523
6000	277.0	981	1292	960	1046	1533
6100	283.0	1036	1329	1016	1088	1569
6200	299.0	1063	1346	1048	1100	1575
6300	302.0	1101	1355	1117	1087	1536
6400	311.0	1138	1359	1157	Buckled	

IMPERFECTION MEASUREMENTS

(x 10^{-3} in)

BCP 9824-A-3-1 AS

	4	0	3	0	-8	-4	-5	-3
	4	-4	0	-4	-10	-6	-1	0
	6	-2	4	-2	-9	-3	3	4
	12	3	7	5	-4	2	11	11
	13	4	8	6	-1	5	11	14
	12	8	7	7	2	8	12	14
	10	10	8	12	6	11	11	12

BCP 9824-A-3-2 AS

	4	1	5	0	-1	0	-5	-5
	0	4	2	3	0	2	-2	-2
	10	0	7	5	1	4	-1	0
	16	4	10	9	5	8	5	6
	20	8	13	13	10	10	10	12
	18	8	11	14	11	13	12	12
	16	12	12	15	13	14	15	16

BCP 9810-B-3-1 AS

	2	-1	0	0	-3	-2	-3	1
	0	-4	-2	-2	-6	-2	-2	2
	4	-2	-2	-1	-5	1	6	8
	10	1	1	3	-3	5	12	12
	11	4	4	7	-1	7	14	15
	12	3	5	5	0	9	16	15
	10	6	7	7	2	8	10	13

BCP 9810-B-3-2 AS

	-3	-1	-2	0	-1	0	-1	-1
	-7	-4	1	0	-3	-2	0	-2
	-10	-3	3	3	-3	0	1	1
	-12	-1	7	5	1	4	5	5
	-13	0	7	6	3	5	7	7
	-10	2	8	6	3	7	6	8
	-2	8	9	13	11	15	15	17

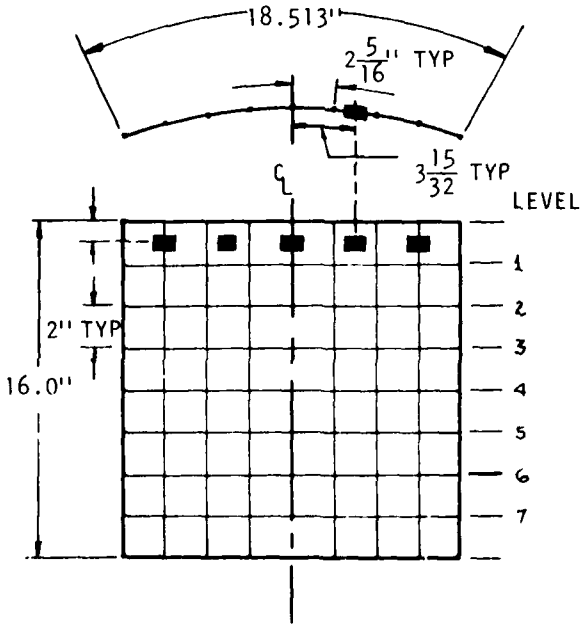

A-4 EXPERIMENTAL DATA FOR 16 x 12 PANELS WITH SIMPLY-SUPPORTED STRAIGHT EDGES

BCP 9921-A8-2 DS

Axial Load(lb)	End Shortening x 10^{-4}	Axial Strain at Gage Number				
		1	2	3	4	5
50	0	-	0	0	0	0
250	5.0	-	44	37	38	60
500	11.0	-	75	69	71	134
750	21.5	-	105	99	97	218
1000	31.0	-	137	133	131	313
1250	41.0	-	174	171	168	392
1500	53.5	-	220	204	210	454
1750	68.5	-	298	240	257	519
2000	80.0	-	394	279	309	592
2250	92.0	-	491	329	368	673
2500	103.0	-	571	375	428	738
2600	110.0	-	605	392	453	761
2700	117.5	-	640	414	481	788
2800	120.0	-	667	431	505	811
2900	126.5	-	698	454	535	841
3000	131.0	-	733	478	566	873
3100	137.5	-	768	502	599	905
3200	141.0	-	798	521	623	927
3300	147.0	-	833	548	658	962
3400	151.0	-	860	566	682	982

BCP 9921-A8-1 DS

	End Shortening x 10^{-4}	Axial Strain at Gage Number				
		1	2	3	4	5
50	0	0	0	0	0	0
250	5.5	49	39	35	39	65
500	19.0	161	87	76	78	171
750	33.0	257	128	110	128	262
1000	48.0	359	179	151	187	375
1250	64.0	447	222	181	228	732
1500	81.0	546	280	215	267	819
1750	94.5	630	345	249	298	892
2000	113.5	718	417	284	337	971
2250	129.0	800	496	315	377	1049
2500	146.0	1065	590	369	434	1103
2750	163.0	1153	674	422	498	1138
3000	181.0	1040	775	482	570	1126
3100	187.5	1282	824	516	599	1145
3200	195.5	-	859	544	620	1163
3300	206.0	-	917	587	627	1156
3400	215.5	-	962	618	626	1144
3500	Buckled					

BCP 9921-A8-2 DS (cont'd)

Axial Load(lb)	End Shortening x 10^{-4}	Axial Strain at Gage Number				
		1	2	3	4	5
3500	158.0	-	891	589	709	1007
3600	161.5	-	927	616	744	1040
3700	169.0	-	959	640	777	1075
3800	173.0	-	991	666	808	1103
3900	179.5	-	1017	686	835	1123
4000	184.5	-	1051	714	871	1159
4100	191.5	-	1091	749	907	1199
4200	193.5	-	1115	769	932	1227
4300	201.0	-	1153	799	965	1254
4400	206.0	-	1181	824	996	1287
4500	211.0	-	1212	850	1025	1313
4600	218.0	-	1248	881	1058	1341
4700	221.5	-	1271	900	1075	1357
4800	223.0	-	1304	931	1114	1395
4900	231.5	-	1332	959	1143	1420
5000	238.5	-	1359	985	1172	1450
5100	241.0	-	1384	1009	1196	1471
5200	248.5	-	1409	1034	1225	1500
5300	253.5	-	1438	1064	1253	1531
5400	259.5	-	1456	1082	1273	1550
5500	265.5	-	1473	1111	1298	1572
5575	Buckled					

BCP 9810-B-1-1 DS

Axial Load(lb)	End Shortening x 10^{-4}	Axial Strain at Gage Number				
		1	2	3	4	5
50	0	0	-	0	0	0
250	4.0	34	-	21	22	35
500	9.0	91	-	52	50	96
750	18.0	146	-	69	71	171
1000	27.0	195	-	87	91	237
1250	38.0	262	-	110	119	319
1500	48.0	332	-	131	145	390
1750	58.0	404	-	150	168	451
2000	68.0	499	-	175	203	527
2250	79.0	577	-	197	235	566
2500	93.0	666	-	225	282	601
2750	107.0	759	-	256	332	610
3000	118.0	842	-	299	398	639
3100	124.0	872	-	315	428	635
3200	128.0	901	-	331	454	649
3300	133.0	926	-	344	478	659
3400	137.0	953	-	360	505	668
3500	144.0	989	-	384	544	681
3600	147.5	1013	-	397	570	682
3700	152.0	1046	-	420	607	696

BCP 9810-B-1-2 DS

	End Shortening x 10^{-4}	Axial Strain at Gage Number				
		1	2	3	4	5
50	0	0	0	0	0	-
250	3.0	34	21	20	25	-
500	11.0	105	67	47	51	-
750	20.0	171	114	65	82	-
1000	30.0	228	156	88	112	-
1250	41.0	292	203	113	144	-
1500	52.0	351	256	141	177	-
1750	64.0	414	319	171	213	-
2000	75.0	466	372	188	244	-
2250	88.0	518	427	207	272	-
2500	100.0	569	486	232	313	-
2750	113.0	630	550	273	378	-
3000	125.0	683	610	307	436	-
3250	143.0	740	686	344	530	-
3500	154.0	777	729	362	578	-
3750	166.0	829	788	392	645	-
4000	175.0	875	840	420	688	-
4100	181.5	890	860	424	699	-
4200	184.0	904	876	432	711	-
4300	192.0	940	912	460	732	-

BCP 9810-B-1-1 DS (cont'd)

Axial Load (lb)	End Shortening x 10^{-4}	Axial Strain at Gage Number				
		1	2	3	4	5
3800	158.0	1078	-	441	644	696
3900	162.0	1103	-	468	675	706
4000	166.0	1121	-	473	696	713
4100	170.5	1144	-	493	726	725
4200	175.0	1158	-	505	742	730
4300	179.0	1178	-	522	769	749
4400	186.0	1198	-	544	802	762
4500	189.0	1206	-	554	820	763
4600	196.0	Buckled				

BCP 9810-B-1-2 DS (cont'd)

	End Shortening x 10^{-4}	Axial Strain at Gage Number				
		1	2	3	4	5
4500	203.0	983	959	508	763	-
4600	206.5	1002	977	526	783	-
4700	211.0	1017	989	543	799	-
4710	Buckled					

IMPERFECTION MEASUREMENTS

($\times 10^{-3}$ in)

BCP 9921-A-8-1 DS

	9	8	4	0	4	6	5	1
	10	5	0	-1	2	7	7	5
	10	7	2	-1	7	12	12	11
	15	8	2	2	9	13	14	14
	15	11	8	8	10	15	19	18
	16	13	11	13	16	17	20	22
	19	14	15	18	20	18	20	22

BCP 9921-A-8-2 DS

	-5	-5	-4	0	6	9	3	-3
	-2	-4	-7	-2	4	6	-3	-4
	1	0	-4	-3	6	8	-2	-5
	9	11	3	1	13	15	3	0
	12	12	4	5	16	18	5	3
	16	14	7	9	16	20	9	5
	15	14	9	11	15	15	14	10

BCP 9810-B-1-1 DS

	1	0	1	0	2	1	-1	-1
	3	2	1	-2	0	-1	-2	-2
	11	9	4	-1	4	3	1	3
	23	19	12	5	9	10	10	9
	34	28	12	4	8	12	13	15
	39	29	12	6	12	14	19	19
	36	29	15	10	16	16	19	21

BCP 9810-B-1-2

	3	3	2	0	-1	-10	-16	-20
	5	5	0	1	0	-15	-23	-24
	12	9	3	3	4	-15	-23	-20
	19	18	10	9	8	-10	-18	-13
	21	18	11	10	9	-6	-12	-8
	21	20	13	12	13	0	-3	2
	20	18	17	16	17	10	3	12

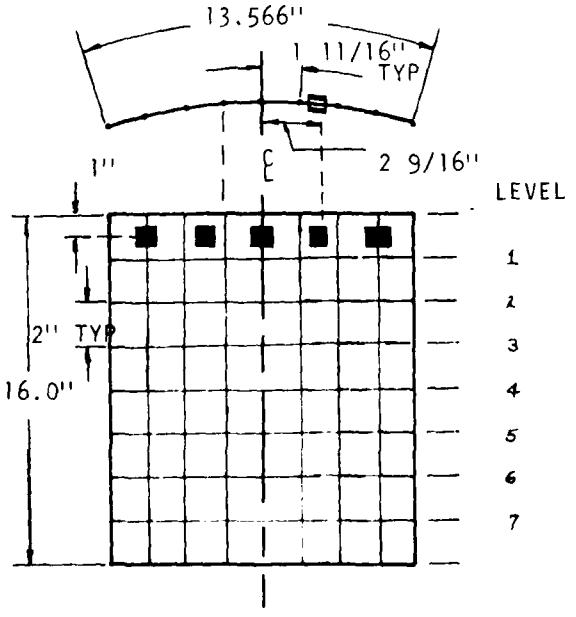

AD-A112 725 DAYTON UNIV OH RESEARCH INST F/G 11/4
EXPERIMENTAL AND NUMERICAL ANALYSIS OF AXIALLY COMPRESSED CIRCU--ETC(U)
OCT 81 N R BAULD F33615-79-C-3030
UNCLASSIFIED AFWAL-TR-81-3158 NL

2 OF 2
AD-A
112 725

END
DATE FILMED
04-82
DTIC

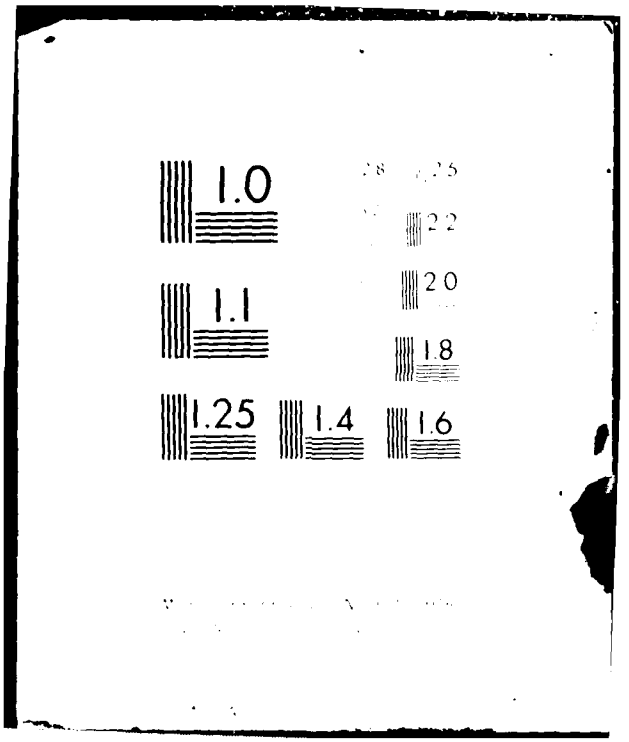
1.0
1.1
1.25
1.4
1.6
2.2
2.0
1.8

A-5 EXPERIMENTAL DATA FOR 16 x 8 PANELS WITH SIMPLY-SUPPORTED STRAIGHT EDGES

BCP 9817-B-7-1 BS

Axial Load(lb)	End Shortening x 10^{-4}	Axial Strain at Gage Number				
		1	2	3	4	5
50	0	0	0	-	0	0
250	4.0	66	56	-	54	71
500	15.0	125	141	-	133	137
750	29.0	208	240	-	212	173
1000	44.0	288	328	-	262	219
1250	60.0	359	398	-	304	292
1500	82.0	436	473	-	349	373
1750	102.0	510	548	-	399	446
2000	127.0	594	613	-	452	518
2250	147.0	675	695	-	505	573
2500*	225.0	1066	-68	-	861	875
2600	238.0	1120	-82	-	920	954
2700	248.0	1139	-83	-	937	974
2800	259.0	1169	-83	-	975	1036
2900	275.0	1233	-92	-	995	1119
3000	303.0	1344	-75	-	864	1272
3100	328.0	1439	-67	-	731	1330
3200	345.0	1506	-54	-	649	1373
3300	361.0	1572	-45	-	568	1417
3400	375.0	1636	-37	-	505	1436

* At 2450 lb some discontinuity in end-shortening vs. load occurred that could not be readily distinguished as bifurcation buckling.

BCP 9817-B-7-2 BS

	End Shortening x 10^{-4}	Axial Strain at Gage Number				
		1	2	3	4	5
50	0	0	0	0	0	0
250	9.0	64	68	53	52	62
500	30.0	187	121	80	73	70
750	51.0	282	185	133	148	110
1000	72.0	385	277	202	231	166
1100	80.0	426	313	226	261	190
1200	88.0	466	353	257	300	224
1300	94.0	489	372	268	318	239
1400	101.0	528	407	297	355	269
1500	108.0	551	430	310	374	278
1600	114.0	588	466	341	414	309
1700	120.0	613	491	362	446	321
1800	126.0	665	541	408	493	362
1900	132.0	691	566	429	518	380
2000	138.0	719	592	451	543	399
2100	142.0	719	592	447	542	394
2200	150.0	770	639	492	589	436
2300	155.0	796	663	513	611	456
2400	162.0	839	707	553	658	501
2500	168.0	871	736	580	688	530

BCP 9817-B-7-1 BS (cont'd)

Axial Load(lb)	End Shortening x 10^{-4}	Axial Strain at Gage Number				
		1	2	3	4	5
3500	389.0	1690	-34	-	442	1447
3600	408.0	1771	-24	-	355	1473
3750	428.0	1857	-13	-	278	1514
4000	459.0	No visible bifurcation				

BCP 9817-B-7-2 BS (cont'd)

	End Shortening x 10^{-4}	Axial Strain at Gage Number				
		1	2	3	4	5
2600	172.5	901	764	605	715	555
2650	177.0	902	772	611	722	560
2700	179.5	923	787	626	738	576
2750	182.0	948	810	648	761	599
2800	184.5	955	817	655	769	605
2850	189.0	975	837	673	788	626
2900	191.5	978	842	677	792	628
2950	194.5	972	832	666	785	620
3000	198.0	982	842	677	796	631
3050	201.0	1010	867	705	821	657
3100	203.0	1020	879	715	832	669
3150	208.0	1033	890	728	844	681
3200	210.5	1042	901	742	857	692
3240	212.5	Buckled				

BCP 9921-A-7-1 BS

Axial Load(lb)	End Shortening x 10^{-4}	Axial Strain at Gage Number				
		1	2	3	4	5
50	0	0	0	0	0	0
500	32.0	24	18	15	16	12
750	56.0	37	28	24	26	24
1000	92.0	54	36	32	33	23
1250	130.0	72	48	41	41	27
1500	165.0	86	63	49	48	30
1750	201.0	1001	781	584	535	393
2000	236.0	1100	882	666	579	475
2250	260.0	1197	980	757	640	563
2500	286.0	1300	1079	854	700	660
2600	293.0	1340	1117	891	729	710
2700	304.0	1385	1162	936	757	762
2300	313.0	1418	1194	968	780	793
2900	322.0	1450	1226	1001	804	823
3000	331.0	1487	1265	1040	835	866
3100	340.0	1523	1304	1078	864	904
3200	349.0	1550	1361	1133	902	961
3300	356 0	1592	1402	1171	946	997
3400	3[illegible]	1621	1448	1212	1000	1046
3440	[illegible]d					

BCP 9921-A-7-2 BS

	End Shortening x 10^{-4}	Axial Strain at Gage Number				
		1	2	3	4	5
50	0	0	-	0	0	0
250	6.0	75	-	54	65	44
500	23.0	204	-	152	127	93
750	37.0	347	-	206	184	143
1000	57.0	543	-	260	237	198
1100	60.0	595	-	287	264	224
1200	66.0	662	-	303	277	251
1300	72.0	737	-	321	294	284
1400	78.0	815	-	339	309	316
1500	84.0	901	-	363	333	355
1600	90.0	974	-	378	347	386
1700	96.0	1044	-	392	360	418
1800	100.0	1096	-	406	374	445
1900	110.0	1180	-	423	393	494
2000	119.0	1275	-	447	420	548
2100	126.0	1351	-	467	441	592
2200	135.0	1416	-	479	457	636
2300	144.0	1500	-	503	487	698
2400	153.0	1571	-	513	505	740
2500	161.0	1640	-	539	540	789

BCP 9921-A-7-2 BS (cont'd)

	End Shorten-ing x 10^{-4}	Axial Strain at Gage Number				
		1	2	3	4	5
2600	170.0	1701	-	556	567	829
2750	182.0	1773	-	595	620	893
2800	187.0	1812	-	618	644	921
2900	191.0	1845	-	640	664	940
3000	200.0	1889	-	669	699	975
3100	209.0	1956	-	716	748	1023
3250	219.0	2006	-	725	764	1036
3300	224.0	2058	-	780	826	1093
3320	Buckled					

IMPERFECTION MEASUREMENTS

($\times 10^{-3}$ in)

BCP 9817-B-7-1 BS

	9	6	0	-3	-7	-5	
	13	10	1	-5	-8	-5	
	18	12	3	-3	-11	-1	
	23	17	7	2	0	3	
	23	17	10	5	4	7	
	21	15	8	7	5	7	
	15	12	9	9	8	9	

BCP 9817-B-7-2 BS

	1	-2	0	1	0	2	
	1	-3	-4	-3	-3	-1	
	6	1	-1	-2	-1	3	
	13	10	5	4	4	7	
	16	9	7	5	6	10	
	20	12	10	10	8	12	
	21	13	15	15	13	15	

BCP 9921-A-7-1 BS

	4	0	0	5	13	15	
	12	1	-2	3	15	19	
	15	3	-1	3	12	19	
	21	9	4	5	13	21	
	22	12	5	4	10	18	
	21	13	7	7	12	17	
	18	13	11	11	12	17	

BCP 9921-A-7-2 BS

	-1	-5	0	9	8	3	
	6	-2	5	25	31	17	
	12	4	15	35	45	31	
	18	11	22	38	41	32	
	23	17	26	36	37	32	
	27	20	25	32	36	38	
	31	27	30	32	33	39	

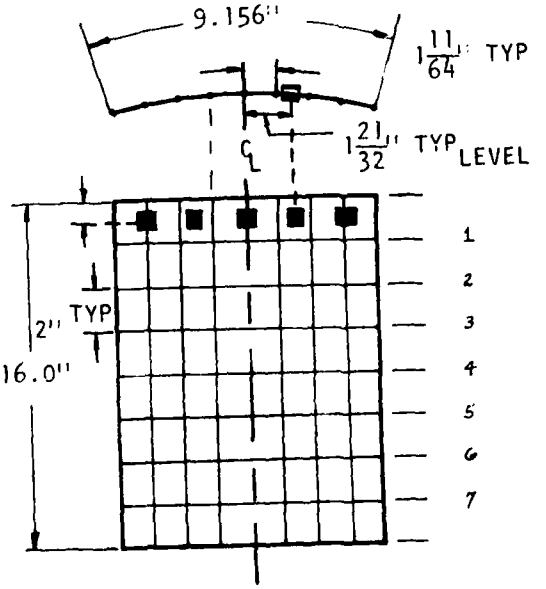

APPENDIX B

STRAIN, END-SHORTENING, AND IMPERFECTION MEASUREMENTS FOR TEST PANELS WITH UNSUPPORTED STRAIGHT EDGES AND CLAMPED CURVED EDGES

TESTING PROGRAM B

B-1 EXPERIMENTAL DATA FOR 8 x 16 PANELS WITH UNSUPPORTED STRAIGHT EDGES*

BCP 9824-A-2-1 CF

Axial Load(lb)	End Shortening x 10^{-4}	Axial Strain at Gage Number				
		1	2	3	4	5
50	0	0	0	0	0	0
250	0	-	39	40	39	47
500	0.9	-	85	91	89	110
750	1.2	-	114	126	125	152
1000	2.0	-	153	165	191	217
1250	3.1	-	196	215	268	282
1500	4.0	-	245	261	331	341
1750	5.1	-	290	297	383	396
2000	6.1	-	347	334	430	457
2250	7.1	-	418	408	476	512
2500	8.6	-	481	487	511	561
2600	9.0	-	505	517	521	573
2700	9.8	-	533	553	542	596
2800	10.0	-	555	580	559	614
2900	10.8	-	574	605	570	626
3000	10.9	-	603	641	591	648
3100	11.3	-	627	672	606	661
3200	12.0	-	656	710	645	680
3300	12.4	-	682	741	644	697
3400	13.0	-	704	768	655	705

BCP 9824-A-2-2 CF

	End Shortening x 10^{-4}	Axial Strain at Gage Number				
		1	2	3	4	5
50	0	0	0	0	0	0
250	0	38	32	31	32	38
500	0.5	98	88	80	94	98
750	1.2	147	143	108	159	139
1000	2.0	180	210	140	232	186
1250	3.0	246	248	185	313	265
1500	4.0	321	293	222	340	337
1750	4.9	420	349	267	383	411
2000	6.0	507	397	309	437	499
2250	7.1	585	441	345	474	574
2500	8.3	668	490	384	523	660
2600	8.8	703	514	403	548	698
2700	9.1	731	532	4k5	567	723
2800	9.4	770	559	438	600	768
2900	9.8	800	573	448	628	803
3000	10.1	828	590	461	655	833
3100	10.4	864	612	477	691	871
3200	11.0	897	630	490	722	909
3300	11.5	933	654	507	758	948
3400	12.0	961	672	519	785	976

* The last letter in a specimen designator (BCP-9824-A-2-1) indicates the fiber pattern. Thus the letter A signifies the pattern [0/±45/90]s and the letter B signifies the pattern [0/90]2s.

BCP 9824-A-2-1 CF (cont'd)

Axial Load(lb)	End Shortening x 10^{-4}	Axial Strain at Gage Number				
		1	2	3	4	5
3500	13.1	-	729	799	670	716
3600	13.8	-	761	841	699	744
3700	14.2	-	782	865	705	742
3800	14.8	-	809	904	734	770
3900	15.0	Buckled				

BCP 9824-A-2-2 CF (cont'd)

Axial Load(lb)	End Shortening x 10^{-4}	Axial Strain at Gage Number				
		1	2	3	4	5
3500	12.3	989	687	528	811	1004
3600	12.7	1017	707	542	838	1027
3700	13.0	1050	730	560	875	1062
3800	13.3	1085	748	573	913	1098
3900	13.8	1120	770	589	952	1133
3975	Buckled					

BCP 9810-B-4-1 CF

Axial Load(lb)	End Shortening x 10^{-4}	Axial Strain at Gage Number				
		1	2	3	4	5
25	0	-	0	0	0	0
200	0.5	-	25	20	18	28
400	1.0	-	54	48	43	59
600	1.4	-	86	78	68	89
800	2.0	-	120	109	91	116
1000	2.5	-	161	148	113	149
1100	3.0	-	180	167	126	167
1200	3.0	-	201	184	134	181
1300	3.5	-	223	204	149	201
1400	4.0	-	251	215	159	219
1500	4.2	-	278	220	170	236
1600	4.9	-	309	229	179	248
1700	5.1	-	333	240	189	259
1800	5.5	-	357	253	202	270
1900	6.0	-	382	266	213	287
2000	6.5	-	410	280	223	301
2050	6.9	-	419	286	228	304
2100	7.0	-	427	294	236	313
2150	7.2	-	435	301	242	321
2200	7.4	-	440	303	244	324

BCP 9810-B-4-2 CF

Axial Load(lb)	End Shortening x 10^{-4}	Axial Strain at Gage Number				
		1	2	3	4	5
50	0	0	0	0	0	0
500	0.2	43	57	72	67	72
750	1.1	71	93	110	107	115
1000	2.1	87	126	119	154	165
1250	3.1	109	167	151	196	213
1500	4.1	134	207	173	247	269
1750	5.1	149	244	190	277	305
2000	6.0	171	296	220	319	362
2250	7.0	186	341	240	345	412
2500	8.0	201	387	277	382	471
2600	9.8	201	345	344	431	562
2700	10.2	201	315	356	434	573
2750	10.2	204	305	372	447	583
2800	10.9	204	280	400	471	602
2850	11.1	200	263	406	475	607
2900	11.2	200	246	417	482	614
2950	12.0	198	201	449	508	635
3000	12.7	158	177	463	512	645
3050	13.0	141	149	483	521	654
3100	13.2	137	123	502	531	663

BCP 9810-B-4-1 CF (cont'd)

Axial Load(lb)	End Shortening x 10^{-4}	Axial Strain at Gage Number				
		1	2	3	4	5
2250	7.7	-	447	311	251	332
2300	7.9	-	453	315	255	337
2350	8.0	-	458	321	258	342
2400	8.2	-	463	326	262	348
2450	8.4	-	467	332	267	354
2500	8.8	-	470	340	275	363
2550	9.0	-	473	345	279	370
2600	9.1	-	474	353	286	379
2650	9.3	-	473	357	290	384
2700	9.7	-	471	364	295	390
2750	10.0	-	466	369	299	396
2800	10.1	-	461	376	306	405
2850	10.3	-	453	386	316	416
2900	10.8	-	442	391	319	422
2950	11.0	-	430	396	324	428
3000	11.0	-	405	412	339	447
3100	11.6	-	381	429	354	465
3200	11.2	-	334	439	363	478
3300	12.8	-	302	446	368	485
3400	13.3	-	259	465	388	507

BCP 9810-B-4-2 CF (cont'd)

Axial Load(lb)	End Shortening x 10^{-4}	Axial Strain at Gage Number				
		1	2	3	4	5
3150	13.8	134	96	515	536	669
3250	14.8	138	35	555	546	683
3300	16.0	Buckled				

BCP 9810-B-4-1 CF (cont'd)

Axial Load(lb)	End Shortening x 10^{-4}	Axial Strain at Gage Number				
		1	2	3	4	5
3500	14.0	-	208	477	404	521
3600	14.5	-	174	488	412	536
3700	17.3	-	-69	197	590	606
3800	18.5	-	-119	108	693	641
3850	Buckled					

IMPERFECTION MEASUREMENTS *

($\times 10^{-3}$ in)

BCP 9824-A-2-1 CF

-4	-6	+1	+7	0	-14	-11	-8	-2
-4	-8	-1	0	-3	-15	-12	-7	+2
-5	-10	-6	-7	-9	-19	-14	-9	+1
-9	-11	-12	-9	-11	-19	-13	-8	+3
-10	-13	-13	-12	-13	-15	-13	-1	+9

BCP 9824-A-2-2 CF

+3	-11	-12	-6	0	-3	+6	+18	+13
+3	-8	-12	-8	0	-5	+5	+16	+18
+4	-8	-10	-7	-3	-4	+5	+14	+21
+4	-6	-10	-7	-5	-7	0	+9	+16
+3	-4	-9	-8	-3	-4	+4	+12	+20

BCP 9810-B-4-1 CF

+20	+12	+4	0	0	-1	+2	+3	+8
+22	+14	+5	+1	+2	+2	+6	+9	+16
+21	+12	+4	+1	+1	0	+7	+9	+19
+33	+25	+16	+9	+8	+6	+9	+11	+18
+33	+26	+17	+12	+10	+8	+11	+14	+20

BCP 9810-B-4-2 CF

+1	+1	+8	+5	0	-10	-21	-28	-15
+1	0	+6	+4	-3	-14	-18	-23	-
0	-2	0	0	-6	-13	-18	-19	-24
0	-4	-1	-5	-10	-14	-14	-16	-6
-4	-9	-7	-10	-10	-11	-6	-6	+6

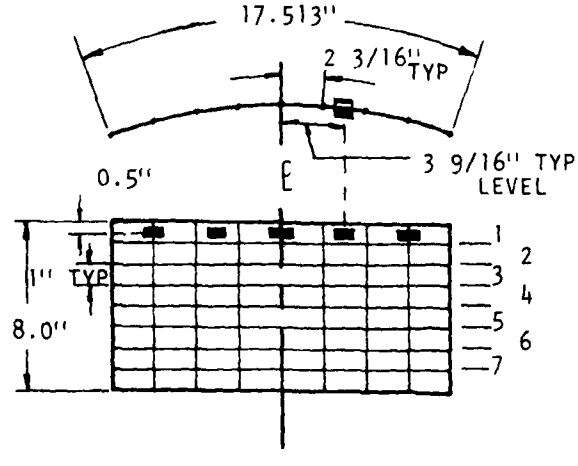

* This imperfection data is questionable. Imperfection measuring device was not mounted accurately enough.

B-2 EXPERIMENTAL DATA FOR 12 x 16 PANELS WITH UNSUPPORTED STRAIGHT EDGES

BCP 9817-B-5-1 EF

Axial Load(lb)	End Shortening x 10^{-4}	Axial Strain at Gage Number				
		1	2	3	4	5
50	0	0	0	0	0	0
250	0.5	29	27	29	25	30
500	1.0	71	59	65	56	65
750	2.0	132	84	92	84	106
1000	3.0	228	110	125	107	140
1250	4.0	320	139	157	133	178
1500	5.0	407	170	192	164	218
1750	6.2	501	194	220	186	261
2000	7.7	590	226	258	219	304
2250	9.0	678	261	296	255	348
2500	10.3	756	288	328	288	382
2600	11.0	790	303	346	308	395
2700	11.8	820	316	361	325	403
2800	12.3	852	333	380	350	406
2900	13.0	880	341	390	365	396
3000	13.8	914	361	415	398	356
3050	14.3	933	372	432	420	322
3100	14.9	940	376	442	434	295
3140	Buckled					

BCP 9817-B-5-2 EF

Axial Load(lb)	End Shortening x 10^{-4}	Axial Strain at Gage Number				
		1	2	3	4	5
25	0	0	0	0	0	0
100	0	13	11	13	9	11
200	0.5	31	25	30	24	27
300	0.8	49	38	45	40	41
400	1.0	69	57	61	57	56
500	1.2	90	61	75	70	73
600	1.6	113	72	89	82	92
700	2.0	140	83	103	91	110
800	2.2	165	96	120	105	128
900	2.6	188	108	134	116	143
1000	3.0	217	122	151	130	164
1100	3.3	246	133	165	141	181
1200	3.8	276	147	181	156	199
1300	4.1	302	157	193	168	213
1400	4.8	334	171	212	185	236
1500	5.1	362	185	230	203	257
1600	5.7	388	198	247	220	276
1700	6.1	420	208	262	233	296
1800	6.8	448	220	278	250	314
1900	7.2	479	231	294	269	335

BCP 9817-B-5-2 EF (cont'd)

Axial Load(lb)	End Shortening x 10^{-4}	Axial Strain at Gage Number				
		1	2	3	4	5
2000	7.8	501	242	309	287	351
2100	8.2	529	250	326	314	377
2200	8.9	553	262	340	342	395
2300	9.2	576	274	357	370	413
2400	9.8	599	284	372	399	430
2500	10.1	621	293	387	432	447
2600	10.8	644	304	401	466	460
2700	11.3	666	314	419	508	464
2800	12.0	688	326	438	550	450
2850	12.3	700	333	449	579	430
2900	12.8	709	340	460	603	412
2950	13.0	717	346	470	630	390
3000	13.5	722	351	480	655	367

BCP 9921-A-6-1 EF

Axial Load(lb)	End Shortening x 10^{-4}	Axial Strain at Gage Number				
		1	2	3	4	5
50	0	0	0	0	-	0
250	0.6	45	41	46	-	52
500	1.9	106	93	83	-	124
750	3.0	166	155	124	-	206
1000	4.0	216	202	164	-	278
1250	5.0	282	271	207	-	377
1500	6.4	348	337	259	-	480
1750	7.8	400	383	300	-	566
2000	9.1	460	433	365	-	640
2100	9.8	481	449	383	-	670
2200	10.2	506	466	413	-	704
2220	Buckled	(Left Side)				
2300	14.8	678	-63	774	-	968
2400	15.3	701	-97	841	-	1012
2500	16.1	731	-139	892	-	1066
2600	17.0	768	-190	966	-	1126
2700	17.9	801	-234	1029	-	1175
2775	Buckled	(Right Side)				

BCP 9921-A-6-2 EF

Axial Load(lb)	End Shortening x 10^{-4}	Axial Strain at Gage Number				
		1	2	3	4	5
50	0	0	0	0	0	0
250	0.8	31	36	37	35	48
500	2.0	94	86	98	86	110
750	3.0	150	141	158	142	174
1000	4.2	212	201	225	204	246
1250	5.8	283	275	297	277	329
1500	7.1	356	347	361	347	406
1750	8.5	433	385	401	413	480
2000	10.0	524	437	446	455	561
2100	10.6	559	467	481	485	601
2200	11.1	593	491	500	505	633
2300	12.0	629	579	530	531	665
2400	12.4	653	532	537	540	680
2500	13.0	680	552	558	560	705
2600	13.8	712	577	583	584	731
2700	14.2	743	601	605	607	753
2800	15.0	774	624	627	631	772
2900	15.5	807	647	647	653	786
3000	16.1	843	673	675	680	789
3050	Buckled					

IMPERFECTION MEASUREMENTS *

($\times 10^{-3}$ in)

BCP 9921-A-6-1 EF

+28	+35	+36	+23	0	-5	+28	+50	+52
+24	+35	+38	+30	+8	+8	+35	+52	+56
+26	+33	+42	+33	+16	+18	+42	+55	+61
+32	+36	+44	+38	+26	+26	+50	+56	+61
+39	+36	+45	+40	+37	+40	+59	+64	+72

BCP 9921-A-6-2 EF

+10	+18	+26	+14	0	+2	+24	+44	+69
+73	+48	+33	+12	+10	+24	+32	+35	+59
+52	+42	+40	+30	+22	+26	+42	+62	+72
+30	+42	+43	+38	+32	+34	+52	+62	+80
+48	+46	+48	+43	+44	+45	+61	+69	+85

BCP 9817-B-5-1 EF

+68	+55	+31	+10	0	+10	+40	+59	+66
+66	+54	+38	+20	+12	+19	+44	+58	+55
+65	+57	+48	+36	+28	+30	+51	+62	+58
+60	+61	+56	+41	+40	+44	+53	+57	+60
+55	+58	+55	+48	+50	+55	+57	+58	+56

BCP 9817-B-5-2 EF

+25	+24	+34	+21	0	+1	+2	+20	+15
+33	+35	+36	+25	+10	+8	+28	+29	+29
+32	+33	+34	+28	+15	+13	+30	+29	+21
+23	+35	+31	+19	+20	+28	+32	+29	+25
+26	+29	+32	+30	+25	+25	+25	+32	+33

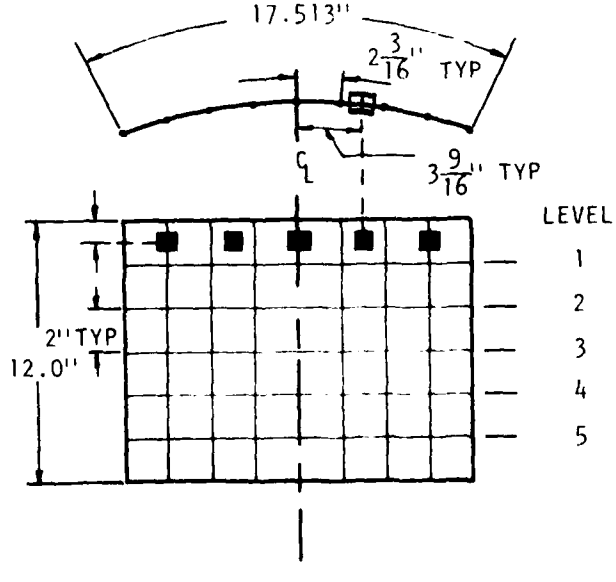

* This imperfection data is questionable. Imperfection measuring device was not mounted accurately enough.

B-3 EXPERIMENTAL DATA FOR 16 x 16 PANELS WITH UNSUPPORTED STRAIGHT EDGES

BCP 9824-A-4-1 AF

Axial Load(lb)	End Shortening x 10^{-4}	Axial Strain at Gage Number				
		1	2	3	4	5
50	0	-	0	0	0	0
250	0.9	-	42	37	38	45
500	1.7	-	74	70	74	69
750	2.5	-	121	117	126	117
1000	3.8	-	172	148	197	161
1250	4.9	-	212	177	270	179
1500	6.0	-	261	211	361	191
1750	7.5	-	325	243	449	208
2000	9.1	-	408	284	541	230
2100	10.0	-	442	296	580	240
2200	10.6	-	474	309	615	247
2300	11.4	-	512	326	656	254
2400	12.4	-	560	347	709	264
2600	13.5	-	618	370	766	270
2700	14.4	-	659	386	820	275
2800	15.1	-	704	407	861	267
2850	16.0	Buckled				

BCP 9824-A-4-2 AF

Axial Load(lb)	End Shortening x 10^{-4}	Axial Strain at Gage Number				
		1	2	3	4	5
50	0	0	0	0	0	-
250	0.7	49	32	43	40	-
500	1.9	118	85	95	100	-
750	3.0	178	137	155	155	-
1000	4.1	235	192	212	212	-
1250	5.3	281	242	264	264	-
1500	6.7	337	300	330	329	-
1750	7.9	385	347	378	381	-
2000	9.0	430	387	402	424	-
2100	9.9	457	416	436	457	-
2200	10.2	475	431	448	465	-
2300	11.0	501	461	481	494	-
2400	11.8	523	484	505	517	-
2500	12.5	552	499	523	534	-
2600	13.1	571	525	552	561	-
2700	14.0	584	543	571	579	-
2750	Buckled					

BCP 9817-B-8-1 AF*

Axial Load(lb)	End Shortening x 10^{-4}	Axial Strain at Gage Number				
		1	2	3	4	5
100	0	0	0	0	0	0
250	0.1	35	-	-	20	-2
500	3.1	185	-	-	3	-53
600	4.5	219	-	-	3	-70
700	5.0	240	-	-	5	-75
800	5.3	249	-	-	11	-69
1000	5.1	244	-	-	38	-47
1200	4.8	230	-	-	77	-20
1400	4.0	214	-	-	104	+10
1600	2.7	197	-	-	128	43
1800	1.4	172	-	-	158	70
2000	0.0	160	-	-	196	99
2200	-1.1	138	-	-	223	110
2400	-3.0	117	-	-	275	115
2500	-6.5	185	-	-	406	102
2600	-7.5	196	-	-	440	92
2650	-8.0	206	-	-	460	86
2700	-8.9	277	-	-	475	77
2750	-13.0	293	-	-	41	125

BCP 9817-B-8-2 AF*

Axial Load(lb)	End Shortening x 10^{-4}	Axial Strain at Gage Number				
		1	2	3	4	5
100	0	0	0	0	0	0
250	1.0	50	42	28	-4	-8
500	4.3	150	141	74	-20	-51
600	5.5	181	179	91	-23	-64
700	6.1	207	215	107	-21	-65
800	6.6	226	243	120	-18	-60
900	6.5	242	271	132	-13	-65
1000	6.1	262	293	148	3	-50
1200	5.2	266	331	175	27	-25
1400	4.0	281	369	204	57	0
1600	3.0	277	413	240	91	33
1700	2.5	277	435	257	108	46
1800	2.0	280	454	272	122	65
1900	1.1	286	474	287	137	80
2000	0.4	280	500	309	156	96
2100	-0.4	281	521	324	160	125
2200	-1.0	282	543	343	175	145
2300	-2.0	282	567	363	203	164
2400	-2.5	281	593	385	221	181
2500	-3.0	278	618	406	230	196

* These data were obtained before the large aluminum lock-nuts were installed on the Tinius-Olsen testing machine.

BCP 9817-B-8-2 AF (cont'd)

Axial Load(lb)	End Shortening x 10^{-4}	Axial Strain at Gage Number				
		1	2	3	4	5
2600	-3.8	279	643	429	246	206
2700	-4.2	278	669	452	264	212
2800	-5.0	275	697	477	278	220
2900	-5.9	273	725	502	282	226
3000	-6.3	271	750	524	295	233
3100	*	184	9	709	256	310

IMPERFECTION MEASUREMENTS*

(x 10^{-3} in)

BCP 9824-A-4-1 AF

+31	+22	+15	+5	0	-2	+5	+10	+11
+32	+25	+16	+4	-2	+1	+8	+13	+20
+34	+26	+19	+6	+4	+4	+11	+17	+22
+39	+31	+22	+10	+8	+10	+19	+25	+29
+45	+35	+27	+16	+14	+17	+26	+30	+37
+45	+37	+29	+21	+22	+24	+33	+40	+46
+43	+37	+34	+28	+31	+33	+43	+50	+62

BCP 9824-A-4-2 AF

+28	+16	+10	0	0	-5	+2	+6	+7
+28	+19	+12	+2	+1	-4	+4	+10	+6
+26	+21	+16	+[illegible]	-2	0	+11	+13	+6
+30	+30	+27	+16	+11	+15	+31	+28	+16
+34	+31	+32	+22	+17	+23	+39	+34	+18
+32	+33	+34	+23	+19	+25	+41	+36	+16
+34	+36	+36	+28	+29	+32	+47	+42	+38

BCP 9817-B-8-1 AF

+30	+14	+6	0	0	-1	+5	+15	+30
+29	+16	+9	+3	+5	+2	+7	+22	+38
+38	+25	+16	+10	+10	+10	+15	+28	+40
+47	+33	+25	+19	+18	+19	+24	+34	+41
+60	+43	+36	+29	+28	+30	+34	+39	+46
+69	+50	+44	+38	+36	+38	+41	+45	+48
+71	+58	+51	+44	+42	+45	+50	+50	+57

BCP 9817-B-8-2 AF

+151	+139	+92	+43	0	-38	-66	-96	-133
+179	+132	+88	+45	+3	-25	-50	-72	-100
+167	+127	+88	+53	+21	-9	-30	-42	-55
+158	+124	+90	+59	+33	+11	-5	-11	-11
+145	+117	+90	+65	+46	+28	+16	+16	+21
+130	+111	+90	+72	+62	+46	+38	+43	+52
+114	+103	+90	+75	+67	+61	+60	+67	+75

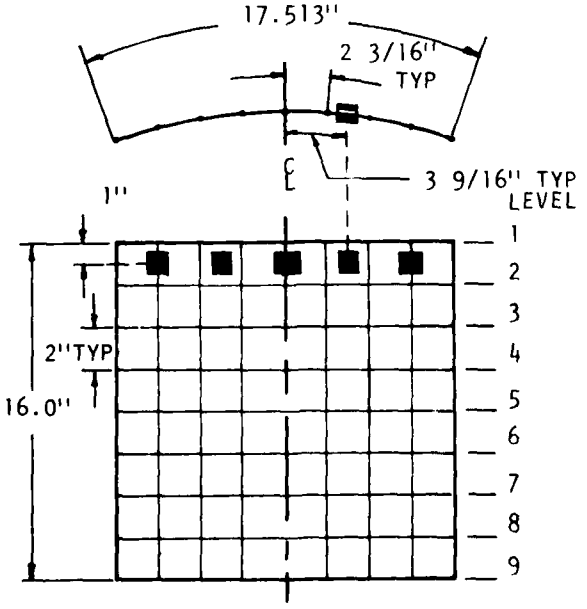

* This imperfection data is questionable. Imperfection measuring device was not mounted accurately enough.

B-4 EXPERIMENTAL DATA FOR 16 x 12 PANELS WITH UNSUPPORTED STRAIGHT EDGES

BCP 9824-A-1-1 DF*

Axial Load(lb)	End Shortening x 10^{-4}	Axial Strain at Gage Number				
		1	2	3	4	5
100	0	0	0	0	0	0
300	-1.1	96	77	56	23	-5
500	-3.0	216	196	96	17	-31
600	-3.6	282	253	115	18	-36
700	-4.0	340	305	138	32	-3
800	-4.0	399	350	163	56	-16
900	-3.3	452	394	187	79	+6
1000	-2.4	490	429	208	98	43
1100	-1.1	524	469	234	123	87
1200	-0.2	548	508	260	137	125
1300	+0.9	569	550	290	159	163
1400	1.8	588	593	322	177	200
1500	3.0	612	666	353	210	311
1600	4.0	630	715	381	247	348
1700	5.1	650	765	409	288	388
1800	6.4	668	815	438	335	423
1900	7.8	687	867	466	385	455
2000	9.0	705	916	492	431	487
2100	10.3	723	966	516	482	514
2200	12.0	744	1018	539	542	543

BCP 9824-A-1-2 DF*

Axial Load(lb)	End Shortening x 10^{-4}	Axial Strain at Gage Number				
		1	2	3	4	5
100	0	0	0	0	0	0
300	-1.0	110	65	-	50	-8
500	-4.0	295	125	-	109	-39
600	-4.1	394	157	-	135	-27
700	-4.1	461	188	-	154	-3
800	-4.0	505	213	-	167	+26
900	-3.1	543	252	-	185	64
1000	-2.3	571	287	-	198	93
1100	-1.5	594	323	-	214	121
1200	-0.5	614	358	-	234	136
1300	+0.5	637	396	-	260	157
1400	1.8	657	431	-	285	166
[illegible]	3.0	674	471	-	309	176
[illegible]	4.0	692	516	-	341	184
1700	5.2	705	563	-	368	188
1800	6.8	720	610	-	395	190
1900	8.1	734	662	-	426	191
2000	9.7	739	722	-	460	187
2090	11.8	Buckled				

* These data were taken before the large aluminum lock-nuts were installed on the Tinius-Olsen testing machine.

BCP 9825-A-1-1 DF (cont'd)

Axial Load(lb)	End Shortening x 10^{-4}	Axial Strain at Gage Number				
		1	2	3	4	5
2300	13.0	766	1063	555	596	565

BCP 9817-B-6-1 DF*

Axial Load(lb)	End Shortening x 10^{-4}	Axial Strain at Gage Number				
		1	2	3	4	5
25	0	6	4	8	13	-1
200	1.0	36	32	43	44	24
400	1.7	70	71	86	80	53
600	2.6	104	118	139	126	85
700	3.0	107	128	152	131	85
800	3.7	115	151	182	151	104
900	4.1	130	179	220	174	129
1000	4.9	148	204	254	186	154
1100	5.6	185	222	286	194	190
1200	6.3	250	260	316	221	237
1300	7.2	284	309	310	245	270
1400	8.1	314	361	327	273	302
1500	9.1	338	413	362	300	329
1600	10.1	359	466	381	327	355
1700	11.1	383	537	405	358	380
1750	11.6	381	559	409	366	383
1800	12.1	385	598	423	384	396
1850	12.9	383	639	436	404	409
1900	13.4	365	701	459	434	431
1930	16.0	297	625	399	472	443

BCP 9817-B-6-2 DF*

Axial Load(lb)	End Shortening x 10^{-4}	Axial Strain at Gage Number				
		1	2	3	4	5
100	0	0	0	0	0	0
300	-2.0	70	-	39	8	-32
500	-4.0	142	-	66	2	-55
600	-4.5	157	-	72	2	-54
700	-5.0	187	-	94	12	-52
800	-5.0	206	-	111	28	-40
900	-4.3	213	-	125	39	-23
1000	-4.0	220	-	142	55	-3
1100	-3.0	226	-	160	78	+19
1200	-2.1	226	-	178	102	38
1300	-1.6	224	-	198	129	54
1400	-0.9	224	-	221	156	68
1500	0.0	224	-	243	177	76
1600	1.0	223	-	268	204	81
1700	1.9	221	-	296	231	84
1800	2.9	219	-	322	252	84
1900	3.8	216	-	354	288	83
2000	4.8	212	-	388	321	79
2100	5.9	202	-	427	358	73
2110	7.0	Buckled				

* These data were taken before the large aluminum lock-nuts were installed on the Tinius-Olsen testing machine.

IMPERFECTION MEASUREMENTS *

($\times 10^{-3}$ in)

BCP 9817-B-6-1 DF

+19	+12	+6	+3	0	0	0	0	-10
+12	+6	-2	-7	-9	-6	-6	-3	-9
+10	+4	-5	-10	-12	-9	-6	+2	+3
+12	+6	-1	-6	-11	-6	-2	+12	+21
+11	+7	0	-3	-7	-5	+3	+18	+31
+5	+2	-3	-4	-9	-5	+3	+19	+31
+14	+9	+6	+4	0	+2	+7	+16	+23

BCP 9824-A-1-2 DF

-10	-12	-16	-11	0	-11	-3	-3	0
-15	-16	-20	-13	-9	-12	-12	-1	+7
-14	-15	-16	-12	-11	-9	-8	0	+13
-9	-10	-11	-8	-7	-6	-4	+7	+17
+1	+1	-3	-2	0	+3	+4	+14	+29
+11	+5	-1	+2	+4	+3	+6	+17	+30
+17	+12	+6	+11	+12	+15	+20	+28	+38

BCP 9824-A-1-1 DF

+7	0	+2	+5	0	-1	-2	+6	+18
+6	+3	+1	+3	+3	+3	-4	+5	+18
+8	+5	+6	+7	+6	+2	+1	+8	+20
+13	+11	+10	+12	+9	+6	+8	+15	+23
+19	+18	+14	+16	+16	+15	+14	+22	+29
+24	+20	+18	+20	+20	+19	+21	+28	+36
+30	+27	+25	+25	+29	+28	+32	+40	+50

BCP 9817-B-6-2 DF

+19	+13	+10	+8	0	+2	+4	+10	+15
+16	+12	+8	+5	-4	-5	-1	+11	+22
+15	+10	+6	+3	-7	-9	-5	+9	+24
+18	+14	+9	+4	-5	-7	-2	+12	+26
+17	+14	+9	+5	-4	-6	-1	+13	+22
+14	+11	+7	+2	-4	-8	+1	+10	+17
+8	+8	+7	+5	+2	+7	+10	+18	+25

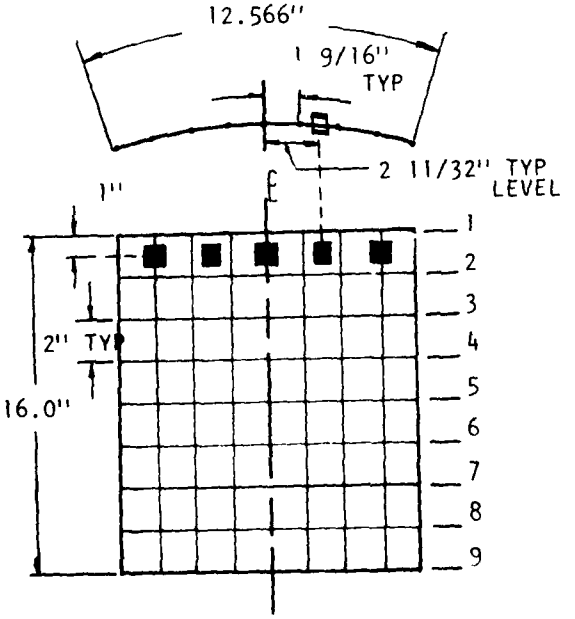

* This imperfection data is questionable. Imperfection measuring device was not mounted accurately enough.

B-5 EXPERIMENTAL DATA FOR 16 x 8 PANELS WITH UNSUPPORTED STRAIGHT EDGES

BCP 9921-A-7-1 BF

Axial Load(lb)	End Shortening x 10^{-4}	Axial Strain at Gage Number				
		1	2	3	4	5
25	0	0	0	0	0	0
100	0.6	19	26	35	36	35
200	1.4	35	63	81	78	76
300	2.6	46	107	122	125	129
350	3.0	55	137	149	154	163
400	3.9	59	153	168	174	190
450	4.5	67	199	217	222	241
500	5.2	99	221	245	248	266
550	6.0	102	235	269	271	289
600	6.8	103	257	294	294	312
650	7.4	99	266	314	315	332
700	8.2	105	291	349	349	364
750	9.2	109	308	378	386	391
800	10.6	104	326	423	442	413
850	12.8	56	331	512	541	438
	Buckled					

BCP 9921-A-7-2 BF

Axial Load(lb)	End Shortening x 10^{-4}	Axial Strain at Gage Number				
		1	2	3	4	5
25	0	0	0	0	0	0
100	0.9	19	18	22	33	25
200	1.8	54	52	64	90	65
250	2.2	73	74	93	128	90
300	2.8	87	93	119	165	108
350	3.2	106	114	147	207	128
400	4.0	118	127	172	252	146
450	4.5	132	142	200	293	163
500	5.1	145	157	229	344	180
550	6.0	153	169	256	387	191
600	6.5	164	187	291	437	203
650	7.2	170	200	321	485	213
700	8.0	179	217	359	536	225
750	8.8	185	236	400	583	234
800	9.7	185	250	441	645	238
850	10.4	185	263	482	697	243
875	11.0	185	270	507	727	247
900	11.4	184	283	538	762	255
925	12.0	183	282	547	773	250
950	12.5	180	295	596	826	255

BCP 9921-A-7-2 BF (cont'd)

Axial Load(lb)	End Shortening x 10^{-4}	Axial Strain at Gage Number				
		1	2	3	4	5
1000	13.7	169	306	653	891	256
1025	14.0	157	308	694	938	256
1046	15.5	Buckled				

BCP 9817-B-7-1 BF

Axial Load(lb)	End Shortening x 10^{-4}	Axial Strain at Gage Number				
		1	2	3	4	5
5						
100						
200						
300						
400						
500						
600						
650						
700						
750						
800						
825						
850						
875						
900						
925						
950						
975						
1000						
1025						

BCP 9817-B-7-2 BF

Axial Load(lb)	End Shortening x 10^{-4}	Axial Strain at Gage Number				
		1	2	3	4	5

BCP 9817-B-7-1 BF

Axial Load(lb)	End Shortening x 10^{-4}	Axial Strain at Gage Number				
		1	2	3	4	5
5	0	0	-	0	0	0
100	0.7	20	-	26	25	26
200	1.2	43	-	58	55	53
300	1.9	65	-	85	83	81
400	2.8	86	-	121	121	117
500	3.6	106	-	166	182	161
600	4.8	116	-	216	259	183
650	5.2	116	-	246	302	187
700	6.0	118	-	276	340	191
750	6.8	114	-	311	384	191
800	7.5	109	-	348	427	188
825	8.0	106	-	365	447	187
850	8.5	104	-	384	468	186
875	9.0	101	-	406	492	186
900	9.6	97	-	429	515	183
925	10.0	95	-	448	536	183
950	10.5	89	-	469	558	180
975	11.0	85	-	492	584	180
1000	12.0	79	-	517	612	180
1025	12.6	72	-	541	637	178

BCP 9817-B-7-2 BF

Axial Load(lb)	End Shortening x 10^{-4}	Axial Strain at Gage Number				
		1	2	3	4	5
5	0	0	0	0	0	0
100	0.7	20	23	24	26	25
200	1.3	52	55	58	61	54
300	2.1	70	74	83	87	75
400	3.1	101	109	123	138	96
500	4.3	124	138	168	194	114
550	5.0	134	152	195	225	123
600	5.6	139	169	225	258	128
650	6.1	144	184	252	289	134
700	7.0	138	191	277	317	132
750	7.6	147	215	319	361	153
775	8.0	141	217	332	373	153
800	8.3	138	220	342	385	147
825	8.8	133	222	356	400	147
850	9.1	128	228	374	418	150
875	9.6	127	240	399	443	156
900	10.0	129	245	415	459	154
925	10.3	120	245	432	474	146
950	10.9	122	262	458	500	151
975	11.3	113	262	476	520	148

BCP 9817-B-7-1 BF (cont'd)

Axial Load(lb)	End Shortening x 10^{-4}	Axial Strain at Gage Number				
		1	2	3	4	5
1050	13.5	60	-	573	671	173
1065	15.0	Buckled				

BCP 9817-B-7-2 BF (cont'd)

Axial Load(lb)	End Shortening x 10^{-4}	Axial Strain at Gage Number				
		1	2	3	4	5
1000	11.8	110	266	496	535	146
1025	12.3	109	278	529	569	144
1050	13.0	109	291	563	599	144
1075	13.9	97	290	601	626	144
1090	15.0	Buckled				

IMPERFECTION MEASUREMENTS

($\times 10^{-3}$ in)

BCP 9921-A-7-1 BF

+30	+27	+22	+14	0	-7	-8	-8	-6
+61	+45	+28	+15	-1	-12	-12	-14	-14
+81	+60	+36	+15	-1	-11	-13	-12	-12
+83	+60	+35	+14	-1	-8	-11	-10	-10
+63	+51	+31	+13	+2	-5	-5	-8	-8
+44	+36	+24	+12	+3	-2	-1	-2	-2
+24	+21	+16	+10	+4	+3	+4	0	+2

BCP 9921-A-7-2 BF

+9	+10	+9	+5	0	-3	-6	-8	-10
+21	+20	+15	+10	0	-10	-20	-29	-36
+34	+25	+17	+11	-4	-16	-26	-40	-57
+39	+30	+21	+11	-2	-14	-26	-48	-71
+36	+33	+24	+12	-3	-16	-26	-43	-64
+33	+30	+22	+12	-2	-12	-17	-25	-38
+21	+19	+13	+7	-3	-8	-8	-11	-15

BCP 9817-B-7-1 BF

+6	+5	+3	+2	0	-2	-3	-8	-12
+12	+8	+3	+2	-1	-5	-8	-10	-16
+13	+8	+3	0	-4	-8	-9	-12	-16
+18	+12	+5	+1	-2	-6	-6	-7	-9
+18	+11	+5	+1	-2	-5	-5	-5	-6
+16	+5	+2	0	-2	-4	-3	-3	-4
+4	+4	+3	+3	+2	0	+1	0	0

BCP 9817-B-7-2 BF

+16	+12	+8	+5	0	+1	+2	+4	-1
+16	+12	+5	-2	-6	-5	0	+5	+2
+20	+13	+8	0	-3	-4	0	+4	+1
+23	+16	+6	+1	-3	-4	-1	+2	-5
+20	+15	+7	+2	-3	-3	-3	-2	-9
+19	+14	+10	+5	0	-1	-2	-2	-13
+14	+12	+10	+8	+4	+3	+2	0	-9

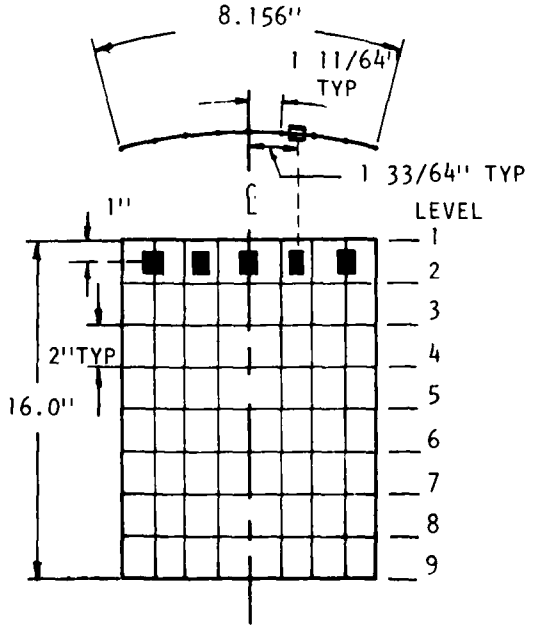

APPENDIX C

STRAIN, END-SHORTENING, AND IMPERFECTION MEASUREMENTS FOR TEST PANELS FOR TESTING PROGRAM B

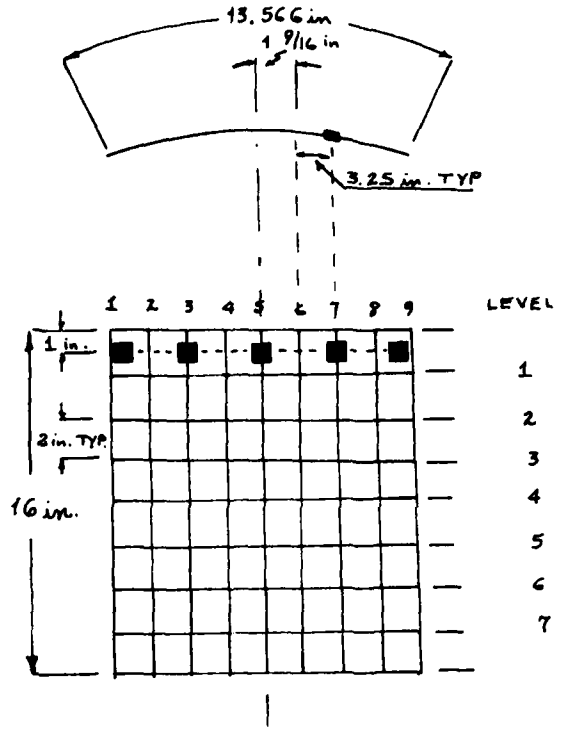

FIGURE Locations for strain and imperfection measurements for 16 x 12 panels with $[0/90]_{2s}$ fiber pattern and unsupported straight edges. For 16 x 12 panels with $[0/\pm45/90]_s$ fiber pattern and simply-supported straight edges only the axial strains at the three interior locations were recorded, and the imperfect data were recorded for the seven interior imperfection grid lines. (Circumferential dimensions shown correspond to the panels with unsupported straight edges. Subtract one inch for simply-supported panels.)

Imperfection measurements ($x10^{-3}$in) for 16x12 panels with fiber pattern $[0/\pm45/90]_s$ and simply-supported straight edges (curved edges clamped). Collapse load in parentheses.

DS-A9-1 (4600 lb) freely

	3	8	8	6	8	6	2	
	-1	7	7	3	4	7	0	
	-2	7	7	3	4	5	-1	
	-2	4	4	3	1	3	-3	
	-4	2	2	-1	-2	1	-2	
	0	2	1	-1	-2	1	-2	
	1	1	0	-1	-2	-1	0	

DS-A9-2 (4975 lb) rounded edges 30 in-lb on side bars

	6	3	3	2	8	6	3	
	5	4	4	3	5	8	7	
	8	4	3	3	4	9	6	
	8	2	3	2	3	7	6	
	4	-2	-2	-1	-1	6	3	
	5	-1	2	2	1	7	3	
	1	1	3	4	3	6	3	

DS-A10-1 (5775 lb) 10 in-lb

	0	4	5	4	7	7	6	
	-4	2	4	4	6	6	9	
	-7	0	7	7	6	7	9	
	-10	-2	3	4	4	4	7	
	-12	-5	2	0	0	3	3	
	-12	-4	1	1	1	1	0	
	-6	-2	0	-1	2	0	-1	

DS-A10-2 (5510 lb) 30 in-lb on side bars

	19	13	6	5	8	12	9	
	33	22	5	2	7	12	10	
	33	28	2	-2	4	15	18	
	30	31	1	-4	2	18	22	
	30	24	0	-10	-3	16	17	
	0	21	-1	-7	-4	10	13	
	19	11	-2	-4	-1	6	8	

DA-A11-1 (5160 lb) nearly freely

	-6	-7	-3	0	0	-6	-2	
	-10	-6	0	5	-1	-8	-8	
	-7	-4	7	10	4	-6	-7	
	-6	-7	6	10	3	-8	-12	
	-10	-10	-1	5	1	-9	-13	
	-6	-7	2	4	0	-7	-8	
	-6	-4	-2	0	0	-4	-7	

Imperfection measurements ($x10^{-3}$in) for 16-12 panels with fiber pattern $[0/90]_s$ and unsupported straight edges (curved edges clamped). Collapse load in parentheses.

DS-B11-1 (2460 lb)

8	8	3	8	9	11	10	11	16
9	7	4	8	10	12	9	9	9
9	6	6	6	8	8	6	6	5
5	2	0	1	2	4	1	3	4
0	2	1	2	3	4	1	6	10
-7	-2	-1	-2	-2	-1	-3	1	6
-7	-3	-3	-3	-3	-3	-3	1	7

DS-B11-2 (2715 lb)

9	6	5	8	6	7	7	8	13
4	3	6	8	9	7	6	10	13
-2	2	7	7	9	8	6	10	12
-8	-2	4	7	7	6	5	8	11
-12	-7	3	6	5	3	2	5	9
-14	-9	0	2	1	1	-1	5	9
-10	-7	0	3	1	1	-2	3	6

DS-B10-1 (2300 lb)

8	3	0	4	8	13	12	13	16
11	5	1	3	9	14	12	9	11
13	6	4	6	10	18	14	9	8
5	-1	-1	0	5	11	8	2	0
4	0	-1	0	4	10	7	0	-2
4	0	-2	-1	3	7	6	0	-4
4	2	-1	1	1	6	4	1	-1

DS-B10-2 (2495 lb)

12	7	5	7	7	9	13	21	33
23	14	10	12	11	13	17	38	33
16	9	5	6	6	8	13	21	31
11	7	5	6	4	8	11	16	23
8	1	3	2	1	4	5	7	10
3	2	1	2	2	4	4	3	5
2	2	1	2	2	3	2	1	4

DS-B9-1 (2165 lb)

-6	-2	3	5	5	10	13	14	23
1	3	6	8	7	13	15	11	11
5	3	3	8	10	14	16	10	8
7	2	1	6	5	9	12	6	2
8	2	-1	3	2	6	6	0	-1
13	4	1	5	6	6	7	4	3
8	3	1	3	3	3	6	3	3

DS-B9-2 (2410 lb)

-4	-2	-2	2	4	8	10	16	23
-1	-1	2	4	7	10	10	16	29
-1	0	2	3	7	12	11	14	23
-1	-2	2	2	5	9	8	12	18
2	1	1	2	3	8	8	10	14
4	3	3	3	3	7	7	9	12
3	1	1	1	1	1	3	4	4

DS-B11-2 $[0/90]_{2s}$ Straight Edges Unsupported

Axial Load lb	End Shortening x 10^{-4} in	Axial Strain at Gage Number				
		1	2	3	4	5
10	0	0	0	0	0	0
100	4.0	12	12	19	16	19
200	8.0	-	27	34	34	41
300	12.2	-	42	50	53	64
400	17.0	-	58	58	63	82
500	21.0	-	69	68	72	97
600	26.0	-	85	87	89	111
700	29.3	-	101	102	104	131
800	33.9	-	118	121	122	152
900	38.0	-	134	146	147	178
1000	43.0	-	151	167	172	198
1100	48.0	-	174	188	202	194
1200	54.0	-	197	211	231	123
1300	60.0	-	225	241	262	44
1400	66.0	-	247	268	283	5
1500	73.5	-	291	311	289	-80
1600	82.0	-	343	346	307	-142
1700	89.0	-	382	370	324	-193
1800	95.5	-	417	398	336	-238
1900	102.5	-	446	429	362	-270

DS-B11-1 $[0/90]_{2s}$ Straight Edges Unsupported

Axial Load lb	End Shortening x 10^{-4} in	Axial Strain at Gage Number				
		1	2	3	4	5
10	0	0	0	0	0	0
100	4.0	15	9	14	13	14
200	8.0	31	12	29	28	34
300	13.0	49	37	48	49	54
400	18.0	65	52	64	63	73
500	23.0	80	71	81	79	93
600	28.0	81	82	98	99	100
700	33.5	33	91	116	118	139
800	40.5	-40	113	138	151	152
900	47.5	-103	131	153	182	105
1000	56.5	-183	155	175	191	25
1100	64.0	-246	176	197	209	-35
1200	72.0	-305	194	217	226	-95
1300	81.0	-373	221	239	242	-168
1400	88.5	-420	247	259	256	-213
1500	96.0	-475	292	281	276	-276
1600	104.5	-531	343	300	291	-325
1700	111.0	-572	378	323	310	-363
1800	119.0	-622	432	340	321	-411
1900	128.0	-678	490	363	341	-456

Continued

DS-B11-2 $[0/90]_{2s}$ Straight Edges Unsupported

Axial Load lb	End Shortening x 10^{-4} in	Axial Strain at Gage Number				
		1	2	3	4	5
2000	109.0	-	495	460	391	-300
2100	115.2	-	531	487	417	-340
2200	122.0	-	568	510	434	-380
2300	128.0	-	601	532	461	-415
2400	136.0	-	649	565	492	-452
2500	142.5	-	681	584	520	-489
2550	146.5	-	701	595	533	-507
2600	151.0	-	725	607	553	-530
2625	152.0	-	729	608	556	-537
2650	154.5	-	739	614	572	-552
2675	157.0	-	755	617	579	-561
2700	159.5	-	766	617	585	-569
2715	buckled					

DS-B11-1 $[0/90]_{2s}$ Straight Edges Unsupported

Axial Load lb	End Shortening x 10^{-4} in	Axial Strain at Gage Number				
		1	2	3	4	5
2000	134.5	-719	532	383	356	-490
2100	142.0	-772	589	408	374	-542
2200	152.0	-828	659	428	392	-588
2250	156.0	-851	683	441	401	-610
2300	161.0	-877	708	451	407	-631
2350	165.5	-904	736	467	420	-657
2400	170.0	-924	754	478	421	-672
2450	175.5	-956	776	500	433	-713
2460	buckled					

DS-B10-1 $[0/90]_{2s}$ Straight Edges Unsupported

Axial Load lb	End Shortening x 10^{-4} in	Axial Strain at Gage Number				
		1	2	3	4	5
10	0	0	0	0	0	0
100	4.0	12	12	8	14	17
200	8.0	24	27	24	31	34
300	13.0	38	41	39	48	51
400	17.0	54	60	57	67	73
500	22.0	66	78	83	71	94
600	27.5	75	102	107	85	112
700	32.0	74	118	127	99	128
800	37.5	63	138	145	112	147
900	43.0	6	160	173	126	163
1000	41.0	10	197	195	147	187
1100	47.5	-24	226	221	164	202
1200	64.0	-65	252	246	180	213
1300	71.0	-113	286	276	197	215
1400	78.0	-152	313	295	207	190
1500	85.0	-193	348	320	232	-50
1600	97.5	-293	409	345	263	-84
1700	106.0	-341	445	368	293	-128
1800	114.0	-390	485	391	326	-168
1900	122.0	-441	522	415	357	-206

DS-B10-2 $[0/90]_{2s}$ Straight Edges Unsupported

Axial Load lb	End Shortening x 10^{-4} in	Axial Strain at Gage Number				
		1	2	3	4	5
0	0	0	0	0	0	0
100	4.2	11	14	15	14	17
200	7.5	24	30	29	31	30
300	13.0	35	48	46	48	40
400	18.0	45	64	62	65	44
500	24.0	53	82	79	85	40
600	31.0	57	104	97	104	28
700	37.0	34	128	117	127	6
800	43.5	-34	152	137	151	-25
900	51.0	-124	188	158	184	-76
1000	58.0	-165	219	178	213	-127
1100	65.6	-205	252	200	245	-176
1200	73.0	-241	283	221	275	-221
1300	80.0	-282	315	240	306	-260
1400	86.5	-322	347	261	337	-291
1500	93.0	-361	378	282	367	-327
1600	99.0	-398	409	301	395	-356
1700	105.0	-438	443	323	424	-382
1800	112.0	-476	476	345	454	-409
1900	118.0	-510	505	365	483	-435

Continued

DS-B10-1 $[0.90]_{2s}$ Straight Edges Unsupported

Axial Load lb	End Shortening x 10^{-4} in	Axial Strain at Gage Number				
		1	2	3	4	5
1950	126.0	-467	544	426	375	-226
2000	130.0	-492	561	439	390	-244
2050	134.0	-514	577	449	404	-261
2100	138.0	-538	596	460	422	-282
2150	141.5	-562	615	470	438	-299
2200	144.5	-585	631	480	455	-317
2250	149.0	-608	646	489	472	-336
2300	155.0	buckled				

DS-B10-2 $[0/90]_{2s}$ Straight Edges Unsupported

Axial Load lb	End Shortening x 10^{-4} in	Axial Strain at Gage Number				
		1	2	3	4	5
2000	124.0	-547	537	386	512	-464
2050	128.0	-568	553	397	528	-476
2100	130.0	-585	572	409	546	-491
2150	133.0	-602	585	418	559	-505
2200	136.0	-618	600	428	575	-518
2250	139.0	-636	615	438	590	-531
2300	142.5	-657	633	448	608	-547
2350	146.0	-671	645	457	623	-559
2400	149.0	-694	664	467	643	-581
2450	153.0	-715	679	474	659	-593
2495	buckled					

DS-B9-1 $[0/90]_{2s}$ Straight Edges Unsupported

Axial Load lb	End Shortening x 10^{-4} in	Axial Strain at Gage Number				
		1	2	3	4	5
0	0	0	0	0	0	0
100	3.0	13	13	14	14	23
200	8.0	17	30	29	27	44
300	13.0	130	46	48	42	71
400	17.5	-	61	64	55	96
500	23.0	-	79	84	68	123
600	28.5	-	98	107	79	149
700	36.0	-	121	131	92	182
800	42.0	-	141	151	106	207
900	49.5	-	169	177	124	234
1000	56.0	-	196	200	140	253
1100	63.0	-	226	220	152	270
1200	70.0	-	257	244	168	286
1300	77.5	-	290	268	184	302
1400	84.0	-	323	288	198	318
1500	90.0	-	357	308	213	333
1600	97.5	-	397	321	225	351
1700	105.0	-	434	342	240	367
1800	112.0	-	473	361	253	382
1900	119.0	-	514	378	265	398

DS-B9-2 $[0/90]_{2s}$ Straight Edges Unsupported

Axial Load lb	End Shortening x 10^{-4} in	Axial Strain at Gage Number				
		1	2	3	4	5
0	0	0	0	0	0	0
100	3.2	15	14	15	16	18
200	7.5	33	29	30	32	37
300	12.5	52	46	47	52	54
400	17.0	71	62	61	69	71
500	21.0	92	78	79	87	85
600	26.0	115	97	98	107	95
700	31.0	138	117	118	128	96
800	37.0	159	137	138	149	49
900	44.0	171	169	157	192	-42
1000	52.5	132	199	180	229	-85
1100	60.0	62	227	202	261	-123
1200	67.5	-30	261	228	299	-176
1300	75.0	-94	292	252	333	-221
1400	82.5	-151	323	276	365	-257
1500	91.0	-206	355	300	397	-295
1600	98.5	-251	384	323	431	-334
1700	107.0	-299	416	348	466	-382
1800	115.5	-345	449	370	502	-430
1900	123.5	-389	481	389	535	-475

Continued

DS-B9-1 $[0/90]_{2s}$ Straight Edges Unsupported

Axial Load lb	End Shortening x 10^{-4} in	Axial Strain at Gage Number				
		1	2	3	4	5
2000	127.0	-	555	398	279	413
2050	131.5	-	576	407	285	419
2100	135.5	-	594	419	294	424
2150	139.5	-	611	432	302	428
2165	buckled					

DS-B9-2 $[0/90]_{2s}$ Straight Edges Unsupported

Axial Load lb	End Shortening x 10^{-4} in	Axial Strain at Gage Number				
		1	2	3	4	5
2000	131.5	-434	514	409	563	-572
2050	135.5	-457	531	421	578	-529
2100	141.0	-479	551	435	588	-536
2150	145.0	-497	567	451	603	-539
2200	148.5	-513	584	464	618	-546
2250	152.0	-525	596	475	634	-561
2300	155.0	-536	608	485	647	-576
2325	156.5	-542	616	491	656	-587
2350	158.0	-552	621	490	658	-598
2375	160.0	-564	620	479	657	-619
2400	162.2	-576	624	477	656	-639
2410	buckled					

Straight Edges
DS-A9-1 $[0/\pm45/90]_s$ Simply-Supported

Axial Load lb	End Shortening x 10^{-4} in	Axial Strain at Gage Number				
		1	2	3	4	5
50	0		0	0	0	
250	7.5		49	47	49	
500	21.0		119	114	116	
750	33.5		197	186	181	
1000	47.0		280	275	236	
1250	60.0		345	347	285	
1500	77.0		420	442	354	
1750	89.0		475	509	401	
2000	101.0		546	586	456	
2250	123.0		616	659	508	
2500	138.0		690	735	572	
2750	152.0		761	803	630	
3000	164.0		820	855	672	
3250	176.5		886	918	732	
3500	189.0		961	987	800	
3750	203.0		1031	1050	866	
3900	212.0		1080	1100	920	
4000	217.0		1101	1108	931	
4100	223.0		1138	1139	970	
4250	230.0		1180	1165	1000	

Straight Edges
DS-A9-2 $[0/\pm45/90]_s$ Simply-Supported

Axial Load lb	End Shortening x 10^{-4} in	Axial Strain at Gage Number				
		1	2	3	4	5
50	0		0	0	0	
250	5.0		43	34	40	
500	13.0		110	84	99	
750	22.0		184	101	128	
1000	35.0		289	140	166	
1250	48.0		393	169	204	
1500	64.0		502	206	253	
1750	77.0		600	235	292	
2000	92.0		703	308	336	
2250	105.0		771	383	368	
2500	120.0		858	481	412	
2750	137.0		938	567	451	
3000	153.0		1018	649	490	
3250	170.0		1107	739	530	
3500	188.0		1181	811	563	
3750	205.0		1263	891	608	
4000	223.0		1336	967	655	
4250	240.0		1416	1047	723	
4500	257.0		1487	1115	794	
4600	263.0		1513	1140	822	

Continued

DS-A9-1 $[0/\pm45/90]_s$ Straight Edges Simply-Supported

Axial Load lb	End Shortening x 10^{-4} in	Axial Strain at Gage Number				
		1	2	3	4	5
4400	248.0		1218	1195	1033	
4500	245.5		1269	1239	1085	
4600	buckled					

DS-A9-2 $[0/\pm45/90]_s$ Straight Edges Simply-Supported

Axial Load lb	End Shortening x 10^{-4} in	Axial Strain at Gage Number				
		1	2	3	4	5
4700	270.0		1545	1170	860	
4800	275.0		1569	1193	888	
4900	282.0		1599	1222	928	
4975	buckled					

DS-A10-1 $[0/\pm45/90]_s$ Straight Edges Simply-Supported

Axial Load lb	End Shortening x 10^{-4} in	Axial Strain at Gage Number				
		1	2	3	4	5
50	0		0	0	0	
250	5.0		43	34	41	
500	13.0		103	78	91	
750	22.0		159	120	134	
1000	32.0		230	178	196	
1250	43.0		296	231	253	
1500	55.0		368	292	320	
1750	67.5		428	341	376	
2000	82.0		505	401	458	
2250	100.0		532	442	558	
2500	118.0		584	492	619	
2750	140.0		633	534	665	
3000	160.0		690	586	716	
3250	182.0		753	639	780	
3500	202.0		814	684	836	
3750	218.0		922	727	892	
4000	231.0		1016	761	930	
4100	236.0		1055	785	959	
4250	245.0		1113	804	970	
4400	254.0		1171	832	1005	

DS-A10-2 $[0/\pm45/90]_s$ Straight Edges Simply-Supported

Axial Load lb	End Shortening x 10^{-4} in	Axial Strain at Gage Number				
		1	2	3	4	5
50	0		0	0	0	
250	6.0		46	34	41	
500	14.0		97	68	75	
750	23.5		158	111	118	
1000	32.5		221	158	168	
1250	43.0		288	212	226	
1500	52.0		334	259	277	
1750	62.0		363	310	334	
2000	74.5		422	367	398	
2250	87.0		483	419	435	
2500	98.5		548	477	467	
2750	113.0		620	547	492	
3000	125.0		680	605	536	
3250	138.0		740	673	567	
3500	150.0		811	738	616	
3750	161.0		885	798	658	
4000	173.0		974	857	704	
4100	179.0		1018	873	729	
4250	187.0		1079	905	766	
4400	194.0		1123	913	783	

Continued

DS-A10-1 $[0/\pm45/90]_s$ Straight Edges Simply-Supported

Axial Load lb	End Shortening x 10^{-4}	Axial Strain at Gage Number				
		1	2	3	4	5
4500	261.0		1211	835	1006	
4600	267.0		1248	849	1026	
4700	272.0		1277	864	1040	
4800	276.0		1302	875	1058	
4900	282.0		1348	909	1093	
5000	289.0		1375	926	1113	
5100	294.0		1414	953	1148	
5200	300.0		1444	973	1177	
5300	305.5		1472	991	1202	
5300	311.0		1502	1011	1230	
5500	316.0		1526	1029	1254	
5600	321.0		1560	1056	1287	
5700	326.0		1589	1080	1319	
5775	buckled					

DS-A10-2 $[0/\pm45/90]_s$ Straight Edges Simply-Supported

Axial Load lb	End Shortening x 10^{-4} in	Axial Strain at Gage Number				
		1	2	3	4	5
4500	200.0		1174	938	822	
4600	205.5		1209	947	832	
4750	213.0		1271	978	876	
4900	221.5		1340	989	909	
5000	228.0		1389	997	936	
5100	233.0		1420	1008	952	
5250	240.0		1471	1036	992	
5400	248.0		1526	1063	1033	
5500	253.0		1561	1069		
5510	buckled					

DS-A11-2 $[0/\pm45/90]_s$ Straight Edges Simply-Supported

Axial Load lb	End Shortening x 10^{-4} in	Axial Strain at Gage Number				
		1	2	3	4	5
50	0		0	0	0	
500	16.0		62	100	77	
750	30.0		100	180	153	
1000	45.0		147	238	245	
1250	60.0		188	313	323	
1500	75.0		226	409	399	
1750	90.0		263	484	458	
2000	107.0		303	582	536	
2250	122.0		344	661	602	
2500	138.0		392	740	673	
2750	153.0		442	810	734	
3000	168.0		503	885	797	
3250	185.0		568	960	859	
3500	201.0		635	1026	908	
3600	207.0		664	1056	930	
3750	215.0		701	1090	953	
3900	225.0		745	1134	983	
4000	232.0		775	1163	1002	
4100	244.0		809	1198	1028	
4250	248.5		849	1234	1048	

Continued

DS-A11-2 $[0/\pm45/90]_s$ Straight Edges Simply-Supported

Axial Load lb	End Shortening x 10^{-4} in	Axial Strain at Gage Number				
		1	2	3	4	5
4500	264.0		929	1314	1104	
4700	276.0		978	1364	1136	
4800	284.0		1012	1395	1154	
4900	291.0		1038	1419	1167	
5000	297.0		1068	1450	1191	
5100	302.0		1094	1474	1208	
5160	buckled					

APPENDIX D

USER'S MANUAL FOR COMPUTER PROGRAM CLAPP

1. TITLE CARD (18A4)

Columns 1-72	Problem description

2. CONTROL CARD (815)

Columns 1-5	IRUN - Takes integer values 1, 2, 3, ..., according as the completion of an analysis requires 1, 2, 3, ..., submissions of the program. IRUN = 1 for the first submission, IRUN = 2 for the second submission, and so forth. Valid for nonlinear analysis only (IBIF = 0). IRUN ≠1for any analysis that is a continuation of a previous application of CLAPP.
6-10	IEX = {0 perfect panel or plate; 1 imperfect panel or plate
11-15	IBIF = {0 nonlinear analysis; 1 linear bifurcation analysis
16-20	NFLAT = {0 flat plate analysis; 1 curved panel analysis
21-25	NAUTO = {0 x and y coordinates must be punched for input. Variable grid capabilities.; 1 Automatic generation of x and y coordinates with uniform, but possibly different, spacings for the x and y directions.
26-30	LGRNG = {0 Initial imperfections are represented by a mathematical expression.; 1 Initial imperfections are represented by a two-dimensional Lagrange interpolating function.

31-35 NUSTRT =

- 0 When the load-deflection curve is generated in segments the tape NTAPE contains the information required by the program to continue the calculations beginning with the last load-level for which a converged solution was obtained. To continue calculations set INDEX = 2, 3, ... and NUSTRT = 0.
- 1 It may happen that it is desirable to adjust the loading sequence to begin calculations for a second segment of the load-deflection curve. To do this set INDEX = 2, 3, ..., NUSTRT = 1 and reset the input data for PZSTRT, PXSTRT, PYSTRT, AND ZINCR, XINCR, YINCR.

36-40 NCURVE = 0

3. CONVERGENCE CRITERION CARD (F10.0, 215)

Columns 1-10 EPSI - Convergence criterion that determines acceptable displacements at a given load-level (order of 10^{-4}).

11-15 ITMAX - Program terminates if convergence at any load-level has not occurred within ITMAX iterations.

16-20 LEMAX - Program terminates after processing LEMAX load-levels as collapse or bifurcation has not occurred. Resubmit program with IRUN = 2.

4. GRID PARAMETERS CARD (815)

Columns 1-5 NSCHM =

- 1 Finite-difference grid points numbered consecutively along a cross-sectional circle
- 0 Finite-difference grid points numbered consecutively along a generator

6-10	ICTOUT = { 0 Panel has no cutout ; 1 Panel has a cutout }
11-15	NCOLS - Number of columns of grid points.
16-20	NROWS - Number of rows of grid points.
21-25	IROW1 - Number of the row in which the side of the cutout nearest the first row of grid points lies.
26-30	IROW2 - Number of the row in which the side of the cutout furtherest from the first row of grid points lies.
31-35	ICOL1 - Number of the column in which the side of the cutout nearest the first column of grid points lies.
36-40	ICOL2 - Number of the column in which the side of the cutout furtherest from the first column of grid points lies.

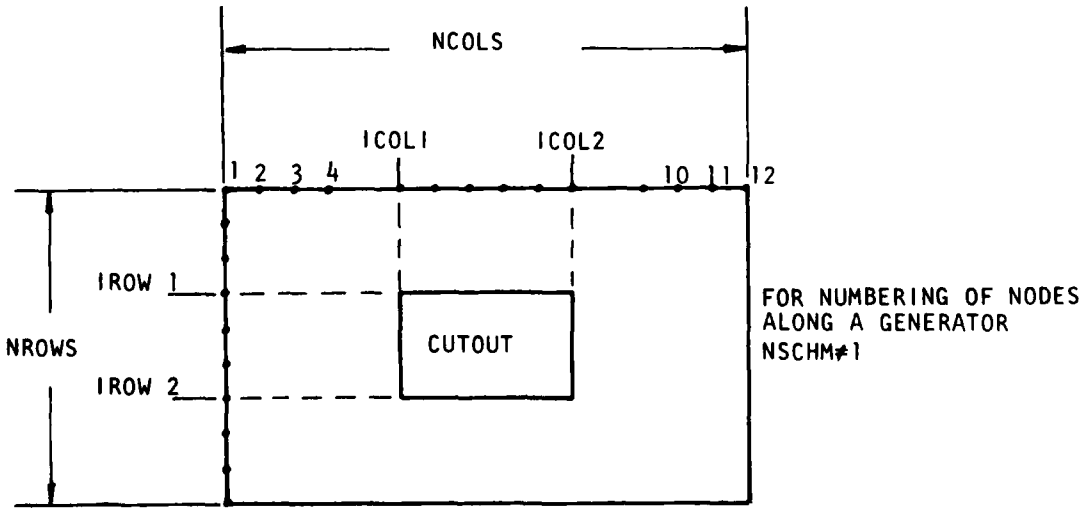

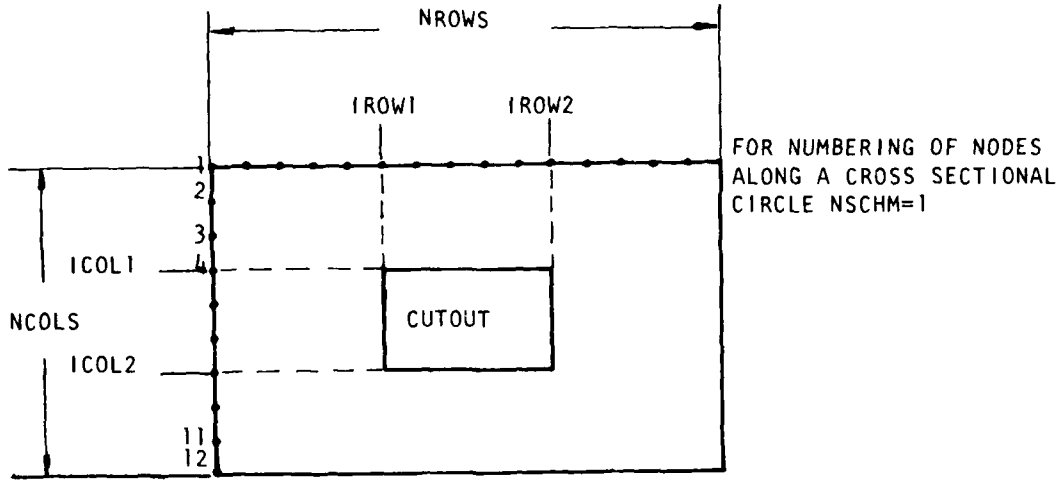

NOTE: Node numbering must originate at the upper left-hand corner of the finite-difference grid.

5. PANEL DIMENSIONS CARD (3F10.0)

Columns 1-10	XDIM - Length of a panel parallel to a generator.
11-20	YDIM - Length of a panel along a cross sectional circle (not the projection).
21-30	R - Panel radius of curvature. (Any number will suffice for a plate.

6. BOUNDARY CONDITION IDENTIFIER CARD (815)

Columns 1-5	NCASE1	=	1
6-10	NCASE2	=	2
11-15	NCASE3	=	2
16-20	NCASE4	=	3
21-25	NCASE5	=	3
26-30	NCASE6	=	4
31-35	NCASE7	=	4
36-40	NCASE8	=	5

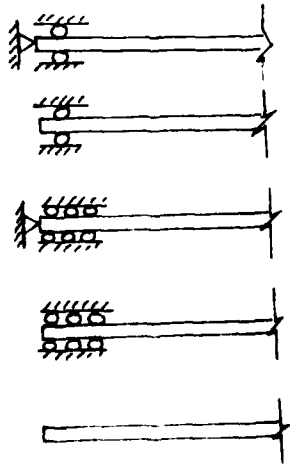

NCASE_ identifies a boundary of the panel as indicated in the accompanying figure. An integer from 1 to 5 is assigned to each NCASE_ according as the desired support condition along the edge identified by NCASE_ is one of those shown above.

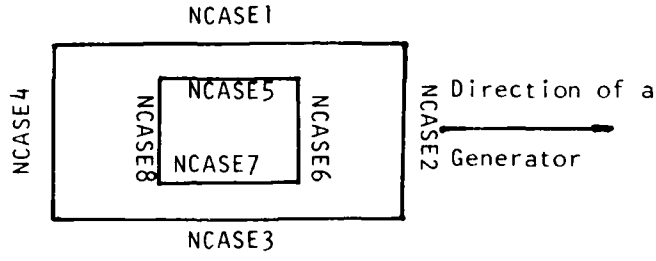

7. RIGID BODY CONDITION CARD (4I5)

Columns 1-5	IRB1	= 1 Tangential displacement parallel to the boundary identified by IRB_ is precluded at the mid-point of the boundary for an even number of grid points, or at the grid point nearest mid-point for an odd number of grid points.
6-10	IRB2	
11-15	IRB3	
16-20	IRB4	0 No modifications to boundary conditions are made.

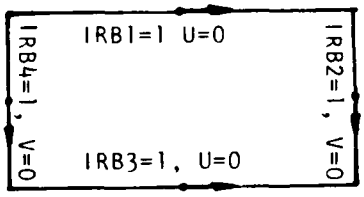

8. INITIAL-LOAD CARD (4F15.0,I5)

Columns 1-15	PZSTRT -	Initial-load normal to the panel surface. (Positive away from the center of curvature.)
16-30	PXSTRT -	Initial-load parallel to a generator of the panel. (Positive in the direction of increasing grid point numbers.)
31-45	PYSTRT -	Initial-load tangent to a cross-sectional circle. (Positive in the direction of increasing grid point numbers.

46-60 XDISPO - Prescribed initial axial end-displacement. Negative for compression.

61-65 MDISP = { 0 Prescribed loads; 1 Prescribed end-displacements

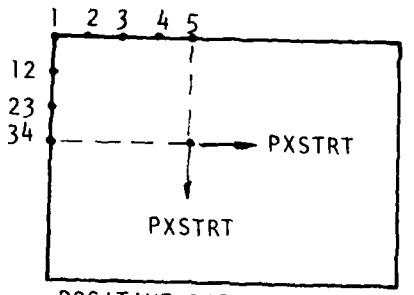

POSITIVE DIRECTIONS FOR PXSTRT AND PYSTRT FOR NSCHM=0

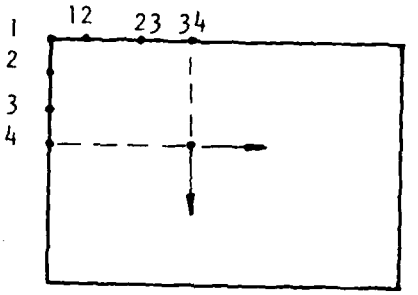

POSITIVE DIRECTIONS FOR PXSTRT AND PYSTRT FOR NSCHM=1.

9. LOAD IDENTIFICATION CARD (415)

Columns 1-5 LCASE = { 1 Concentrated load at grid point number LNODE.; 2 Line-load along row number LROW of the finite-difference grid.; 3 Line-load along column number LCOL of the finite-difference grid.; 4 Uniform distributed load over the entire surface.

6-10 LNODE - Number of the finite-difference grid-point at which a concentrated load is applied.

11-15 LROW - Number of the row of finite-difference grid points along which a line-load is applied.

16-20 LCOL - Number of the column of finite-difference grid points along which a line-load is applied.

10. LOAD INCREMENT CARD (3F10.0)

Columns 1-10	ZINCR - Load increment normal to the panel surface.
11-20	XINCR - Load increment parallel to a generator of the panel.
21-30	YINCR - Load increment tangent to a cross-sectional circle of the panel.

Positive directions for load-increments are the same as those for the initial loads.

If IEX ≠ 1 cards 11, 12, and 13 are not required.

11. INITIAL IMPERFECTION CARD (5F10.0,I5) Required only if LGRNG = 0 and IEX = 1

Columns 1-10	WO - Amplitude of initial geometric imperfection.
11-20	CONS1 - Wave number of the imperfection associated with the direction of a generator of a panel (π/half length of panel)
21-30	CONS2 = 0 Clamped curved edges and unsupported straight edges. b Clamped curved edges and simply-supported straight edges. b is one half of the circumferential length of a panel
31-40	XO - x-coordinate of geometric center of panel measured from lower left hand corner
41-50	YO - y-coordinator of geometric center of the panel measured from the lower left hand corner
51-60	IMPFORM = Initial imperfection has the form $WO(x,y) = WI*(1+\cos \pi\xi/a)(1-(\eta/b)^2)$ (Clamped at curved edges - simply-supported along the straight edges) Initial imperfection has the form $WO(x) = WI*(1+\cos \pi\xi/a)$ (Clamped along the curved edges - free at the straight edges)

12. IMPERFECTION-GRID PARAMETER CARD (2I5) Required only if LGRNG = 1 and IEX = 1

Columns 1-5	MX = Number of grid points along a generator for which discrete values of initial imperfection are known. Spacing of these points is required to be uniform.
6-10	MY = Number of grid points along a cross sectional circle for which discrete values of initial imperfection are known. Spacing of these points is required to be uniform.

MX or MY can not exceed 10 for the present dimensions of the program.

13. IMPERFECTION DATA CARD (10F8.0) Required only if LGRNG = 1 and IEX = 1

A single card contains the known discrete value of initial imperfection for every grid point in a row of the imperfection-grid. Thus, MY cards are required: one for each row of the imperfection-grid. A row is considered to be parallel to a generator of the panel. Imperfection values are positive away from the center of curvature of the panel.

Imperfection-grid size cannot exceed 10 grid points in either direction unless internal dimensions are modified.

Imperfection-grid is parallel to finite-difference grid with origin as shown in the figure.

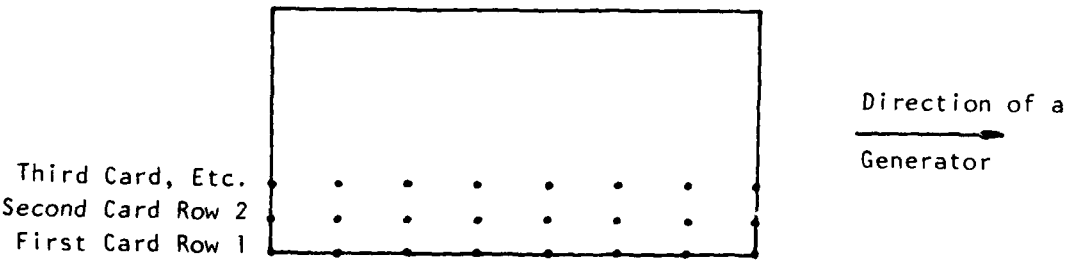

14. NODAL COORDINATE CARD (2F10.0) Required only if NAUTØ = 0

Columns 1-10	x-coordinate of a finite-difference grid point
11-20	y-coordinate of a finite-difference grid point

These cards are required only when NAUTO = 0; i.e., whenever a variable finite-difference grid is required.

15. STIFFENER CARD (4I5)

Columns 1-5	NSTFR = {0 no stiffeners; 1 stiffeners included}
6-10	NSTYP = {1 through 8 - cross section type (see below)}
11-15	NSLOC = {0 located on outside of panel (+); 1 located on inside of panel}
16-20	ISSPC = {0 spaced on all grid lines; 1 variable spacing}

16. STIFFENER CROSS SECTION INPUT CARDS only if NSTFR = 1

The number and required input of these cards depend on the choice of stiffener cross section type (NSTYP) above.

NSTYP = 1 (2F10.0) (2F10.0) rectangular plate

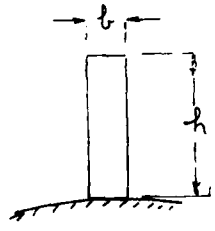

(1)	Columns 1-10	HGHT = h
	11-20	WDTH = b
(2)	Columns 1-10	SEMOD = elastic modulus
	11-20	SGMOD = shear modulus

NSTYP = 2 (4F10.0) (2F10.0) symmetric I beam

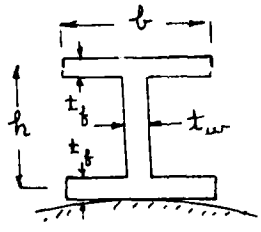

(1)	Columns 1-10	HGHT = h (total - t_f)
	11-20	WDTH = b
	21-30	FLTHK = t_f
	31-40	WTHK = t_w
(2)	Columns 1-10	SEMOD = elastic modulus
	11-20	SGMOD = shear modulus

NSTYP = 3 (5F10.0) (2F10.0) non-symmetric I beam

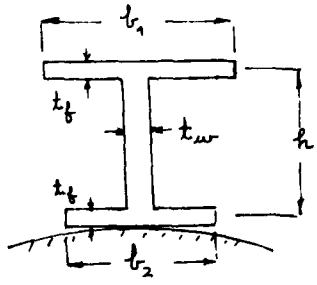

(1)	Columns 1-10	HGHT = h (total - t_f)
	11-20	TWDTH = b_1
	21-30	BWDTH = b_2
	31-40	FLTHK = t_f
	41-50	WTHK = t_w
(2)	Columns 1-10	SEMOD = elastic modulus
	11-20	SGMOD = shear modulus

NSTYP = 4 (4F10.0) (2F10.0) inverted T

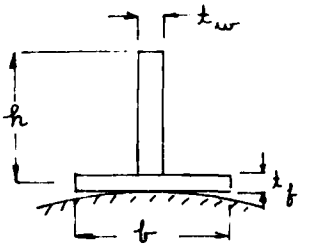

(1)	Columns 1-10	HGHT = h (total - $t_f/2$)
	11-20	WDTH = b
	21-30	FLTHK = t_f
	31-40	WTHK = t_w
(2)	Columns 1-10	SEMOD = elastic modulus
	11-20	SGMOD = shear modulus

NSTYP = 5 (4F10.0) (2F10.0) T beam

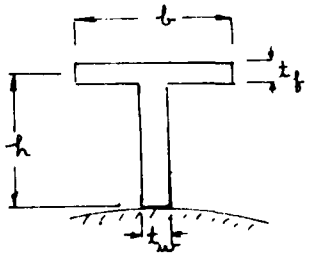

(1)	Columns 1-10	HGHT = h (total - $t_f/2$)
	11-20	WDTH = b
	21-30	FLTHK = t_f
	31-40	WTHK = t_w
(2)	Columns 1-10	SEMOD - elastic modulus
	11-20	SGMOD - shear modulus

NSTYP = 6 (4F10.0) (2F10.0) C beam

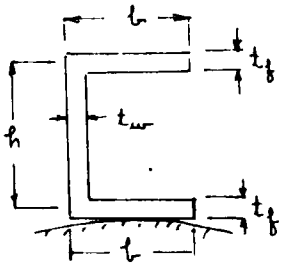

(1)	Columns 1-10	HGHT = h (total - t_f)
	11-20	WDTH = b
	21-30	FLTHK = t_f
	31-40	WTHK = t_w
(2)	Columns 1-10	SEMOD = elastic modulus
	11-20	SGMOD = shear modulus

NSTYP = 7 (4F10.0) (2F10.0) L beam

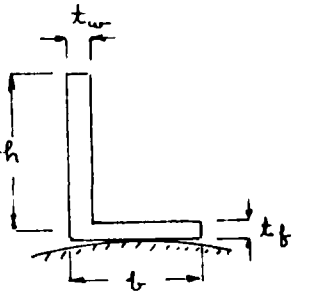

(1)	Columns 1-10	HGHT = h (total - $t_f/2$)
	11-20	WDTH = b
	21-30	FLTHK = t_f
	31-40	WTHK = t_w
(2)	Columns 1-10	SEMOD = elastic modulus
	11-20	SGMOD = shear modulus

NSTYP = 8 (4F10.0) (5F10.0) (2F10.0) user's choice

(1)	Columns 1-10	SAREA = cross section area
	11-20	CEI = 1st principal moment of inertia, $I_{\xi\xi}$
	21-30	ETAI = 2nd principal moment of inertia, $I_{\eta\eta}$
	31-40	ALPHA = angle from horizontal to ξ-direction, in radians
(2)	Columns 1-10	CED = distance to contact point, ξ-direction
	11-20	ETAD = distance to contact point, η-direction
	21-30	CES = distance to shear center, ξ-direction
	31-40	ETAS = distance to shear center, η-direction
	41-50	CONSTJ = twisting constant, J

(3) Columns 1-10 SEMOD - elastic modulus
11-20 SGMOD - shear modulus

Refer to figure on the next page for an example of these quantities for the user's choice stiffener, type 8.

NSTYP = 9 (4F10.0,I5)(5F10.0) QUASI-ISOTROPIC HAT SECTION

(1) Columns 1 - 10 HGHT = h

11 - 20 WDTH = b

21 - 30 FLNGW = b_1

31 - 40 STHK = t

41 - 45 NLAYER = No. of layers.

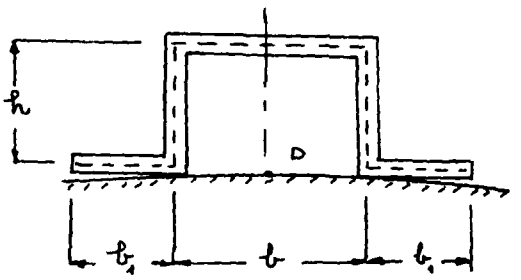

UNIFORM SECTION THICKNESS.

(2) Columns 1 - 10 E11 = elastic modulus parallel to the fibers of a lamina.

11 - 20 E22 = elastic modulus perpendicular to the fibers of a lamina.

21 - 30 G12 = lamina shear modulus

31 - 40 PNU12 = Poisson ratio associated with stress along fiber direction.

41 - 50 PNU21 = Poisson ratio associated with stress perpendicular to fiber direction.

This stiffener cross section type accomodates fiber-reinforced stiffeners where the fiber directions are alternately zero and 90 degrees. Midplane symmetry is assumed.

Note that the stiffeners when located on the inside of the panel are inverted as depicted below.

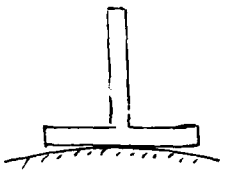

STIFFENER ON THE OUTSIDE OF PANEL

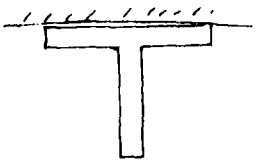

STIFFENER ON THE INSIDE OF PANEL.

17. NUMBER OF STIFFENERS (I5) needed only if ISSPC = 1, NSTFR = 1

Columns 1-5	NST = number of stiffeners if they are not on each grid line

18. VARIABLE SPACING STIFFENER CARDS (I5) only if ISSPC = 1, NSTFR = 1

Columns 1-5	NSROW = row number that locates stiffener (if NSCHM = 0) column number that locates stiffener (if NSCHM = 1)

One card is required for each stiffener, so there will be the same number of cards as NST above. The row (or column) numbers must be in increasing order, i.e., 1,4,7,10, etc. not 1,7,4,10.

19. NUMBER OF LAYERS CARD (I5)

Columns 1-5	KN - Number of layers in the laminate.

20. LAYER LOCATION CARDS (F10.0)

Columns 1-10	Distance (inches) between a layer surface nearest the center of curvature and the laminate reference surface. First layer is considered to be the one nearest the center of curvature. Distances measured toward the center of curvature are negative.

A card for the most remote surface of the last layer is required. Thus, there is required KN+1 LAYER LOCATION CARDS.

21. MATERIAL PROPERTIES CARDS (6F10.0) One card is required for each layer.

Columns 1-10	Modulus of elasticity parallel to the fibers of a given layer (lb/in^2)
11-20	Modulus of elasticity perpendicular to the fibers of a given layer (lb/in^2)
21-30	Poisson ratio associated with strain parallel to the fiber axis due to a stress perpendicular to the fiber axis
31-40	Poisson ratio associated with strain perpendicular to the fiber axis due to a stress parallel to the fiber axis.
41-50	Shearing modulus of elasticity (lb/in^2)
51-60	Angle between the fiber direction and a generator of the panel. This angle is positive whenever the fiber direction is situated in a clockwise orientation relative to the positive x-direction.

EXAMPLE THAT DEFINES INPUT QUANTITIES
FOR USERS CHOICE STIFFENER

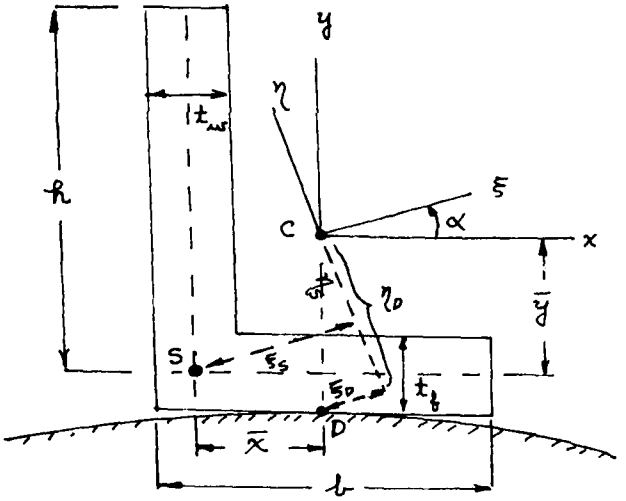

C —	CENTROID
S —	SHEAR CENTER
D —	CONTACT POINT BETWEEN PANEL AND STIFFENER

$$\text{AREA} = \left(h - \frac{t_f}{2}\right) t_w + b\, t_f$$

$$I_{\xi\xi} = \frac{I_{xx} + I_{yy}}{2} + \sqrt{\left(\frac{I_{xx} - I_{yy}}{2}\right)^2 + I_{xy}^2}$$

$$I_{\eta\eta} = \frac{I_{xx} + I_{yy}}{2} - \sqrt{\left(\frac{I_{xx} - I_{yy}}{2}\right)^2 + I_{xy}^2}$$

$$\alpha = \frac{1}{2}\ \text{ARCTAN}\left(\frac{-2 I_{xy}}{I_{xx} - I_{yy}}\right)$$

CED ≡ ξ_D : HERE $-(\bar{y} + \frac{1}{2} t_f)\sin\alpha$

ETAD ≡ η_D $-(\bar{y} + \frac{1}{2} t_f)\cos\alpha$

CES ≡ ξ_S $-(\bar{y}\sin\alpha + \bar{x}\cos\alpha)$

ETAS ≡ η_S $-(\bar{y}\cos\alpha - \bar{x}\sin\alpha)$

$$\text{CONSTJ} \equiv J = \sum_{i=1}^{N} \frac{1}{3} h_i t_i^3 \quad : \quad \frac{h t_w^3 + b t_f^3}{3}$$

☆U.S.Government Printing Office: 1982 — 559-005/4055

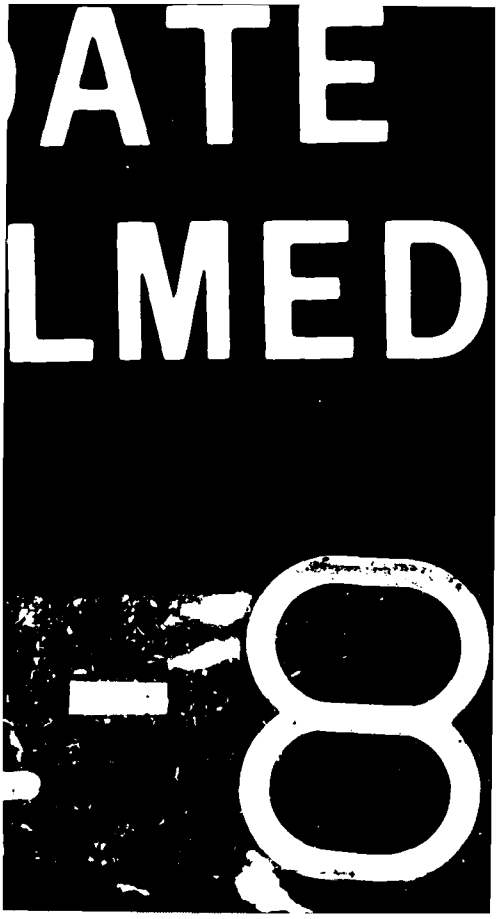
ATE
LMED
8